Channel Estimation and ICI Cancellation for Adaptive OFDM Systems in Doubly Selective Channels

Dissertation
zur Erlangung des akademischen Grades

Doktoringenieur
(Dr.-Ing.)

von **M.Sc. Ali Ramadan M. Ali**
geb. am 1. January 1974 in Faum, Ägypten

genehmigt durch die Fakultät für Elektrotechnik und Informationstechnik
der Otto-von-Guericke-Universität Magdeburg

Gutachter:

Prof. Dr.-Ing Abbas S. Omar
Prof. Dr.-Ing Christian Diedrich
Dr.-Ing Lutz Rauchhaupt

Promotionskolloquium am: 26. April 2010

Dedications

This work is dedicated to the memory of my mother and my father

Ali

Acknowledgements

I would like to express my thanks and gratitude to all those gave me the support to complete this work.

First of all I am deeply indebted to my supervisor Prof. Dr.-Ing Abbas Omar for the opportunity to become a member of his group and for his help, guidance, and support during the time that I spent at the Institute for Electronics, Signal Processing and Communications at the Otto-von-Guericke University. He was always available to give me timely and indispensable suggestions and advices. His big experience and knowledge provided me with the required sprit and motivation to complete this work.

I express my appreciation to the Administration of Educational Missions in Libya for the financial support during my study in Germany. I would like to express my thanks to Prof. Christian Diedrich and Dr. Lutz Rauchhaupt for agreeing to referee this thesis.

I am expressing my sincere gratitude to Atallah Balalem, Tariq Kanzada, Moftah Elzobi, for their kind help in reviewing the text. I am also thankful to Berthold Banzner, Julia Braun, Abdallah Farid and Michael Maiwald for their help. I would like to thank Prof. Jan Machac from Czech Technical University, and Dr. Ali Aassie for their cooperation. My sincere thanks to Dr. Adel Abdel-Rahman, Ahmed Boutejdar, Ahmed Hassen, Mohammed Khair and all my colleges in the HF group and my friends in Magdeburg for their help and support. I have had a great time with them both socially and on the job.

I am so grateful to my parents, my sisters and brothers for everything they did for me. Their love and support have always nurtured me throughout my life, so I thank them in every possible way.

Finally, I would like to thank my wife Tahani. Without her effort, patience, and understanding, this work would not be possible.

Ali Ramadan Ali
Magdeburg, October, 2009.

Zusammenfassung

Im Rahmen dieser Dissertation wurde eine Studie über die Leistungsfähigkeit des OFDM-Systems in zeitvarianten Kanälen mit Mehrwegeausbreitung durchgeführt, unterstützt durch mathematische Analyse und Simulation in MATLAB sowie die Messung des OFDM-Signals, um eine neue Kanalschätzung und Entzerrungsalgorithmen zur Verbesserung der Leistungsfähigkeit und zur Verringerung des Rechenaufwandes zu entwickeln.

In dieser Arbeit werden zwei Reduzierungsmethoden der Inter-Carrier-Interferenz (ICI) für das System Digital Radio Mondiale (DRM) erläutert und weiter entwickelt. Aufgrund der langen Symboldauer des DRM, leidet dieses Übertragungssystem unter hohen ICI. In der Literatur wird diesem System weniger Aufmerksamkeit geschenkt als den anderen Anwendungen des OFDM-Systems.

Es werden Vorschläge für neue Algorithmen gemacht, die mit geringer Komplexität zur Reduktion von ICI für das OFDM-basierte DRM-System in den schnellen zeitvarianten Kanälen geeignet sind. Diese Algorithmen verwenden die Angleichung der Zeitvariation des Kanals mit Hilfe von numerischen Methoden, wie der Newton- und Lagrange-Polynome-Angleichung. Die Algorithmen nutzen die begrenzte Anzahl von Koeffizienten in der Kanalimpulsantwort (engl. CIR).

In der Arbeit wird eine andere Methode mit geringer Komplexität für DRM-Systeme erläutert. Sie basiert auf einer Vorverarbeitung des empfangenen Signals im Zeitbereichs, um das Signal-Rausch-plus-Interferenz-Verhältnis (SNIR) so zu erhöhen, dass Entzerrungsschemen mit geringer Komplexität anwendbar werden. Es wird ein Hamming-Fenster verwendet, um die Kanal-Matrix auf verschiedene Doppler-Spread Werte dünn besetzt zu machen.

Die Verbesserung der Fähigkeiten des Empfängers in den zeitvarianten Kanälen ist nicht ausreichend für eine zuverlässige Kommunikation. Um eine zuverlässige Kommunikation und einen breiten Bereich von Anwendungen für unterschiedliche Nutzer zu erzielen, sind einige weitere Änderungen für das gesamte System erforderlich, wie die Anpassung des Systems an langfristige Änderungen des Kanals. In der Dissertation wird eine Methode für die Anpassung des Zeit-Interpolators des Schätzers auf der Empfängerseite vorgeschlagen. Bei dieser Methode folgt der Schätzer den kurz- und langfristigen Veränderungen des Kanals und passt den Grad der Polynom Angleichung Methode an die Zeit-Interpolation an, um die Bit-Fehler-Rate (BER) als Gegenstand der Verarbeitungsverzögerung und der Komplexität zu minimieren. Weiterhin werden zwei Link-Anpassungsmethoden für OFDM-basiertes WLAN-System vorgeschlagen. Die erste ist die Cyclic-Präfixlänge-Anpassung, bei der die langfristige Veränderung der Kanalverzögerung mit dem Root-MUSIC Algorithmus geschätzt und dann für die Anpassung der Guard Interval (GI) verwendet wird. Die zweite Methode befasst sich mit dem adaptiven Pilot-Distribution, wobei die Distanz zwischen den Piloten in der Zeit und Frequenz der Doppler- und Delay-Variationen-Verbreitung des Kanals entspricht. Das Ziel dieser Methoden ist eine Erhöhung der Kapazität des Systems.

Abstract

One of the major aspects of the emerging wireless communication systems is the use of the orthogonal frequency division multiplexing (OFDM) as a modulation scheme for data transmission. This is motivated by its ability to work efficiently in multi-path channels. However, the system suffers in time-varying channels from the performance degradation and the increase of computational complexity.

Throughout this thesis, a study of the performance degradation of OFDM systems in multipath time-varying channels is carried out supported with mathematical analysis, simulation in MATLAB as well as measurements of the OFDM signals, in order to find new and robust channel estimation and equalization algorithms capable to enhance the performance, and reduce the computational effort.

In this thesis some inter-carrier interference (ICI) reduction methods for digital radio mondiale (DRM) system, which is one of OFDM system applications, are introduced. As a consequence of its long symbol duration, DRM system suffers from high ICI even with medium vehicle speeds. However, in the literature, this system got less attention than other OFDM applications.

A Wiener filtering channel estimation algorithm for DRM system is introduced in this thesis. To reduce the model mismatch, the estimator makes use of a combined Matrix pencil delay estimation algorithms and Wiener filtering.

New low complexity algorithms used for reducing the ICI for OFDM-based DRM system in rapidly time-variant channels are proposed. These algorithms make use of approximating the time variation of the channel by means of numerical methods, such as Newton and Lagrange polynomial approximation. Instead of using the channel transfer function (CTF) for the approximation, the methods exploit the limited number of taps in the channel impulse response (CIR). Another low complexity estimation method for DRM system is introduced. The method applies a time domain preprocessing at the received signal to maximize the signal-to-noise plus interference ratio (SNIR), and aiming at making the channel matrix sparse so that low complexity equalization algorithms become applicable. The Gaussian shaped Doppler spectrum of the DRM system is considered in implementing this algorithm. In addition, a modified Hamming window is applied in order to squeeze the channel matrix for different squeezing factors and Doppler spread values.

In case of mobile scenarios, improving the receiver capabilities is not enough to achieve a reliable communication. In order to deliver a wide range of applications to different users, some further modifications for the entire system are required, such as adapting the system parameters according to the long-term variation of the channel. Some adaptive methods are introduced in this thesis. A method of adapting the time interpolator of the estimator at the receiver is proposed in which the estimator tracks the short and long-term variations of the channel, and then adapts the degree of the polynomial approximation used for time interpolation, aiming at minimizing the bit-error rate (BER) subject to prescribed processing delay and complexity. On the other hand, two link adaptation methods for OFDM-based WLAN system are proposed. The first one is cyclic prefix length adaptation algorithm in which the long-term variation of the delay spread is estimated using root multiple signal classification (root-MUSIC) algorithm, which then used

to adapt the guard interval (GI) length of the transmitted signal. The second method deals with adapting the pilot distribution. The pilot separations in time and frequency are adapted according to the Doppler and delay spread variations of the channel, aiming at maximizing the throughput of the system without significantly sacrificing the BER performance.

Contents

List of Figures

List of Tables

Mathematical Notation

Symbol	Description
$\mathbf{H}$	Bold uppercase letters denote matrices in frequency domain
$\mathbf{h}$	Bold lowercase letters denote matrices in time domain
$\underline{\mathbf{H}}$	bold uppercase underlined letters denote frequency domain vectors
$\underline{\mathbf{h}}$	bold lowercase underlined letters denote time domain vectors
h	Lowercase letters denote variables in time
H	Uppercase letters denote variables in frequency
$\{.\}^*$	Conjugate operator
$\{.\}^T$	Transpose operator
$\{.\}^H$	Hermitian operator
$E\{.\}$	The mathematical expectation
$\mathcal{D}\{.\}$	Vector to diagonal matrix conversion
$\mathcal{C}\{.\}$	Vector to circulant matrix conversion
$\mathcal{M}\{.\}$	Masking operator
$\bar{\mathcal{M}}\{.\}$	Complementary masking operator
$diag(\mathbf{H})$	The diagonal of a matrix
$\odot$	Wise element multiplication (Hadamard product)
$*$	mathematical convolution
$\|\cdot\|_F$	Frobenius norm

List of Symbols

Chapter 1

Introduction

During the last two decades, the wireless communications have experienced a huge growth in both capacity and variety. This growth is going to shrink the world to a small village in which users with different requirements are efficiently accommodated anywhere and at any time. This will be resulted in an increased demand for new services that provide higher bit rate and higher capacity. It is expected that the wireless communication systems of the near future will require data rates up to few hundreds of mega bits per second (Mbps), which are able to deliver bandwidth hungry applications such as web browsing and video streaming. The required data rate of the next generation of wireless communication systems will be achieved by efficiently increasing the amount of the allocated bandwidth and using more advanced technologies, both in hardware and software [1].

One of the major themes in today's broadband systems is the use of the orthogonal frequency division multiplexing (OFDM). OFDM is a modulation scheme suitable for frequency selective channels and for providing high speed data transmission, which makes it one of the promising solutions for the next generation of wireless communications. However, there is a need for more developments of OFDM systems in terms of complexity reduction and adaptation, therefore reconfigurable solutions are needed to achieve the user requirements. This is necessary because the end users require lightweight, compact size and power efficient devices besides the high bit rate capabilities. Furthermore, combining the communication systems with the new techniques such as multiple-input-multiple-output (MIMO), can also enhance the capacity and the bit rate of the emerging systems.

1.1 Today's Wireless Communication Systems

Currently, there is a very wide range of wireless applications used for serving users with a variety of services such as voice, video, and data. Many newcomers have found employment in the area of wireless communications. These include broadcasting systems such as digital audio and video broadcasting (DAB) [2] and (DVB) [3], fixed point-to-point wireless communications and mobile cellular systems, medium and short range wireless networks including the wireless metropolitan area network (WMAN), wireless local area network (WLAN) [4], and sensor networks such as Zigbee as well as the very short range networks such as near field communication (NFC), personal area networks (PAN) and ultra-wideband (UWB) systems. The current wireless networks operate over a wide range of data rate (from 20 Kbps for Zigbee to 500 Mbps for wireless USB), and over a coverage range between 5 cm for NFC to 50 Km for WMAN, in between, there is a huge number of applications that are designed to serve a wide variety of users with different needs.

1.1.1 Mobile Revolution

In cellular systems, the geographic area to be covered is divided into small cells, thus the same frequency can be reused many times to enhance the system capacity. The history of mobile cellular systems started with the first generation (1G) in the mid of eighties in USA. These systems were based on analog technology and were designed only for voice transmission. The users in a cell were sharing the common channel using frequency division multiple access (FDMA), and the connection between the base station and mobile station was based on frequency division duplex (FDD). Several standards have been established for different countries, such as the advanced mobile phone service (AMPS) that was popular in USA, the nordic mobile telephone (NMT) that was used in the Scandinavian countries, and C-Nentz that was used in West Germany.

In the early nineties, the digital technology became the backbone of the second generation systems (2G), which are still in use in many countries till now. These systems use different multiplexing methodologies such as time division multiple access (TDMA) and code division multiple access (CDMA). Compared to the 1G communication systems, 2G systems have higher capacity, and enjoy improvements in the power and cost efficiencies. Global system for mobile communications (GSM) [5] is one example of the 2G systems that has been established firstly by Radiolinja in Finland in March 1991, and became very popular in Europe. In September 2002, there were 460 GSM networks serving 747.5 million subscribers worldwide [6]. Currently, the GSM system is used in more than 170 countries worldwide. This system uses a combination of FDMA and TDMA, and provides data rate up to 9.6 Kbps. Other examples of 2G systems are personal digital communications (PDC) [7] that is used in Japan and IS-95 [8] that is popular in USA and South Korea. Although the 2G systems are digital, they were designed for voice transmission only. Furthermore, these systems were unsuitable for accessing the Internet, since they were based on circuit switched networks. This put some limitations on the systems, since the demand for transmitting data and accessing the Internet through the mobile services increases every day. Because it was difficult to remove the existing infrastructures and think in different systems, the mobile communication companies started to develop technologies to enhance the capabilities of the existing 2G systems. Nowadays, users can access the Internet using the general packet radio service (GPRS) which is available for GSM users. GPRS makes GSM users able to transmit voice as well as low rate data like short message service (SMS). The data rate for GPRS exceeds 115 Kbps. An important issue is that GPRS is based on packet switched networks, therefore it does not allocate the entire channel continuously, but only when there are data to be sent. Another development on the 2G systems is the enhanced data services for GSM evolution (EDGE). This system is usually referred as 2.5G system. It utilizes advance modulation techniques as eight-phase shift keying (8PSK) and forward error correction (FEC) coding to increase the bit rate of the GSM system. EDGE systems provide intermediate multimedia services with bit rate of 384 Kbps.

In 2001, the standardization of the third generation 3G mobile communication systems has been started by the European telecommunication standard institute (ETSI) [9]. The new systems are designed for both voice and data transmission with higher bit rate than that for 2G. The 3G systems provide streaming video capabilities that can support movie downloads and video conferencing along with Internet access with several Mbps. One

example of 3G systems is the universal mobile telecommunication system (UMTS). This system uses wideband CDMA (WCDMA) as an air interface with channel bandwidth of 5 MHz. The UMTS system supports transmission speed of about 2 Mbps. For mobility cases, this rate reduces to around 144 Kbps. Another example of 3G systems is cdma2000, which is popular in South Korea.

To further enhance the system capabilities, 3G systems are being developed under a worldwide project called 3G partnership project (3GPP) [10, 11], which is responsible for improving the performance of UMTS systems. One release of this project is the high speed packet access (HSPA), which is referred as 3.5G system. HSPA contains different standards like high speed downlink packet access (HSDPA), which is defined in 3GPP UMTS Release 5 specifications and has been established in June 2002. It provides improvements on the downlink speed up to 10 Mbps by utilizing different spreading factors as well as adaptive modulation and coding schemes according to the signal quality. The second standard is high speed uplink packet access (HSUPA), which increases the speed of the up link up to 5 Mbps. It is standardized as part of 3GPP UMTS Release 6 specifications and has been approved in March 2005. A new standard which is still under development is called high speed OFDM packet access (HSOPA). This system uses different air interface to improve the spectrum efficiency and bit rate. OFDM provides high speed data transmission and has less reception complexity in multipath channels. HSOPA has variable bandwidth between 1.25 MHz-20 MHz. The downlink speed reaches 100 Mbps while that of the uplink is 50 Mbps. HSOPA is a fraction of the so called long term evolution (LTE) of the 3GPP. This evolution will lead to the fourth generation (4G) mobile systems in the next few years. This system takes the advantages of both, OFDM modulation and single carrier modulation. The downlink is based on orthogonal frequency division multiple access (OFDMA) to increase the bit rate, and the uplink is based on single carrier- frequency division multiple access (SC-FDMA) that has better power efficiency. In this new modulation scheme, the time domain signal is first spread using precoding stage making use of the discrete Fourier transform (DFT), and then converted back to the time using inverse fast Fourier transform IFFT, in order to get the advantages of OFDM in multipath channels as well as better power efficiency than OFDM system [12]. For high bit rate targets, OFDMA can provide benefits over a CDMA-based system when the bandwidth increases. LTE system will use MIMO technology for both base station and mobile station. Two MIMO configurations (2×2 and 4×4 have been standardized, however, it is expected that only 2×2 antennas will be available for the first commercial LTE systems.

In addition to 3GPP, there is another project goes in parallel called (3GPP2), which has two standards, the evolution data and voice (1xEV-DV) and the evolution data-optimized (1xEV-DO). These standards are defined as evolutions responsible for enhancing the capabilities of 2G: IS-95 and 3G: cdma2000 systems, respectively. By tracking the cellular history, we find that there were always two candidates in a competition for each emerging mobile generation. Fig. 1.1 shows the adopted radio accesses over the last two decades. In the discussion about the 2G systems, two candidates for multiplexing were considered, TDMA and CDMA. At the end, TDMA was adopted as a standard [13]. However, some systems used CDMA like IS-95. In late 1999, again two candidates for 3G systems were in the competition, CDMA and an OFDM-based multiple access system. CDMA has finally been adopted in the form of WCDMA and cdma2000. OFDM-based

techniques look very promising for the 4G systems, which may be put in service by 2010.

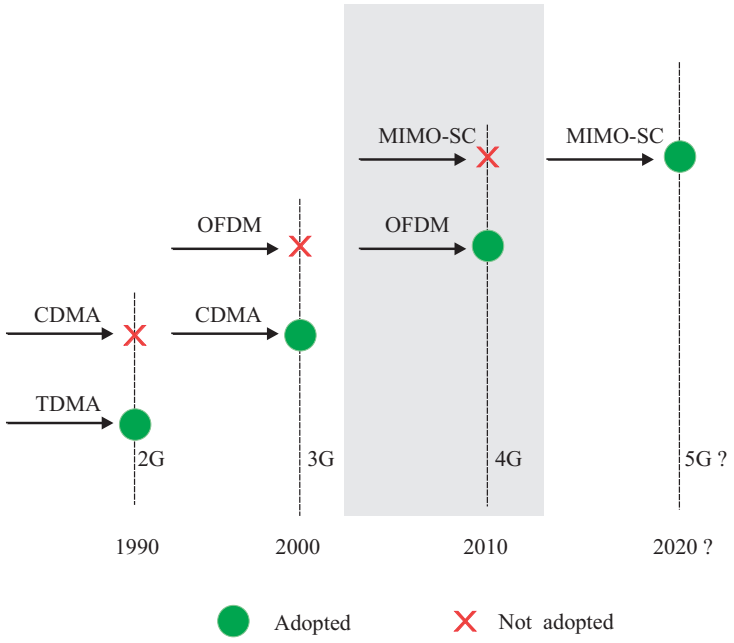

Figure 1.1: Adopted radio access techniques for mobile generations.

1.1.2 Modern Wireless Internet Access Networks

The world is going to have faster wireless connections, and within the next decade people will gain high-speed wireless Internet access. The wireless network is designed to provide wireless access between computing devices, and usually implemented as a final link between the existing network and the client PC. WLAN is an example of the wireless network that provides wireless connections between some local computers used in temporary offices, or other places where the installation of cables is expensive.

In 1999, the institute of electrical and electronics engineers (IEEE) has approved the standard IEEE802.11b WLAN, which is also called Wireless Fidelity Wi-Fi. It works at 2.4 GHz and has a bandwidth of 20 MHz, which is larger than that of 3G systems. The system uses direct sequence spread spectrum DSSS as an air interface and provides data rates up to 11 Mbps. Two other standards that use OFDM as an air interface, which allows higher data rate, are IEEE802.11a that has been approved in 1999 and works at 5.2 GHz and IEEE802.11g that has been approved in 2003 and works at 2.4 GHz. The bit rate of the last two systems can reach 54 Mbps by using adaptive modulation and coding schemes. The European version of IEEE802.11a is called High Performance LAN 2 (HiperLAN/2), which has been approved in 2000. It is equivalent to IEEE802.11a in the physical layer but differs in the medium access control (MAC) layer. In 2004, a new standard IEEE802.11n has been developed. This system uses MIMO technology to enhance the capabilities of the OFDM system in terms of the bit rate and coverage. IEEE802.11n provides data rates up to 200 Mbps according to the number of used antennas at the receiver and the transmitter. Currently WLANs are distributed as hot spots at airports,

universities or conferences. They are designed to provide in-building or campus coverage (around 100 m), therefore the system does not support high speed mobility.

On the other hand, WMANs, usually referred to IEEE802.16, provide wireless connections between multiple locations within a city where WLANs can not cover. One example of the emerging WMAN systems is the worldwide interpretability for microwave access (WiMAX). It works for long distances (several km's) and allows for higher mobility with bit rates up to 70 Mbps. There are some standards of WiMAX, one of them is the aforementioned IEEE802.16, approved in 2002. This system uses SC modulation and designed for fixed line of sight (LOS) connections. The other one is IEEE802.16-2004, which is designed for fixed non-LOS situations and uses OFDM as an air interface and OFDMA for multiplexing. The third type is IEEE802.16e-2005, which is designed for mobile non-LOS situations. IEEE802.16e-2005 uses a scalable OFDM with different bandwidth allocation from 1.25 to 20 MHz to comply with varied worldwide requirements. Now, more than 150 WiMAX trials are underway in Europe, Asia, Africa and North and South America [14]. Another type of wireless networks is the WPAN that replaces the short range cables with RF technology. One example of WPAN is the famous Bluetooth system which works at 2.4 GHz and provides peak data rate up to 1 Mbps. In Bluetooth, frequency hopping (FH) technology is used for multiple access. Bluetooth has low cost, low power (1mW), and works for short range (10 m).

A new type of emerging wireless networks is ultra-wideband (UWB) that works in frequency range between 3.1-10.6 GHz. UWB system, also referred as WiMedia IEEE 802.11.15a, allows users to work with very high bit rate around 500 Mbps with channel bandwidth of 500 MHz by using very narrow pulses (nanoseconds). UWB devices work at very low power (many times lower than Bluetooth for the same range), and cover short distances (5 m). Similar to the most of the emerging technologies, UWB systems use OFDM air interface to deal with the multipath channels.

1.1.3 The Fourth Generation (4G) Systems

The research on 4G systems has just recently begun. In the past, the term "new generation" referred always to mobile cellular systems. However, 4G systems will combine many applications simultaneously and will integrate various networks like cellular systems with WiMAX and WLAN to allow users to move freely between the different standards. The aim of 4G technology is to extend the capabilities of 3G systems, allowing a wider range of applications. One of the main focuses of the 4G systems will be the efficient utilization of the finite spectrum. 4G will also provide flexible connectivity to the users (stay connected anywhere, anytime) with higher data rates, stronger security, higher mobility, and higher quality of services (QoS) than the current systems. Fig. 1.2 shows the mobility scenarios versus the achievable bit rate for the modern communication systems and the position of the 4G systems [15]. 4G systems will be designed to deal with the fading and the multipath problems. Low power consumption (increased battery life), compact size, and low cost efficiency are the important issues in designing the next generations of communication systems. As a common solution for most of the next generation requirements, OFDM system becomes a very preferable modulation scheme because of its robustness in severe multipath scenarios.

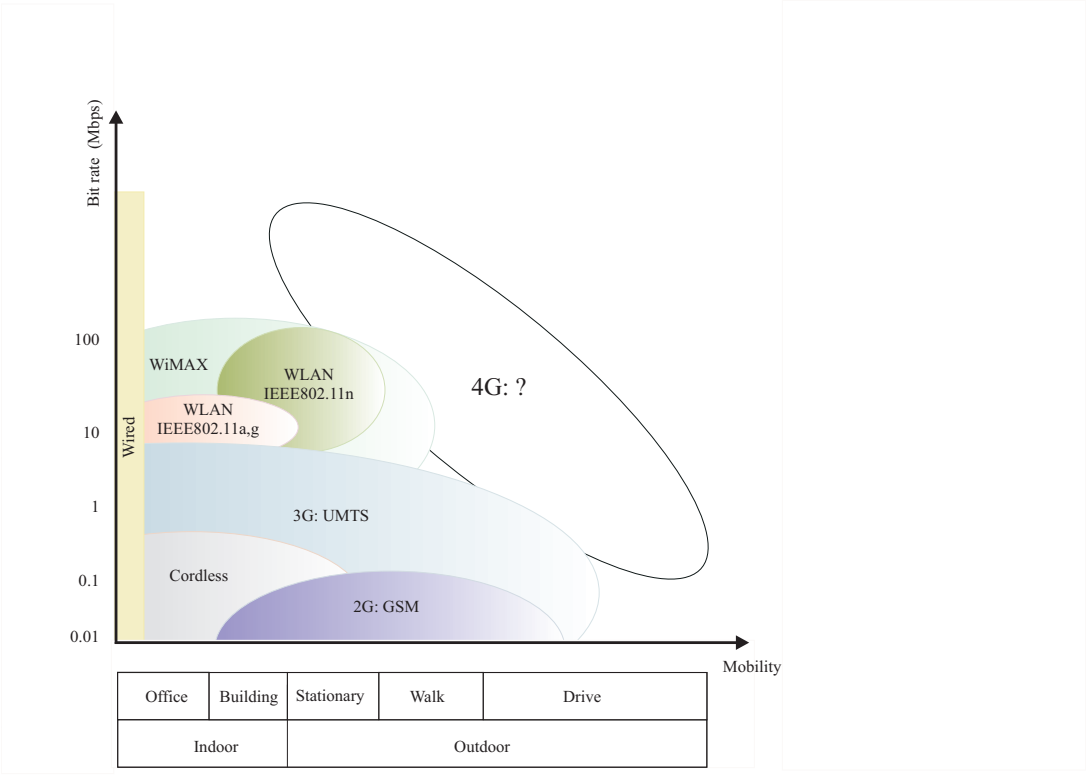

Figure 1.2: User mobility versus the achieved bit rate in the modern communication systems.

1.2 Design Challenges and Motivations

As it was described in the previous section, the world of communications is moving towards the use of OFDM system as an air interface like in WLAN, WiMAX, and LTE. OFDM is also becoming the promising technique for many of the communication systems of the future because of its spectrum efficiency and its robustness against fading channels. However, OFDM technique is still facing many design challenges that need to be addressed. The main design issues and challenges for the next generation of wireless communications are summarized in the following points:

1.2.1 Complexity Issue

System complexity is one of the important issues to be addressed in designing the future communication systems. The wireless channel introduces distortions to the transmitted signal and complicates the reception process. In addition to the noise that is added to the transmitted signal, the signal strength falls down rapidly with distance due to the path loss. Path loss is a function of distance and frequency; (the signals with high frequencies get attenuated more). This puts a challenge on broadband systems that are able to transmit more data rates, but unfortunately to a shorter range. Small scale fading is also one of the channel impairments. This kind of fading leads to huge variations in signal power over short distances, times, or frequencies. Fading can cause different types of interferences, such as inter-symbol interference (ISI) due to the superposition

of signals coming from different paths, self interference, inter-carrier interference (ICI) in time-variant channels, and co-channel interference in cellular systems. All of these impairments distort the transmitted signal and complicate the reception process. In order to deal with the channel effects, the receiver must be able to estimate the channel and its parameters, such as the maximum delay spread, Doppler spread, and noise variance. Then, it compensates for the distortions caused by the channel imperfections. These processes require high processing time and power, and thereby increase the complexity of the digital signal processing (DSP) algorithms. The processing complexity is measured by the number of floating point operations per second (FLOPs) for an algorithm.

OFDM system is one of the most powerful systems regarding the immunity against the frequency selectivity of the channel because of its ability to deal perfectly with the ISI by means of time guard interval (GI). Consequently, the OFDM system has less reception complexity in multipath channels than the single carrier systems, since one tap equalizer can cancel the effect of the frequency selectivity. However, the system suffers in high speed mobilities because of the ICI. This also put a challenge against designing an OFDM system that is suitable for the vehicle speed scenarios of the next mobile generation. The channel estimator must take into account the time variations of the channel, in order to cancel the effect of the resulting ICI. Many signal processing algorithms [16–21] have been developed to deal with ICI and time-frequency synchronization. However, in most of the ICI cancellation algorithms, the processing time and power increase as a function of vehicle speed and number of OFDM carriers. This is because the equalization algorithms require non-trivial matrix inversion in the dimension of the number of carriers, which can reach thousands in some applications. During the last decade, researchers were looking for advanced and efficient ICI cancellation methods that require less processing efforts, or by introducing some signal processing algorithms to reduce the system complexity. Adapting the equalization process according to the channel situations can partially solve the problem of processing complexity. For good channel conditions, low complexity algorithms can be used, while for bad conditions, more advanced algorithms are applied.

1.2.2 Capacity Issue

In 1948, Claude Shannon [22] has defined the upper bound on the amount of data that can be transmitted over a channel by the following equation

$$C = B \log_2(1 + \mathrm{SNR}) \tag{1.1}$$

where C is the maximum bit rate, B is the Nyquist bandwidth, and SNR is the signal-to-noise ratio. As it can be seen from the equation, the spectrum bandwidth is one of the parameters that plays a role in the achievable capacity of a system. The radio frequency (RF) spectrum today has become more crowded, because many wireless communication systems are continually being developed. Satellite systems, navigation systems, cellular systems, and other wireless networks all have to share a limited amount of spectrum and sometimes overlap each other. This makes licensing the spectrum the most expensive parameter in designing a new mobile communication system. Cellular systems achieve the required capacity by reusing the available spectrum using small cells, which result

from dividing the geographic area to be covered. However, reducing the cell size increases the interference and complicates the hand-off schemes.

As has been described above, OFDM-based systems have higher spectral efficiency than that of the 3G systems. The orthogonality allows the sub-carriers to overlap each other. Therefore, OFDM is able to transmit with higher bit rate than other systems. The other parameter that can increase the bit rate or the capacity of the system is the signal-to-noise ratio (SNR). MIMO technology increases the SNR by using multiple antennas at the transmitter and the receiver, and thus, adds a space diversity factor. Since the noise is uncorrelated for each antenna, the space diversity helps to enhance the SNR, and thus, increasing the bit rate of the system. The combination of OFDM and MIMO technology [23–26] is the forthcoming technology that can work with high bit rate. However, the limit is the hardware effort and the increased size of the system specially at the user terminal. On the other hand, OFDM loses some of its capacity due to inserting the GI for avoiding ISI and because of transmitting pilot signals that carry no information and used only for synchronization and channel estimation. The capacity loss increases with increasing the length of the GI and the number of pilots. 4G systems require high data rates greater than 100 Mbps and high quality of service QoS of about 99%. To achieve these requirements, the new communication systems need to be more flexible and adaptive. Adapting the system parameters can increase the capacity and the QoS of the system. In addition to the modulation scheme, the number of pilots, the number of carriers or the GI can also be adapted according to the channel state information.

1.2.3 Power Consumption Issue

The existing mobile communication devices have internal batteries that need to be recharged every one or two days. Increasing the battery life is a challenge for the 4G systems. 3G systems have introduced power control schemes that allows the users to transmit with the minimum possible power to increase the battery life, and to solve the so called near-far problem [27]. OFDM is known as a power hungry system. The high peak-to-average power ratio (PAPR) of the OFDM signal causes more power consumption, since the power amplifier in the transmitter must work with higher linear range to cover the wide amplitude range of the signal. Pre-coding or clipping algorithms [28–31] can help to reduce the effect of the PAPR. The power consumption problem of OFDM is a transmitter issue, therefore some of the new mobile communication standard like LTE uses OFDM only for the downlink, since the power at the base station is not an important issue. For the uplink, a single carrier system is used. In addition to the PAPR, the signal processing also consumes power, specially when high complexity algorithms for channel estimation and equalization are used. Therefore, reducing the computation complexity leads to enhance the power efficiency of the system.

The above challenges are addressed throughout this thesis, guided by the motivation to enhance the performance of the next generation of communication systems that adopt OFDM as an air interface. The aim of this thesis is to extend the previous work on the subject of channel estimation and equalization for the OFDM system. Furthermore, it is intended to deliver some improvements on implementing low complexity algorithms for ICI cancellation, and to propose new adaptive techniques to enhance the system capacity.

1.3 Thesis Outline and Contributions

The outline of the thesis and the author's contributions are organized as following:

Chapter 2: OFDM Systems in Doubly Selective Channels

Chapter 2 presents an introduction to the multipath time-variant channels and their influences on the transmitted signal. Different statistical characteristics of the wireless channels, which are considered in the remainder of this thesis, are studied. The basics of OFDM systems and their robustness against frequency selectivity are explained in detail. Furthermore, the orthogonality principle and the transceiver structure are described.

The effect of the doubly dispersive channel on the performance of the OFDM system is analyzed and simulated according to the wide sense stationary uncorrelated scattering (WSSUS) assumption. Different channel impairments such as Additive white Gaussian noise (AWGN), frequency and time selectivity are tested on the system. The chapter also describes the channel matrix in time and frequency domains and shows the effect of time variation on the properties of the channel matrix.

Chapter 3: Channel Estimation and Equalization for OFDM Systems

The chapter discusses the pilot-based channel estimation for OFDM systems. It explains some of the common estimation algorithms such as least square (LS) and minimum mean square error (MMSE) criteria. The equalization algorithms used for detecting the OFDM signal is also discussed.

In this chapter, an MMSE Wiener filtering estimation algorithm for digital radio mondiale (DRM) system is developed. The Wiener filter is designed according to the Gaussian shaped Doppler spectrum, and combined with the Matrix Pencil (MP) algorithm as a pre-stage to estimate the channel statistical parameters required for optimizing the Wiener filter. The effects of the number of pilots, the modulation level, the number of channel taps, and the number of antennas are shown through the simulation results.

The chapter also discusses some experimental studies of multipath channels, and explains a measurement system used for testing OFDM signal. A discussion of the transmission, reception and channel estimation of an OFDM-based WLAN system in indoor wireless channel is provided. A joint channel and frequency offset estimation method is introduced for equalizing the received OFDM symbols. The performance of the OFDM system with pilot-based Wiener filtering channel estimator is tested with different modulation schemes subject to different conditions, such as the transmission power, the antenna orientation and the distance between the transmitter and the receiver.

Chapter 4: Low Complexity ICI Reduction for OFDM Systems

The chapter discusses the ICI phenomenon and analyzes its generation mechanism in OFDM-based DRM system. The effect of loosing the orthogonality due to time variations is studied on the system performance.

New low complexity algorithms used for reducing ICI for OFDM in rapidly time-variant channels are proposed. These algorithms make use of predecting the time variation of the channel by means of numerical methods, such as Newton and Lagrange polynomial approximation. A Lagrange extrapolation method has been applied to reduce the processing delay. A low complexity estimation method for DRM system is introduced. The method applies a time domain preprocessing to the received signal to maximize the signal-to-noise plus interference ratio (SNIR) and make the channel matrix sparse. It allows thereby for low complexity equalization. Low complexity iterative detection schemes that depend on hard and soft feedback equalization are implemented and verified using simulations.

Chapter 5: Adaptive Techniques for OFDM Systems

This chapter presents different adaptive techniques for OFDM systems and suggests new techniques for both, receiver and link adaptation that allow the system to work in a wide range of channel conditions.

A new receiver adaptation scheme for OFDM systems based on long-term tracking of the channel is proposed. The scheme adapt the polynomial degree of the channel approximation (discussed in Chapter 4), aiming at minimizing the bit-error-rate (BER) subject to processing delay. Adaptive GI length for OFDM-based WLAN systems is proposed. In this method, the delay spread is estimated using root-multiple signal classification (Root-MUSIC) algorithm, and is used to adapt the GI length at the transmitter aiming at maximizing the system throughput for a given BER performance. In this chapter, a new adaptive pilot distribution method is also proposed. The pilot spacing in time and in frequency domains is adapted according to the channel state information (CSI). Doppler spread used for adapting the time pilot spacing is estimated in terms of the off-diagonal elements of the channel matrix. In order to guarantee a robust Doppler estimation process, the pilots are gathered in blocks of three symbols and used for estimating the channel matrix via linear channel approximation. The separation between these blocks is adapted instead of adapting that between the pilots. The delay spread used for adapting the frequency pilot spacing is estimated using Root-MUSIC algorithm.

Chapter 6: Conclusion and Future Work

The chapter concludes the thesis, lists out the introduced contributions, and highlights possible future work.

Chapter 2

OFDM Systems in Doubly Selective Channels

This chapter is organized as follows: Section 2.1. discusses the wireless multipath time-variant channel and its statistical models. Section 2.2. gives a detailed discussion about the OFDM system, its structure and the related signal generation. It also explains the effect of doubly selective channels on system performance.

2.1 Wireless Doubly Selective Channels

A wireless channel models the mechanism of the electromagnetic propagation from the transmitter to the receiver. Unlike wired communication channels that are stationary and can be predicted, wireless channels are extremely random and cause severe variations in the spectrum characteristics of the transmitted signal. Time and frequency dispersion of the received signal due to multipath propagation is a dominant source of impairment in wireless communication systems. It places fundamental limitations on the system performance and leads to a complex reception.

2.1.1 Multipath Effect (Frequency Selectivity)

In a multipath radio channel, the transmitted electromagnetic wave reaches the receiver from different directions due to reflections, diffractions, and scattering caused by the obstacles that lie on the way of the transmitted signal. At the receiver side, the number of reflections, the time and the direction of arrivals play a role in the reception process. Fig. 2.1 illustrates an example of the multipath channel. In multipath channels, the frequency characteristics of the transmitted signal is distorted. This distortion is usually known as frequency fading, which appears to be deep at some frequencies of the spectrum of the transmitted signal.

As a consequence of the multipath time-variant channel, the received signal $y(t)$ is composed of an infinite number of delayed and attenuated replicas of the transmitted signal $x(t)$. The received time domain signal results from a convolution between the transmitted signal and the channel impulse response as

$$y(t) = \int_{-\infty}^{\infty} h(\tau, t)x(t-\tau)d\tau + v(t) \tag{2.1}$$

where $v(t)$ is the additive white Gaussian noise (AWGN) caused by the channel and by the system electronic circuits, and $h(\tau, t)$ is the response of the channel at time t of an

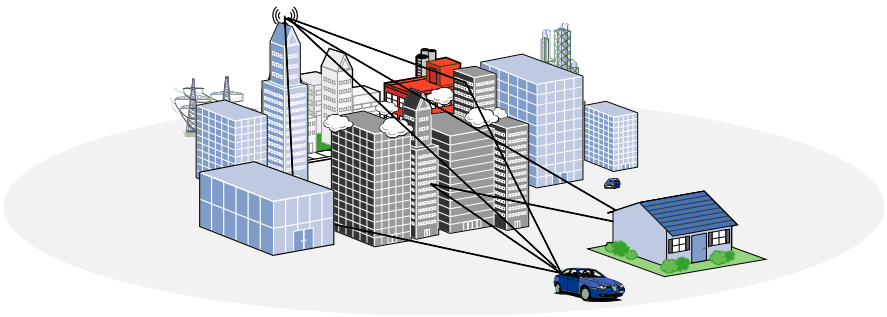

Figure 2.1: The multipath time-variant channel.

impulse applied at time $t - \tau$, and can be expressed as

$$h(\tau, t) = \sum_{l=0}^{L-1} \beta_l(t)\delta(\tau - \tau_l)$$

where $\beta_l(t)$ is a time-variant complex random variable describes the channel amplitude and phase. Applying the Fourier transform to the channel impulse response $h(\tau, t)$ with respect to the delay τ gives the time-dependent channel transfer function $H(f, t)$.

$$H(f, t) = \int_{-\infty}^{\infty} h(\tau, t)e^{-j2\pi f\tau}d\tau \tag{2.2}$$

The transfer function gives a view of the frequency selectivity of the channel caused by the multipath effect.

If the frequency components of the transmitted signal are equally attenuated, the fading is considered to be flat. Narrowband systems usually experience flat fading, since the signal bandwidth is much smaller than the so called coherence bandwidth of the channel C_f. The coherence bandwidth is defined as the bandwidth over which the channel is considered flat. The coherence bandwidth is related to the maximum delay of the channel. It is expressed as

$$C_f \propto \frac{1}{\tau_{max}} \tag{2.3}$$

In other words, the channel is said to be flat if the bandwidth of the transmitted signal is less than the coherence bandwidth, otherwise, it is frequency selective, which is the case of wideband systems. Frequency selectivity degrades the performance of wireless communication systems by introducing inter-symbol interference (ISI) between the transmitted symbols, and hence, complicates the reception process, specially for single carrier systems such as CDMA in which a matched filter with number of taps equal to the relevant channel paths is required in order to deal with the multipath [27].

2.1.2 Doppler Effect (Time Selectivity)

In a dynamic wireless communication channel, the received signal from different paths is fluctuated in its envelope, frequency, and phase over time. Due to the relative velocity

between the transmitter, the receiver or/ and the obstacles, some shifts on the frequency contents of the transmitted signal occur due to Doppler effect. Besides the velocity, Doppler shifts f_{sh} depend on the angle of arrival θ of the received signal and the carrier frequency f_c as

$$f_{sh} = f_c \frac{\mathsf{v}}{c} \cos\theta. \tag{2.4}$$

where c denotes the speed of light and v denotes the relative velocity. This kind of channels is known as time-variant channels. The fashion of variation describes the time selectivity of the channel. In order to understand the phenomenon caused by Doppler effect, a function is derived by applying the Fourier transform to the time-variant impulse response of the channel with respect to the time t as

$$s(\tau, \nu) = \int_{-\infty}^{\infty} h(\tau, t) e^{-j2\pi\nu t} dt \tag{2.5}$$

$s(\tau, \nu)$ is known as the Doppler-dependent impulse response of the channel, which describes the frequency dispersion of the channel for each time delay [32]. Basically, the channel can be classified as fast or slow time-selective channel. A parameter that characterizes this selectivity is called the coherence time C_t, which is the time duration over which the channel can be considered static. A fast selective channel is a channel through which the symbols with length longer than the coherence time are transmitted, whereas, the channel is said to be slow if the transmitted symbols are shorter than the coherence time. The coherence time of the channel is related to Doppler spread f_d of the channel as

$$C_t \propto \frac{1}{f_d} \tag{2.6}$$

To get a clear picture about the channel, we can apply a two-dimensional Fourier transform to $h(\tau, t)$ with respect to both delay and time to get the so called Doppler-variant transfer function

$$T(f, \nu) = \int_{-\infty}^{\infty} \int_{-\infty}^{\infty} h(\tau, t) e^{-j2\pi(\nu t + f\tau)} dt\, d\tau \tag{2.7}$$

Fig. 2.2 shows the doubly selective channel, which has dispersions in both time and frequency directions. It is clear that all derived functions are related through Fourier pairs as shown in Fig. 2.3, which shows these function and their mutual relations.

2.1.3 Statistical Models of Wireless Channels

In many situations, it is difficult to describe all channel processes that determine the time-variant multipath components. It is rather often preferable to describe the statistical behavior of these components [33].

2.1.3.1 Correlation functions

We are interested in the statistical behavior of the channel, since the channel distortions can be interpreted as random processes. The channel impulse response and the

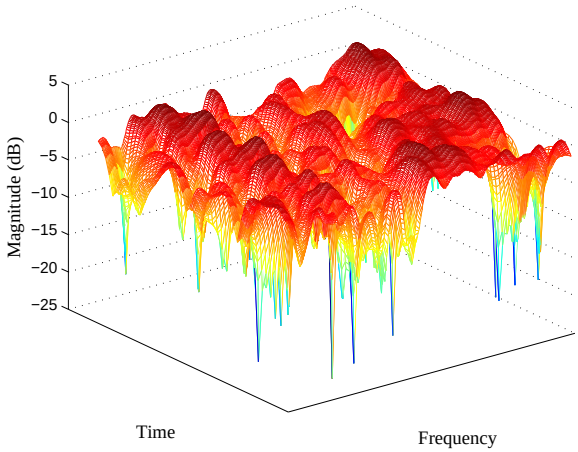

Figure 2.2: The doubly selective channel.

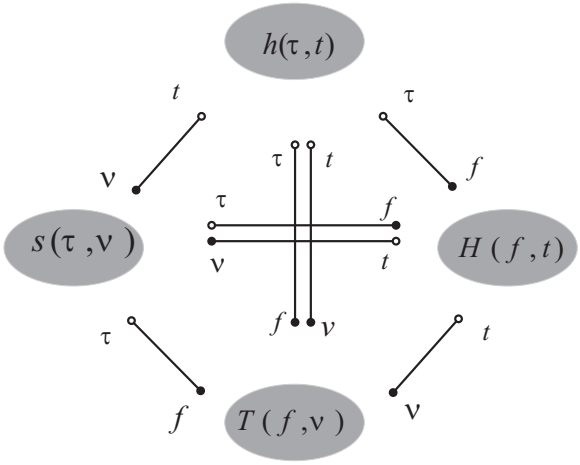

Figure 2.3: Fourier transform relationships between the channel functions.

channel transfer function can be considered as the stochastic system functions, whose autocorrelation functions in both frequency and time domains are written as [32]

$$r_{hh}(\tau_1, \tau_2; t_1, t_2) = E\{h^*(\tau_1, t_1)h(\tau_2, t_2)\} \tag{2.8}$$

$$r_{HH}(f_1, f_2; t_1, t_2) = E\{H^*(f_1, t_1)H(f_2, t_2)\} \tag{2.9}$$

It can be seen that the Fourier transform pair are also valid for these correlation functions.

2.1.3.2 WSSUS model

Wide sense stationary uncorrelated scattering (WSSUS) assumption [34] is an important and frequently used description of the short range variation of the wireless channels, and leads to simplify the channel correlation functions. According to WSSUS assumption, the wireless channel can be completely characterized by their statistical properties up to the

second order, such as the mean and the autocorrelation. The wide sense stationary (WSS) assumption states that the autocorrelation function of the channel impulse response is invariant over time for a constant time shift, which can be represented by the following equations

$$r_{hh}(\tau_1, \tau_2; t, t + t') = r_{hh}(\tau_1, \tau_2; t'), \tag{2.10}$$

$$r_{HH}(f_1, f_2; t, t + t') = r_{HH}(f_1, f_2; t') \tag{2.11}$$

where t' is a small shift in time. In general, the channel is said to be WSS channel, if the mobile terminal moves for few tens of carrier wavelength. The uncorrelated scattering (US) assumption states that the scatterers from different paths are statistically uncorrelated, which can be expressed as

$$r_{HH}(f, f + f'; t_1, t_2) = r_{HH}(f'; t_1, t_2) \tag{2.12}$$

where f' is a small shift in frequency, thus the channel is stationary in frequency. In real life, it is reasonable to assume that the channel is stationary in both time and frequency (WSSUS), so the autocorrelation function of the channel can be written in the following form

$$r_{HH}(f, f + f'; t, t + t') = r_{HH}(f', t') \tag{2.13}$$

The later function is known as the time-frequency correlation function. Two important functions that have a major role in characterizing the wireless channel, can be obtained from the time-frequency correlation function [32]. The first one is called Doppler power spectral density, which provides information about the time selectivity of the channel and can be written as

$$D(\nu) = \int_{-\infty}^{\infty} r_{HH}(f', t') e^{-2\pi\nu t'} dt'|_{f'=0} \tag{2.14}$$

Doppler power spectral density of a channel describes the spectral broadening that the channel causes to a pure sinusoid passes through it. The other function is called Delay spectral density, which represents the frequency selectivity of the channel caused by the multiple reflections.

$$K(\tau) = \int_{-\infty}^{\infty} r_{HH}(f', t') e^{2\pi\tau f'} df'|_{t'=0} \tag{2.15}$$

2.1.3.3 Rayleigh and Ricean channels

The channel frequency fading is caused by the multipath phenomenon. The receive antenna receives a large number of reflected, refracted, and scattered waves. Due to the addition and the cancellation effects of all these received components, the received power can be described as a random variable. In many practical situations, the line of site (LOS) between the transmit and the receive antennas is lost. In such a case, the received signal becomes a superposition of many scattered components only. According to the central limit theorem [35], the time-variant channel can be modeled by Gaussian process with zero mean. The type of channels where the LOS is lost is known as Rayleigh fading channels. The probability density function (PDF) of a Rayleigh channel is written as [27]

$$P(a) = 2ae^{-a^2} \tag{2.16}$$

where a is a random variable results from a summation of the attenuations from many scatterers. In the presence of LOS, a constant mean value is added. This channel becomes a Ricean fading channel. The probability density function in this case turns to be a Gaussian distribution process with non-zero mean

$$P(a) = 2a(1+K)e^{-(K+a^2(1+K))}J_0(2a\sqrt{K(1+K)}) \tag{2.17}$$

where $J_0(\cdot)$ is the zeroth order modified Bessel function of the first kind and K is the Ricean K-factor, which defines the ratio between the signal power of the LOS over the scattered power. It can be seen that for $K = 0$, the channel turns to be a Rayleigh channel, while for $K = \infty$, the channel becomes an AWGN channel. Fig. 2.4 shows the PDF of the Ricean function for different K-factor values.

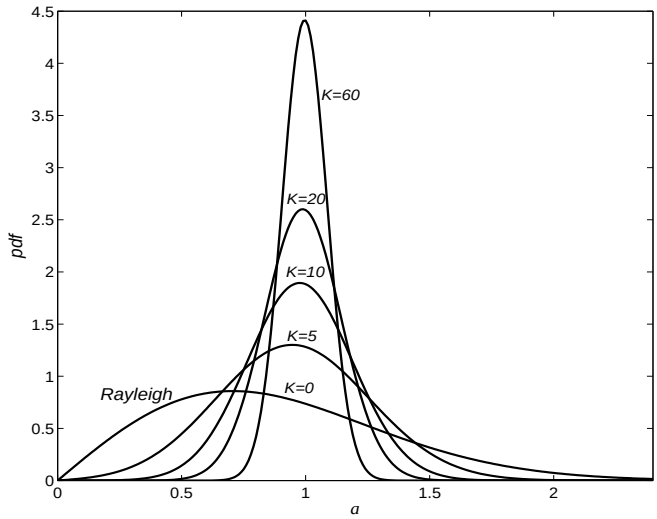

Figure 2.4: Probability density function of Ricean channel.

For indoor and short range propagation, Jakes Doppler spectral density has been proven to be the suitable assumption, whose model is described by the following equation

$$D(\nu) = \frac{1}{\pi\nu_{\max}\sqrt{1-(\frac{\nu}{\nu_{\max}})^2}} \tag{2.18}$$

where $\nu_{\max}$ is the maximum Doppler shift. On the other hand, it has been shown that Doppler spectral density of far echoes has a different shape than Jakes model. Gaussian shape of Doppler spectral density is a suitable assumption for long range propagations like propagations through ionosphere [36], which is a typical propagation scenario for broadcasting systems. Gaussian Doppler spectral density is represented by the following expression

$$D(\nu) = \frac{1}{f_d\sqrt{\frac{\pi}{2}}}e^{-\frac{2\nu^2}{f_d^2}} \tag{2.19}$$

where $f_d = 2\nu_{\max}$ is the Doppler spread. Fig. 2.5 illustrates the two models of Doppler spectral density functions.

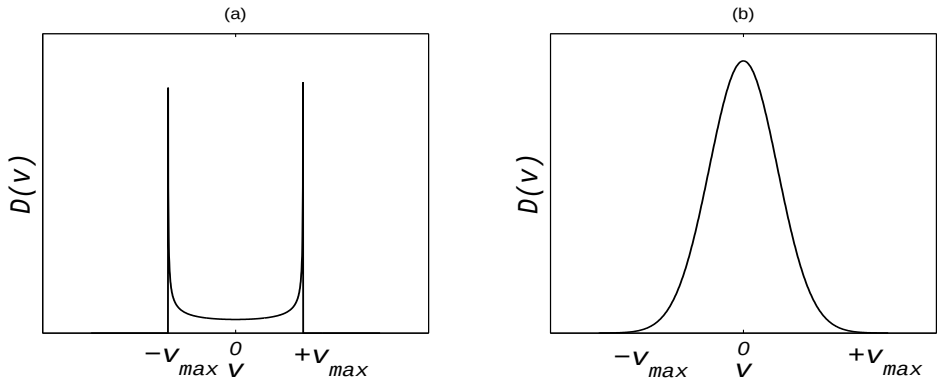

Figure 2.5: Doppler spectral density of Jakes model (a) and Gaussian model (b).

In order to understand the channel distortion caused by the scattering components, the WSSUS is often represented by a tapped-delay line model, which has been widely used for simulating the wireless channels [37, 38]. The tapped delay line model appears in Fig. 2.6. The model can be understood as a superposition of a number of discrete fading paths each corresponds to a certain propagation delay value τ_l. In order to have a complete channel effect, the delay of each tap, the corresponding amplitude, and Doppler spectrum are specified. Basically, the stationary stochastic channel consists of two important contributions. The first one is a stochastic one, which can be generated by filtering the white Gaussian noise (WGN) by a suitable Doppler filter for each tap. The second part is a purely deterministic process. The deterministic part is fully predictable from a sufficient set of measurements [39].

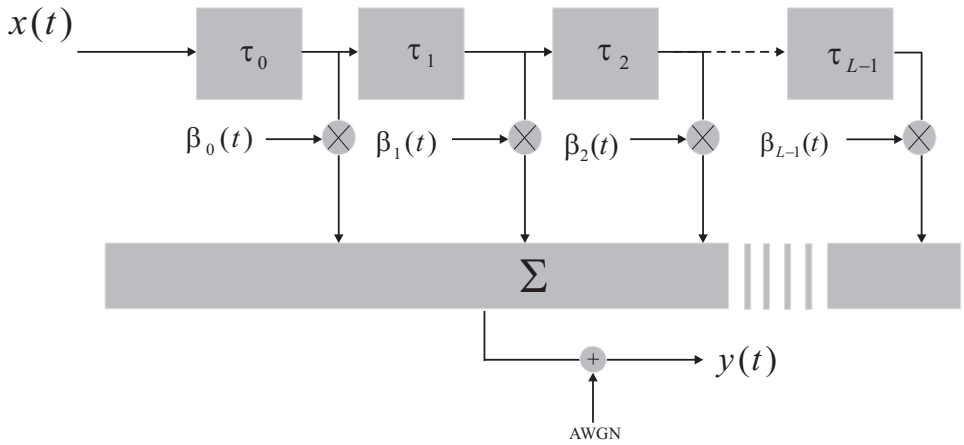

Figure 2.6: Tapped delay line model.

2.2 OFDM Systems

OFDM is a modulation technique that allows for high data rates over multipath channels. OFDM can also be seen as a multiplexing technique in the form of OFDMA, which allows many users to share the orthogonal bands. OFDM mitigates the effect of multipath

channel by essentially dividing the source spectrum into many narrow sub-bands that are transmitted simultaneously. The bandwidth of the sub-bands are designed to be narrow enough so that the channel exhibit a flat fading over each sub-band.

2.2.1 History

Transmitting data over multibands is known since 1966, when Chang [40] had shown that the multicarrier modulation could solve the impairments caused by the multipath channels without reducing the data transmission rate. Five years later, in 1971, Weinstein and Ebert [41] showed that the generation of the multicarrier signal can be accomplished by means of discrete Fourier transform (DFT), which is the technique that is known today as orthogonal frequency division multiplexing (OFDM). In 1985, Cimini [42] was the first one who suggested OFDM for the wireless communications. After that many of the key issues in the OFDM system have been investigated. However, the first practical application that used OFDM as a modulation scheme, was considered in early 90's for digital subscriber line (DSL) system. At that time, this system was known as discrete multitone system (DMT). By the end of 90's, many practical systems were using OFDM scheme like wireless LAN standard IEEE.802.11a [4]. Later on, OFDM was also utilized for some broadcasting systems like digital video broadcasting DVB [3], digital radio mondiale DRM [36], and digital audio broadcasting DAB [2]. In 2002, OFDM has been adopted in metropolitan area networks WMAN under revision IEEE802.16a, which is known as worldwide interoperability for microwave access WiMAX that allows for high data rate and supports user mobility. A new standard of WLAN IEEE802.11n has been implemented in 2003. This standard uses OFDM as an air interface as well as multi-input multi-output (MIMO) technology to enhance the bit rate capabilities for WLAN systems. In 2006, OFDMA was chosen as multiple access for the 3GPP LTE standard in the downlink, which is promising a downlink speed up to 100 Mbps for the UMTS usres. Recently, OFDM combined with MIMO is becoming a very attractive technique for the 4G mobile communication systems.

2.2.2 Orthogonality Principle

In OFDM, the source bitstream is split into N parallel streams, which are modulated using N sub-carriers. Because of using many sub-carriers, the symbol duration T_s becomes N times larger. This reduces the effect of ISI in multipath channels, and thereby reduces the equalization complexity. In case of FDMA, frequency guard bands between the sub-carriers and couple of filters are needed at the receiver side in order to decompose these carriers. On the other hand, if these sub-carriers are orthogonal, a very simple equalization method is able to decompose the carriers without requiring frequency guard bands or filters. To make the sub-carriers orthogonal, their frequencies must be located at $f_m = \frac{mB}{N}$, where m is an integer and B is the total available bandwidth. Basically, the sub-carriers can be generated using N local oscillators that oscillate at frequencies f_m [43], as shown in Fig. 2.7, however, the hardware cost of implementing N oscillators for one system is very high. A much easier alternative implementation is accomplished digitally using inverse discrete Fourier transform (IDFT), which is applied on the block of N symbols so that the resulting time domain carriers become orthogonal. In practical

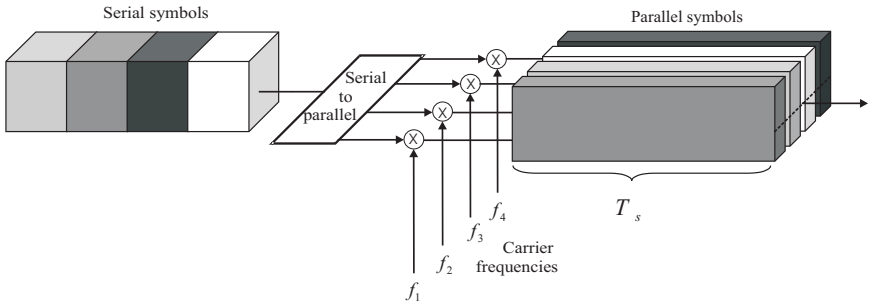

Figure 2.7: OFDM signal generation.

implementation, the block length N is chosen to be a power of 2 and the IDFT is realized efficiently as inverse fast Fourier transform (IFFT), which speeds up the multiplication operation. Orthogonality condition in time domain requires all the sub-carriers to have an integer number of cycles during the symbol duration. For a certain carrier in frequency domain, at the maximum of each sinc shaped carrier, the contributions from other carriers must be zero as shown in Fig. 2.8. Orthogonality allows the carriers to overlap each

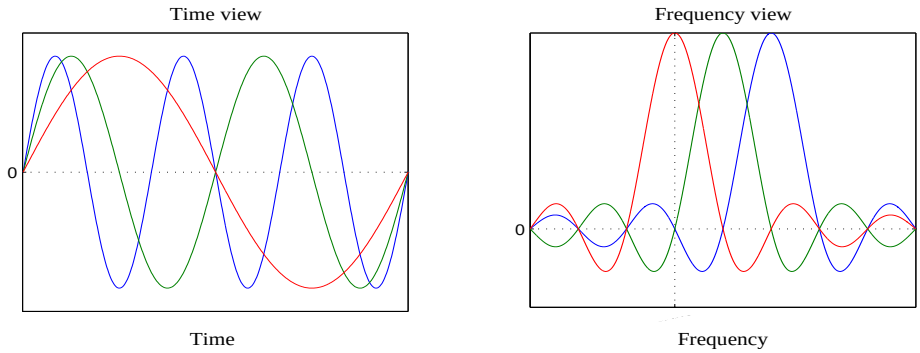

Figure 2.8: Orthogonality in time and frequency domains.

other, which squeezes the spectrum about 50%. This spectrum efficiency is one of the key advantages of the OFDM system. Fig. 2.9 presents an OFDM spectrum compared with the conventional FDMA that requires much larger bandwidth for transmitting the same amount of information. To understand the orthogonality, let us look at one OFDM symbol in passband, which can be written as

$$x(t) = Re\{\sum_{m=0}^{N-1} S(m)e^{j2\pi(f_c - \frac{m}{T_s})t}\}, \qquad 0 \leq t \leq T_s, \tag{2.20}$$

where $S(m)$ is the original data symbols to be transmitted, and f_c is the carrier frequency. In literature, the equivalent baseband notation is mostly used, which is given by

$$x(t) = \sum_{m=0}^{N-1} S(m)e^{j2\pi\frac{m}{T_s}t}, \qquad 0 \leq t \leq T_s \tag{2.21}$$

The orthogonality is guaranteed because of the wise spacing between the sub-carriers $\frac{m}{T_s}$. At the receiver side, the k^{th} subcarrier is detected by demodulating (downconverting) the

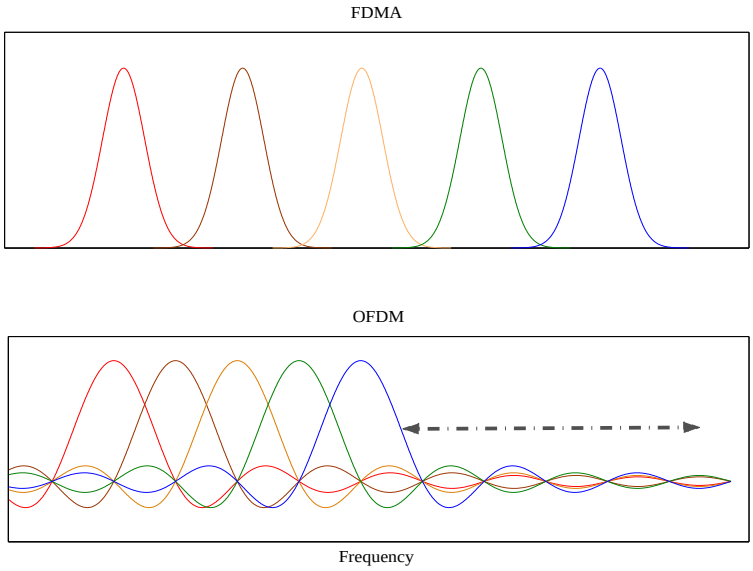

Figure 2.9: Spectrum efficiency of the OFDM signal.

signal with frequencies $\frac{k}{T_s}$, and then integrating it over the symbol duration T_s, which gives

$$\int_0^{T_s} e^{-j2\pi\frac{k}{T_s}} \sum_{m=0}^{N-1} S(m) e^{j2\pi\frac{m}{T_s}t} dt =$$

$$\sum_{m=0}^{N-1} S(m) \int_0^{T_s} e^{j2\pi\frac{m-k}{T_s}t} dt = \begin{cases} T_s S(k), & \text{for } k = m; \\ 0, & \text{else.} \end{cases} \tag{2.22}$$

It can be seen that the detector gives a value only at the carrier of interest, while for all other carriers, the integration is zero, since the difference $(k - m)$ produces an integer number of cycles during the symbol duration T_s [44].

2.2.3 System Structure

Fig. 2.10 illustrates a block diagram of an OFDM system. The user information (data, audio, video etc.) is encoded using one of the channel coding methodologies, which is used to correct the errors that are caused by the channel. Therefore, it is some times called forward error correction (FEC) scheme. As discussed in the previous section, channel fading causes distortions in the transmitted signal, and thereby decreases the system performance. The channel encoder adds some redundant bits to the original message to increase the hamming distance between the different code words, thus, the frequency diversity of the fading channel is exploited. Different types of channel coding schemes can be applied for OFDM system like Reed-Solomon, convolutional, or concatenated coding. The last type is very popular in modern communication systems, which has two coding stages, the inner coding stage (closer to the channel), which is often a convolutional encoder, and the outer coding stage, usually Reed-solomon encoder. In order to achieve

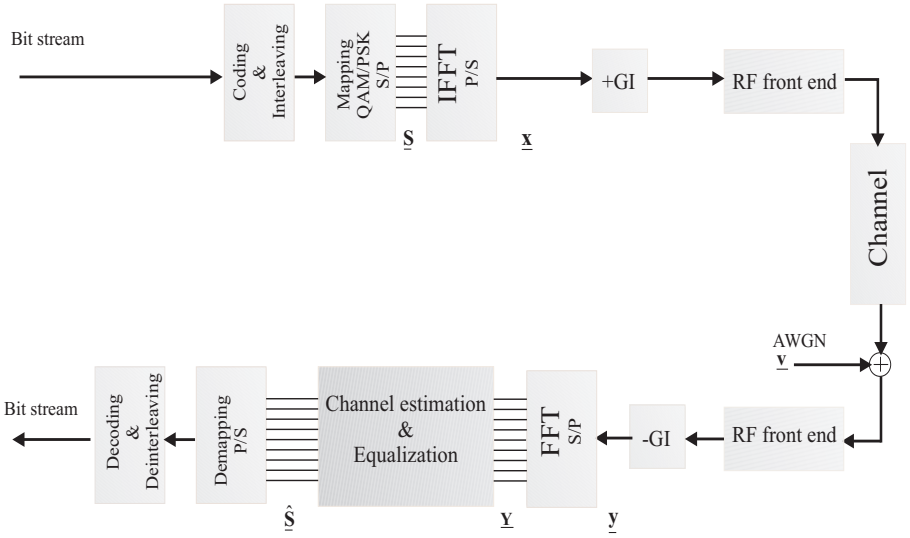

Figure 2.10: Simple block diagram for an OFDM system.

the full diversity gain, the coding stage in OFDM is followed by an interleaving stage. Interleaving means separating the bits that correspond to one code word, in order to randomize the fading caused by the channel. After the interleaving stage, the bitstream is modulated using a common modulation scheme like quadrature amplitude modulation (QAM) or phase shift keying (PSK) and then distributed over multiple carriers by means of IFFT. The transmitted OFDM symbol can be written in digital form as

$$x(n) = \frac{1}{\sqrt{N}} \sum_{m=0}^{N-1} S(m) e^{j\frac{2\pi nm}{N}} \qquad 0 \leq n \leq N-1 \tag{2.23}$$

where $S(m)$ is the QAM symbol at the m^{th} sub-carrier. Notice that through the rest of this thesis, the discrete notation of the OFDM signal will be considered. In order to avoid ISI caused by the delay spread of the channel, a guard interval (GI) is added to the time domain transmitted signal. ISI can be completely eliminated if a suitable GI, usually longer than the channel impulse response (CIR) ($T_g \geq \tau_{max}$), is added to the transmitted time domain signal. In OFDM, a so called cyclic prefix guard interval is used, which inserts the last portion of the time domain symbol in the beginning. Cyclic prefix extension maintains the orthogonality between the sub-carriers and allows the circular convolution with the channel. Fig. 2.11 shows the cyclic prefix GI, where T_g is the guard time period, T_u is the useful part of the symbol, and $T_s = T_u + T_g$ is the total symbol duration.

The generated OFDM symbol has a rectangular shape, which has a very large bandwidth because of the infinite side lobes at both sides of the spectrum. To satisfy the spectrum mask that is licensed to transmit an OFDM signal, a pulse shaping window is applied on the signal to decrease the side lobes, and thereby reduce the signal power transmitted out of band. In practical OFDM system, a raised cosine window is commonly used, however, any window shape can be designed to achieve certain application requirements. In order to transmit the OFDM signal through the channel, a digital to analog converter (ADC) is needed and then an up-converter to modulate the signal with

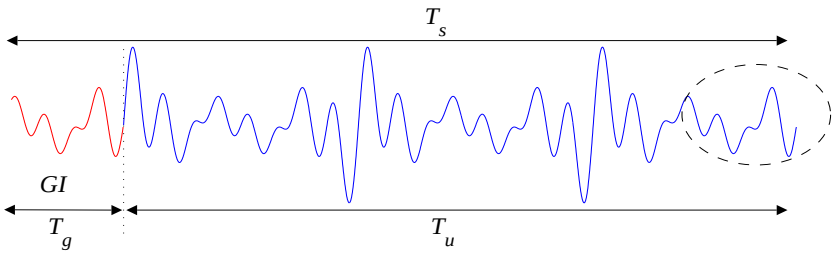

Figure 2.11: Cyclic prefix guard interval.

the suitable carrier frequency. At the OFDM transmitter, adding many orthogonal subcarriers produces some large peaks of the signal at certain instants. Therefore, OFDM has a large peak-to-average power ratio (PAPR), which is one of the severe drawbacks of the OFDM system that reduces the performance and leads to power consumption. In order to transmit the signal that has wide amplitude range without distortion, the power amplifier needs to have a very wide linear range, thereby requires more power. There are many methods to reduce the effect of PAPR such as clipping and precoding methods, however, the detail description of PAPR reduction algorithms is out of scope of this thesis.

2.2.4 Channel Effect on OFDM Signals

Because of the cyclic prefix GI, the transmitted signal is circularly convolved with the impulse response of the multipath time-variant channel. The received OFDM symbol can be expressed as

$$y(n) = \sum_{l=0}^{L-1} h(l,n)x(n-l) + v(n) \tag{2.24}$$

where $h(l,n)$ and l are the complex random variable and the corresponding tap delay that characterize the l^{th} path of the multipath channel, respectively, and $v(n)$ denotes the AWGN at sample instant n. Notice that $h(l,n)$ is the digital form of $h(\tau,t)$. Basically, $h(l,n)$ can be interpreted as the time n response to an impulse applied at time $n-l$. At the receiver side, the guard interval is removed and then an FFT operation is applied to convert the received signal to frequency domain. The frequency domain signal at the k^{th} carrier becomes

$$Y(k) = \frac{1}{\sqrt{N}} \sum_{n=0}^{N-1} y(n) e^{-j\frac{2\pi nk}{N}} \tag{2.25}$$

substituting (2.24) in (2.25) gives

$$Y(k) = \frac{1}{\sqrt{N}} \sum_{n=0}^{N-1} \Big(\sum_{l=0}^{L-1} h(l,n)x(n-l) + v(n) \Big) e^{-j\frac{2\pi nk}{N}} \tag{2.26}$$

by inserting (2.23) in (2.26), we can rewrite the received signal considering the two operations, IDFT at the transmitter and DFT at the receiver as

$$Y(k) = \underbrace{\frac{1}{\sqrt{N}} \sum_{n=0}^{N-1} (\sum_{l=0}^{L-1} h(l,n) \underbrace{\frac{1}{\sqrt{N}} \sum_{m=0}^{N-1} S(m) e^{j\frac{2\pi(n-l)m}{N}}}_{IDFT} + v(n)) e^{-j\frac{2\pi nk}{N}}}_{DFT} \tag{2.27}$$

In time-variant channels, the orthogonality between the sub-carriers of OFDM systems is lost because of Doppler effect. The sub-carriers shift right or left according to the instantaneous Doppler frequency, which causes ICI. ICI results from the contributions of all sub-carriers to the carrier of interest. An example of losing the orthogonality between four received sub-carriers appears in Fig. 2.12. A simplified [45] version of (2.27) can be

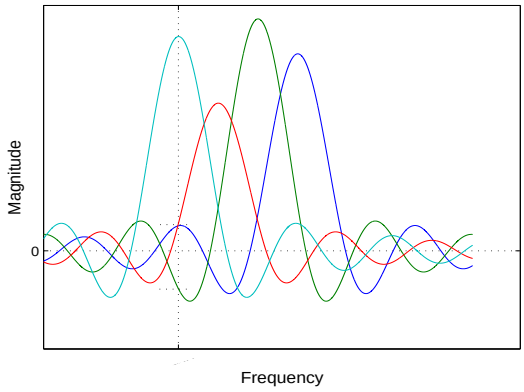

Figure 2.12: Losing the orthogonality between the sub-carriers.

given in the following form

$$Y(k) = S(k)H_{k,k} + \underbrace{\sum_{m=0}^{N-1} S(m)H_{m,k}}_{ICI} + V(k) \tag{2.28}$$

In Eq. (2.28), the second term on the left hand side represents the ICI coefficients, which appear on the off-diagonals of the channel matrix $\mathbf{H}$. Eq. (2.28) can be written in the vector form as

$$\underline{\mathbf{Y}} = \mathbf{H}\underline{\mathbf{S}} + \underline{\mathbf{V}} \tag{2.29}$$

where

$$\underline{\mathbf{Y}} = [Y(0), Y(1), ..., Y(N-1)]^T,$$

$$\underline{\mathbf{S}} = [S(0), S(1), ..., S(N-1)]^T,$$

$$\underline{\mathbf{V}} = [V(0), V(1), ..., V(N-1)]^T,$$

and

$$\mathbf{H} = \begin{pmatrix} H_{0,0} & H_{0,1} & \dots & H_{0,N-1} \\ H_{1,0} & H_{1,1} & \dots & H_{1,N-1} \\ \vdots & & \ddots & \vdots \\ H_{N-1,0} & H_{N-1,1} & \dots & H_{N-1,N-1} \end{pmatrix} \tag{2.30}$$

Notice that for time-invariant channels, the channel matrix is diagonal (only the main diagonal is filled), while for the time-variant channels, the channel matrix loses its diagonality. The channel variation effect on $\mathbf{H}$ is shown in Fig. 2.13. The element $H_{m,k}$ of

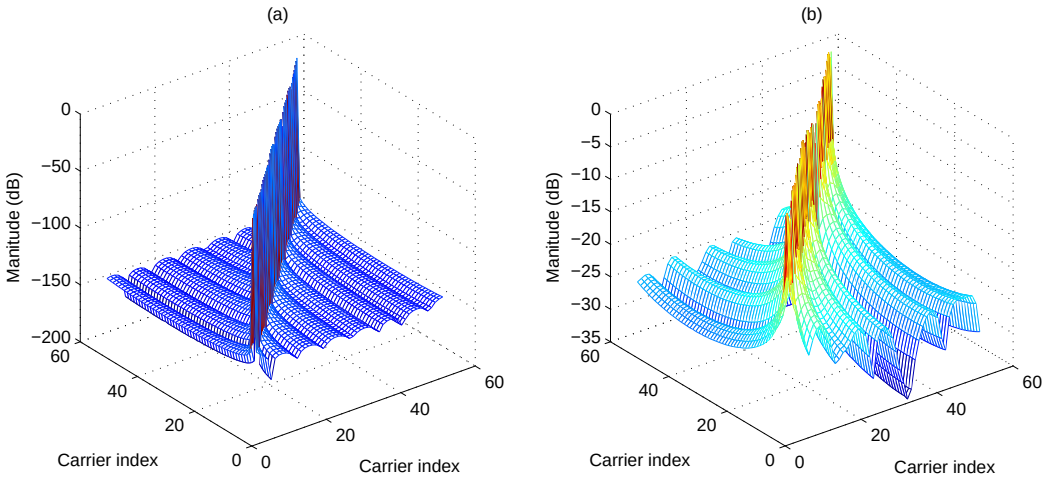

Figure 2.13: Time variation effect on the frequency domain channel matrix $\mathbf{H}$; (a): Time-invariant, (b): Time-variant.

the channel matrix is expressed as

$$H_{k,m} = \frac{1}{N} \sum_{n=0}^{N-1} \underbrace{\sum_{l=0}^{L-1} h(l,n) e^{-j\frac{2\pi l m}{N}}}_{U(m,n)} e^{-j\frac{2\pi}{N} n(k-m)} \tag{2.31}$$

where $U(m,n)$ denotes the channel weights at carrier m and time instant n, which is the digital form of the time-variant CTF described in Section 2.1 ($U(m,n) \equiv H(f,t)$). On the other hand, the system equation in time is given by

$$\underline{\mathbf{y}} = \mathbf{h}\underline{\mathbf{s}} + \underline{\mathbf{v}} \tag{2.32}$$

where $\mathbf{h}$ is the channel matrix in time domain, which can be calculated as

$$\mathbf{h} = \mathbf{F}^H \mathbf{H} \mathbf{F}, \tag{2.33}$$

where $\mathbf{F}$ is the DFT matrix whose elements are given by

$$F_{m,k} = e^{\frac{-j2\pi(m-1)(k-1)}{N}}$$

If the channel is time-invariant, $\mathbf{h}$ is circulant and written as follows

$$\mathbf{h} = \begin{pmatrix} h_0 & 0 & 0 & h_{L-1} & \vdots & h_1 \\ h_1 & h_0 & 0 & 0 & h_{L-1} & \vdots \\ \vdots & h_1 & h_0 & 0 & 0 & h_{L-1} \\ h_{L-1} & \vdots & h_1 & h_0 & 0 & 0 \\ 0 & h_{L-1} & \vdots & h_1 & h_0 & 0 \\ 0 & 0 & h_{L-1} & \vdots & h_1 & h_0 \end{pmatrix} \tag{2.34}$$

The effect of the time variation of the channel leads to losing the circularity of $\mathbf{h}$. Fig. 2.14 shows the channel variation effect on the channel matrix $\mathbf{h}$. Fig. 2.15 presents the

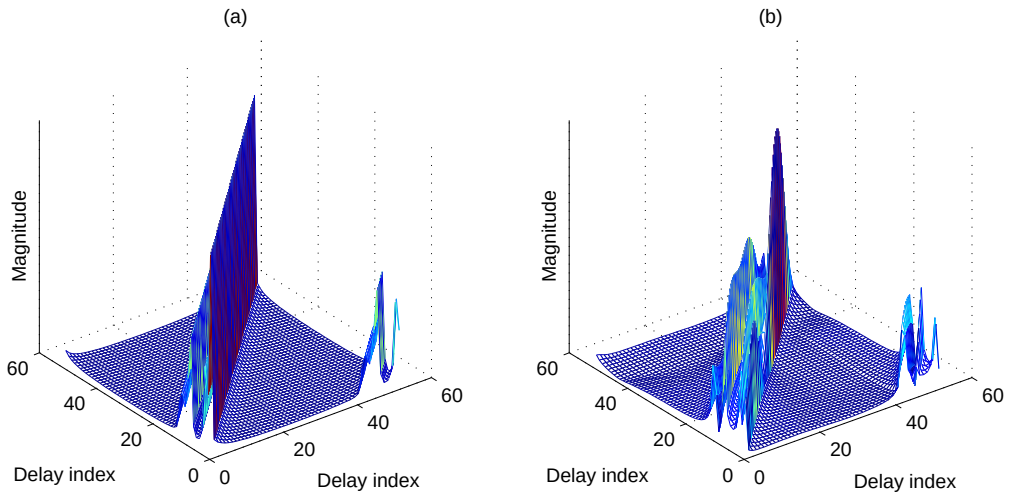

Figure 2.14: Time variation effect on the time domain channel matrix $\mathbf{h}$; (a): Time-invariant, (b): Time-variant.

constellation diagram of a transmitted 16QAM-mapped OFDM signal. Fig. 2.16 shows the received OFDM signal with different channel effects. The AWGN effect appears as clouds on the constellation diagram. The system exhibits an error-free performance as long as these clouds do not intersect. The delay caused by multipath effect leads to rotation in the constellation according to the delay of each tap. The Doppler effect leads to shifting the symbols in a random manner. In order to cancel the effect of multipath time-variant channel, channel estimation and equalization algorithms must be applied. The subsequent chapter will discuss some of the common estimation and equalization schemes.

2.2.5 Optimal Values of System Parameters

In the presence of time selectivity and frequency selectivity at the same time, choosing the optimal values of system parameters, when designing the OFDM system, becomes critical. The transmission becomes more sensitive to the time selectivity as the number

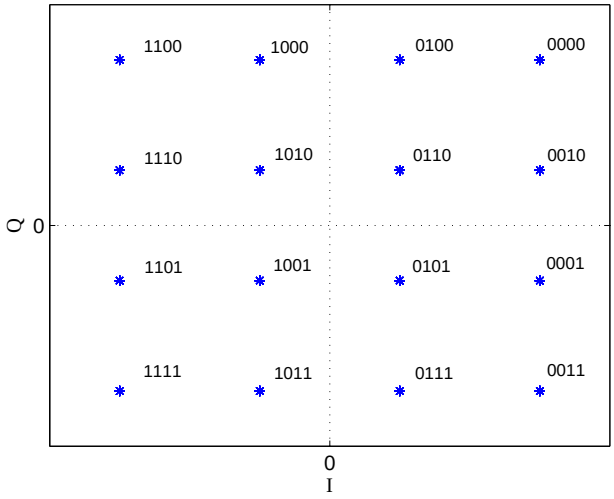

Figure 2.15: The constellation diagram of 16QAM mapped symbols.

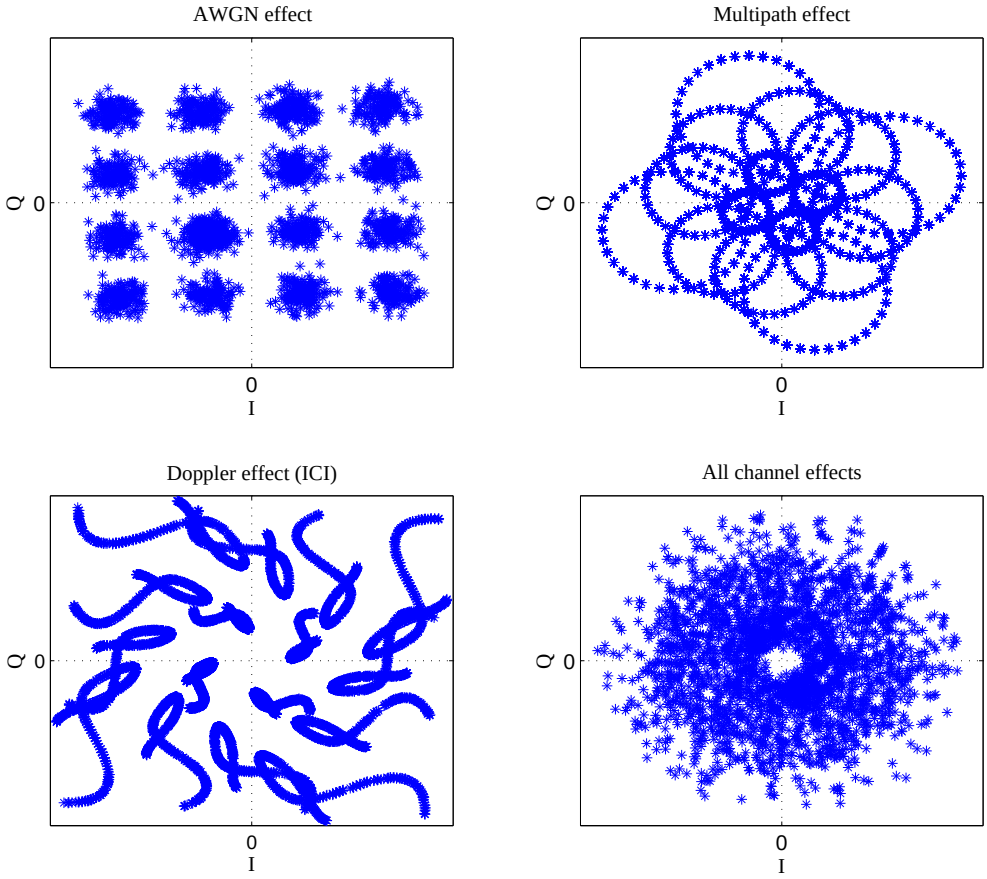

Figure 2.16: The channel effects on the OFDM / 16QAM symbols.

of carriers increases, since increasing the number of carriers makes the OFDM symbol longer, and hence the channel variations becomes obvious during the symbol duration. This variations increases the values of the ICI coefficients. On the other hand, in case of frequency selective channels, increasing the number of carriers helps to mitigate the ISI. However, increasing the number of carriers complicates the equalization process at the receiver side. Fig. 2.17 shows simulation results of the OFDM system performance as a function of delay and Doppler spread for different symbol lengths. The simulated system is 4QAM-DRM system in the presence of doubly selective channel with 4 taps and at SNR = 40 dB. Also, the robustness against ISI can be achieved by having longer

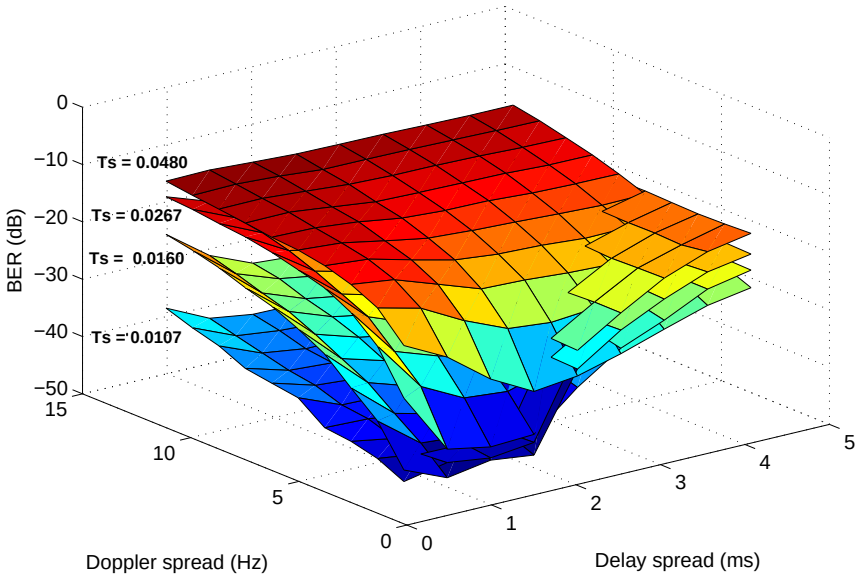

Figure 2.17: The effect of the symbol length T_s (in seconds) on the system performance at different channel conditions.

GI, however, increasing the GI length leads to power and spectrum losses. Therefore, the optimum number of carriers and the optimum length of the GI must be designed according to the expected Doppler spread and the expected delay spread as well as the QoS requirements.

2.2.6 OFDM Features

The main OFDM features are highlighted as follows:

Advantages

- Spectrum efficiency: OFDM system has high spectrum efficiency, since it allows for carrier overlapping without interfering. This feature increases the system capacity and allows the higher bit rate transmission.
- Low complexity: The use of FFT and IFFT reduces the implementation complexity of the OFDM system. Furthermore, the equalization at the receiver side can be

accomplished using one-tap equalizer. The number of operations required for one OFDM symbol is on the order of $Nlog(N)$, while for single carrier systems, NL_e operations are required, where L_e is the number of taps in the equalizer.

- Immunity against multipath effect: Because of using many sub-carriers and becuase of its long symbol duration, as well as the insertion of the GI, OFDM is very robust against multipath channel impairments such as frequency selectivity and ISI.
- Adaptation: Different modulation schemes can be used on individual sub-carriers which are adapted to the transmission conditions on each sub-carrier

Disadvantages

- High PAPR: Because of transmitting many coherent sub-carriers simultaneously, OFDM signal has high PAPR, which makes the power amplifiers expensive and power hungry.
- Sensitivity to frequency offsets: One of the disadvantages of the OFDM system is its sensitivity to frequency offsets and phase noise. The offset between transmitter and receiver oscillators can cause an effective ICI, hence degrades the system performance. Time-variant channel also introduces a severe ICI to the transmitted signal because of Doppler effect.
- Guard interval overhead: Insertion of GI causes loss in spectral and power efficiency.

Chapter 3

Channel Estimation and Equalization for OFDM Systems

The properties of the multipath time-variant channel have been discussed in Chapter 2. Many of the OFDM imperfections caused by the channel have also been studied. For a reliable communication in the doubly selective channels, the OFDM receiver must be able to recover the transmitted information from the noisy and distorted received signal. The first step of recovering the information is estimating the channel and then compensating for the distortions by means of equalization processes. There are two main types of channel estimation. The first one is pilot-based channel estimation that exploits some pilots that are inserted among the transmitted carriers. These pilots are known for both the transmitter and the receiver, they carry no information and used only for the channel estimation purpose. The receiver compares between the transmitted and received pilots to retrieve the channel state information (CSI). More details about pilot-based channel estimation can be found in [46–55]. The second type is the blind channel estimation with no prior information about the transmitted signal [56–62]. The blind estimation can be accomplished by exploiting some structural or statistical information of the received OFDM signal. One example of the blind channel estimation algorithms is using the maximum likelihood (ML) method to exploit the redundancy in the cyclic prefix GI [63]. The virtual carriers, that are used in many OFDM systems to provide frequency guards, can also be used to estimate the channel and its parameters [64]. The blind estimator has less capacity and power losses comparing with the pilot-based estimator. However, it has higher complexity and less performance than the prior one, which makes it unsuitable for many of the real applications. Throughout this thesis, only the pilot-based channel estimation is considered.

The chapter is organized as follow: The first section discusses the pilot-based channel estimation schemes such as LS and MMSE criteria. A proposed MMSE scheme for DRM system is introduced and evaluated by the simulation results. The second section explains the common equalization schemes used for OFDM signal detection such as ZF and LMMSE equalization schemes. The third section shows the simulation results of the proposed algorithm with different channel conditions. The last section discusses an experimental study of the OFDM system in indoor wireless channel. A method of joint channel estimation and frequency offset estimation is introduced. The performance of the OFDM system with pilot-based Wiener filtering channel estimator is tested with different modulation schemes over different conditions, such as the transmission power and the distance between the transmitter and the receiver.

3.1 Pilot-Based Channel Estimation

The pilot-based channel estimation is rather preferred due to its simplicity and its high performance. To be able to track the channel variations in both time and frequency directions, the pilots are inserted in two dimensions as shown in Fig. 3.1. The figure shows the well known three types of pilot insertion. In the block type, the pilots are

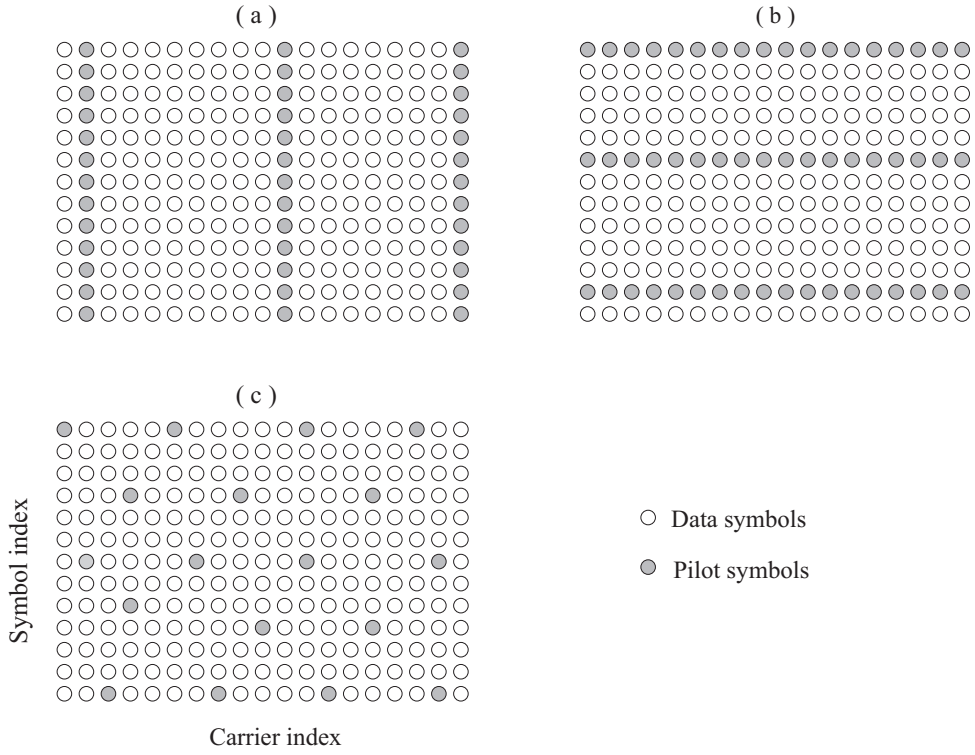

Figure 3.1: Different types of pilot insertion; a: Comb type, b: Block type, c: Scattered pilots type.

inserted in all sub-carriers (frequency direction) in a specific time period. This type of pilot distribution is suitable for channels that have high frequency selectivity and slow time variation. The second type is the comb type in which the pilots are inserted in few sub-carriers for all symbols. This type is suitable for time-variant channels with low frequency selectivity. Finally, the third type is called scattered-pilot type. Since the pilots are scattered in both time and frequency directions, this type is used for the doubly selective channels. In order to fulfill the Nyquist sampling condition, the spacings between the pilots in frequency direction D_f and in the time direction D_t are chosen according to the coherence bandwidth C_f and the coherence time C_t of the channel that are represented by (2.3) and (2.6), respectively [65]. The condition to be fulfilled is

$$D_f \leq C_f \quad , \quad D_t \leq C_t$$

Basically, channel estimation in wireless communication systems can be divided into two phases, which are the acquisition phase and the tracking phase. The acquisition phase is responsible for determining the number of the channel paths as well as some of channel statistical information. This is done by transmitting pure training symbols (pilots) for a

certain time duration at the beginning of the transmission period [1]. In the tracking phase, which is continued until the end of the transmission period, the channel is estimated over the distributed pilots and then interpolated in order to estimate the channel response over all sub-carriers. In general, the channel estimator at the receiver side can be implemented either in time or in frequency domains, however, the complexity in frequency domain is lower since the channel is simply multiplied by the transmitted frequency domain signal as described by (2.29).

3.1.1 Least Square (LS) Channel Estimator

As we have described in Chapter 2, the frequency response of a time-invariant channel can be represented as a vector, which is the main diagonal of the channel matrix $\mathbf{H}$. Assuming that $\underline{\mathbf{S}}_p$ is a vector that contains the transmitted pilots and $\underline{\mathbf{Y}}_p$ is a vector containing the received noisy pilots, the system equation (2.29) can be rewritten as

$$\underline{\mathbf{Y}}_p = \mathbf{S}_p \underline{\mathbf{H}}_p + \underline{\mathbf{V}}, \tag{3.1}$$

where $\mathbf{S}_p$ is a diagonal matrix whose diagonal is the transmitted pilots $\underline{\mathbf{S}}_p$, and $\underline{\mathbf{H}}_p$ is the channel frequency response on the pilots. The simplest frequency domain channel estimator can be obtained by dividing the received by the transmitted pilots [66] as following

$$\widehat{\underline{\mathbf{H}}}_p = \mathbf{S}_p^{-1}\underline{\mathbf{Y}}_p = \underline{\mathbf{H}}_p + \underbrace{\mathbf{S}_p^{-1}\underline{\mathbf{V}}}_{\text{Estimation error}} \tag{3.2}$$

which is a solution generated by minimizing the term

$$(\underline{\mathbf{Y}}_p - \mathbf{S}_p\underline{\mathbf{H}}_p)^H(\underline{\mathbf{Y}}_p - \mathbf{S}_p\underline{\mathbf{H}}_p)$$

where $(.)^H$ is the conjugate transpose operator. This estimation scheme is known as least square (LS) estimator [67–69]. The main advantage of this kind of estimators is its low complexity (one complex multiplication per one frequency pin), which can be represented by the big O notation as $\mathcal{O}(N)$. The disadvantage of this estimator is the poor performance (it has high mean square error MSE), since the frequency and time correlation of the channel are not taken into account. In order to enhance the performance, the estimation can be averaged over many successive pilot symbols, which averages the noise. Basically, the LS estimator is preferred when the channel and the noise statistics are not available. After estimating the channel response on pilots, some interpolation schemes are applied in order to estimate the channel over all data sub-carriers. The interpolation can be done either in frequency direction or in time direction as 1-D interpolator. If we need to estimate the channel over all sub-carriers for each symbol, a 2-D interpolator is required as shown in Fig. 3.2. In order to estimate the channel over a data subcarrier, the channel estimations over all the adjacent pilots are utilized. This kind of interpolations assumes that the channel is not varying within the symbol duration T_s. However, there are some other 2-D schemes that make use of the channel correlation functions in order to estimate the channel over all time samples.

[1] In OFDM-based systems such as WLAN, the transmitted OFDM symbols are put in frames each one contains many OFDM symbols. The training phase occupies the first two OFDM symbols of the frame as preambles.

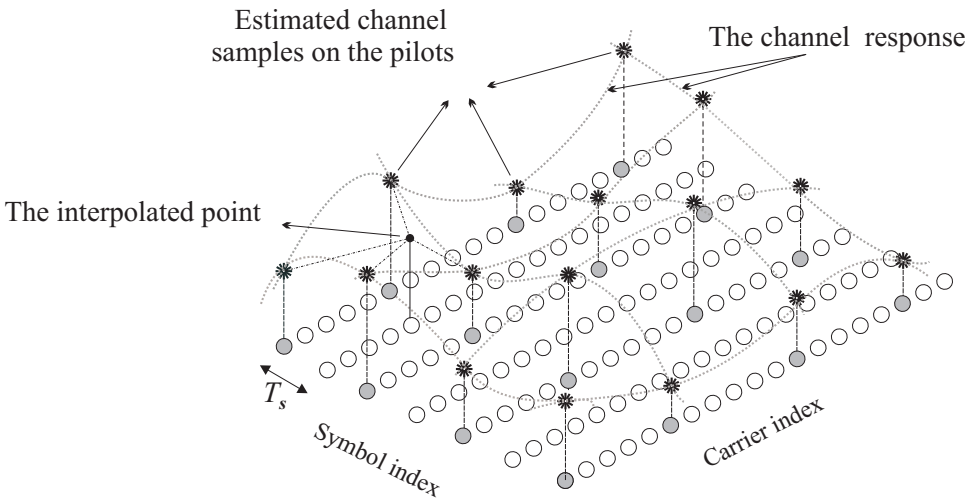

Figure 3.2: 2-D interpolation for OFDM channel.

3.1.2 An MMSE-Based Wiener Filtering Estimator Combined with Matrix-Pencil Algorithm for DRM System

Minimum mean square error (MMSE) estimator is the estimator that minimizes a certain cost function [70–72]. For channel estimation, the cost function is the error (e) between the actual channel values and the estimated values. Unlike the LS estimator, MMSE exploits the second order statistics of the channel such as noise variance, Delay spread, Doppler spread, and the correlation functions. The frequency domain MMSE estimator minimizes the following formula

$$E\{|e|^2\} = E\{|\underline{\mathbf{H}}_p - \underline{\widehat{\mathbf{H}}}_p|^2\}$$

In this section, we describe an estimator scheme to estimate the channel matrix $\mathbf{H}$ for DRM system based on a combination between Matrix Pencil algorithm for estimating the delay contents of the channel and Wiener filtering for tracking the time-variant channel magnitude. DRM system is an OFDM-based digital audio broadcasting technology designed to work over the frequency band of AM radio. The DRM system uses low frequency (LF), medium frequency (MF), and high frequency (HF) broadcast radio channels, which are multipath channels because the surface of the earth and the ionosphere are involved in the mechanism of electromagnetic wave propagation [73]. The frequency domain channel matrix can be estimated by linearly filtering the received signal for each channel element. The estimated element (m, k) of the channel matrix is expressed as follows

$$\hat{H}_{m,k} = \underline{\mathbf{W}}_{m,k}^H \underline{\mathbf{Y}}, \tag{3.3}$$

where $\underline{\mathbf{W}}_{m,k}$ is the Wiener filter vector that is used to estimate the channel matrix element (m, k). The Wiener filter for each channel element is designed and optimized according to the MMSE criterion as follows

$$\underline{\mathbf{W}}_{m,k}^{(opt)} = \arg \min_{\underline{\mathbf{W}}} E\left\{\left|H_{m,k} - \underline{\mathbf{W}}_{m,k}^H \underline{\mathbf{Y}}\right|^2\right\}. \tag{3.4}$$

The solution of (3.4) is given in [74], which reads

$$\underline{\mathbf{W}}_{m,k}^{(opt)} = \mathbf{R}^{-1}\underline{\mathbf{P}}_{m,k}, \tag{3.5}$$

where $\mathbf{R} = E\{\underline{\mathbf{Y}}\underline{\mathbf{Y}}^H\}$ is the autocorrelation of the received frequency domain signal and $\underline{\mathbf{P}}_{m,k} = E\{H_{m,k}^*\underline{\mathbf{Y}}\}$ is the cross correlation between the received signal and the actual frequency response of the channel. Notice that in order to estimate the whole channel matrix, N^2 Wiener filters are needed. In order to calculate these filters, $\mathcal{O}(N^4)$ multiplications are required. This requires high computational effort and high storage specially for large number of carriers N. In practical implementations, only few elements of the channel matrix are considered. Only the main diagonal and some of the adjacent diagonals can give reasonable accuracy for slow varying channels, while for rapid varying channels, the whole channel matrix is required. Assuming that $\mathbf{H}$, $\underline{\mathbf{S}}$, and $\underline{\mathbf{V}}$ are uncorrelated and making use of (2.28), the element (k, k') of $\mathbf{R}$ can be written as

$$R_{k,k'} = E\{Y(k)Y(k')^*\} = E\Big\{\Big(\sum_{m=0}^{N-1} H_{m,k}S(m)\Big)\Big(\sum_{m'=0}^{N-1} H_{m',k'}^*S(m')^*\Big)\Big\} + E\{V(k)V(k')^*\} \tag{3.6}$$

From (3.6), $\mathbf{R}$ can be separated into two parts, the pure correlation matrix and the noise

$$\mathbf{R} = \mathbf{R}' + \sigma_v^2\mathbf{I} \tag{3.7}$$

where σ_v^2 is the noise variance, which is the first statistical parameter that needs to be estimated at the receiver. Also the element k' in $\underline{\mathbf{P}}_{m,k}$ is calculated as

$$P_{m,k}^{k'} = E\{Y(k')H_{m,k}^*\} = E\Big\{\sum_{m'=0}^{N-1} H_{m',k'}H_{m,k}^*S(m')\Big\} + E\{V(k')H_{m,k}^*\} \tag{3.8}$$

Assuming a WSSUS channel model, $R'_{k,k'}$ and $P_{m,k}^{k'}$ can be given by the following equations [75]

$$R'_{k,k'} = \sigma_s^2 \sum_{m\notin\underline{\mathbf{S}}_p}\sum_{l=0}^{L-1}\int_{-\infty}^{\infty}\Phi_{l,\nu}(k-m,k'-m)d\nu +$$

$$\sum_{m,m'\in\underline{\mathbf{S}}_p} S(m)S^*(m')\sum_{l=0}^{L-1} e^{-j2\pi(m-m')\Delta f\tau_l}\int_{-\infty}^{\infty}\Phi_{l,\nu}(k-m',k'-m')d\nu \tag{3.9}$$

$$P_{m,k}^{k'} = \sum_{m'\in\underline{\mathbf{S}}_p} S(m')\sum_{l=0}^{L-1} e^{-j2\pi(m-m')\Delta f\tau_l}\int_{-\infty}^{\infty}\Phi_{l,\nu}(k'-m',k-m)d\nu \tag{3.10}$$

where

$$\Phi_{l,\nu}(a,b) = \mathrm{sinc}(\nu T_s - a)\,\mathrm{sinc}(\nu T_s - b)D_l(\nu)$$

where $\mathrm{sinc}(\cdot)$ is the sinc function. In addition to the transmitted pilots $\underline{\mathbf{S}}_p$, the previous equations require the knowledge of statistical channel parameters such as Doppler spectral density $D_l(\nu)$ and the time delays τ_l for each path. The tap delays are estimated using Matrix-Pencil algorithm [76], which is one of the super resolution techniques. The

algorithm makes use of the initially estimated channel transfer function that can be estimated once at the beginning[2] of the frame using simple least square estimation. The elements of $\underline{\mathbf{H}}_p$ are arranged in the following matrix

$$\mathbf{A} = \begin{pmatrix} \hat{H}_p(1) & \hat{H}_p(2) & \dots & \hat{H}_p(K+1) \\ \hat{H}_p(2) & \hat{H}_p(3) & \dots & \hat{H}_p(K+2) \\ \vdots & & \ddots & \vdots \\ \hat{H}_p(N-K) & \hat{H}_p(N-K+1) & \dots & \hat{H}_p(N) \end{pmatrix}, \tag{3.11}$$

where K is the pencil parameter that can be chosen by default as $(K = \frac{N}{3})$ [76]. Matrix pencil algorithm applies a singular value decomposition [77] which reads

$$\mathbf{A}' = \mathbf{U}\mathbf{S}\mathbf{V}^H$$

where $\mathbf{A}'$ contains the last K columns of $\mathbf{A}$.

$$\mathbf{A}' = \begin{pmatrix} A_{1,2} & A_{1,3} & \dots & A_{1,K+1} \\ A_{2,2} & A_{2,3} & \dots & A_{2,K+1} \\ \vdots & & \ddots & \vdots \\ A_{N-K,2} & A_{N-K,3} & \dots & A_{N-K,K+1} \end{pmatrix}.$$

In order to estimate the time delay of each tap, eigenspace analysis is applied on the following matrix

$$\mathbf{T} = (\mathbf{S}')^{-1}\mathbf{U}'^H\mathbf{A}''\mathbf{V}' = \mathbf{E}\Lambda\mathbf{E}^{-1}$$

where $\Lambda = \mathcal{D}\{\lambda_1, \lambda_2, ..., \lambda_L\}$ is a diagonal matrix which contains the eigenvalues of $\mathbf{T}$, while $\mathbf{E}$ is a matrix whose columns are the corresponding eigenvectors. $\mathbf{S}'$ is a sub-matrix from $\mathbf{S}$, which contains the first L rows and first L columns. $\mathbf{U}'$ and $\mathbf{V}'$ contain the first L columns of $\mathbf{U}$ and $\mathbf{V}$, respectively. $\mathbf{A}''$ contains the first K columns of $\mathbf{A}$. Finally, the time delay of the l^{th} path is calculated as

$$\tau_l = \frac{\mathrm{lm}\{\ln(\lambda_l)\}}{2\pi\Delta f},$$

where Δf is the frequency spacing between the OFDM carriers. The Wiener filtering method has been designed for digital radio mondiale (DRM) system which has a Doppler spectrum with Gaussian shape

$$D(\nu) = \frac{1}{\sqrt{2\pi}f_d} e^{-\frac{\nu^2}{2f_d^2}}. \tag{3.12}$$

The power density spectrum (PDS) is modeled by filtering the white Gaussian noise (WGN) with the proper filter and the stochastic processes belonging to each path become Rayleigh processes.

[2]The channel transfer function is estimated from the training symbols in the preamble.

3.2 Equalization Algorithms

In OFDM systems, the estimation stage is followed by an equalization stage to compensate for the channel distortions in order to detect the transmitted signal. The detected frequency domain signal at the equalizer output is written as

$$\underline{\widehat{\mathbf{S}}} = \mathbf{G}\underline{\mathbf{Y}} \tag{3.13}$$

where $\mathbf{G}$ is the equalization matrix. There are many ways to equlize the received signal, some of them depend on forward equalizations and others utilize feedback equalization to adapt the filter coefficients. In this section, two of the most popular equalization schemes are considered, ZF and MMSE equalizers.

3.2.1 Zero Forcing Equalizer

Zero forcing (ZF) equalizer applies direct channel inversion to eliminate the effects of the channel [78]. The equalization matrix is given by

$$\mathbf{G} = \mathbf{H}^{-1} \tag{3.14}$$

By considering only the main diagonal of $\mathbf{H}$, which is the case of time-invariant channels, the equalizer coefficient for each channel element is given by

$$G_{m,m} = \frac{H^*_{m,m}}{|H_{m,m}|^2} \tag{3.15}$$

The drawback of ZF equalization is that at deep fading, where the channel amplitudes are small, the equalizer enhances the noise. This makes ZF equalizer unsuitable at low SNR values.

3.2.2 Linear MMSE Equalizer LMMSE

MMSE equalizer minimizes the error between the transmitted signal and the equalizer output. The cost function to be minimized is given by

$$Z(m) = E\{|\varepsilon(m)|^2\} = E\{|S(m) - G_{m,m}Y(m)|^2\} \tag{3.16}$$

To minimize Z_m, the equalizer coefficients are chosen such that the error $\varepsilon(m)$ is orthogonal to the received signal $Y(m)$ [27], which can be described as

$$E\{\varepsilon_m Y(m)^*\} = 0 \tag{3.17}$$

The equalizer coefficients at the main diagonal of the channel matrix are given by

$$G_{m,m} = \frac{H^*_{m,m}}{|H_{m,m}|^2 + \sigma_v^2}. \tag{3.18}$$

As it is shown in (3.18), the noise variance at the denominator helps to avoid the noise enhancements. Considering the whole channel matrix, $\mathbf{G}$ is given by

$$\mathbf{G} = \mathbf{H}^H(\mathbf{H}\mathbf{H}^H + \sigma_v^2\mathbf{I})^{-1} \tag{3.19}$$

This kind of equalizer is called linear MMSE equalizer (LMMSE), since there is no feedback path. It can be seen from (3.19) that at very high SNR ($\sigma_v^2 \approx 0$), The LMMSE equalizer becomes identical to the ZF equalizer. Therefore, LMMSE equalizers are not recommended at high SNR because of the higher complexity.

3.2.3 Channel Equalization for MIMO OFDM Systems

As has been discussed in Chapter 1, combining the MIMO technique with the OFDM system is a very promising technology in the future, since it enhances the capacity and the coverage capabilities. The idea is to transmit different data streams by multiple transmit antennas M_t and receive them using multiple receive antennas M_r. In order to exploit the space diversity, space-time coding algorithms such as Alamouti encoder [79] are applied. The OFDM channel matrix in case of MIMO is given by

$$\mathbb{H} = \begin{pmatrix} \mathbf{H}_{(1,1)} & \mathbf{H}_{(1,2)} & \dots & \mathbf{H}_{(1,M_r)} \\ \mathbf{H}_{(2,1)} & \mathbf{H}_{(2,2)} & \dots & \mathbf{H}_{(2,M_r)} \\ \vdots & & \ddots & \vdots \\ \mathbf{H}_{(M_t,1)} & \mathbf{H}_{(M_t,2)} & \dots & \mathbf{H}_{(M_t,M_r)} \end{pmatrix} \tag{3.20}$$

where $\mathbf{H}_{(i,j)}$ is the channel matrix for the path between the i^{th} transmit antenna and the jth receive antenna. Fig. 3.3 presents a 2X2 MIMO-OFDM system using Alamouti space-time coding (STC) in which the transmitted symbols at the first transmit antenna is written as

$$\underline{\mathbf{S}}_{(1)} = \begin{bmatrix} -\underline{\mathbf{S}}^*[1] & \underline{\mathbf{S}}[0] \end{bmatrix}$$

and at the second antenna as

$$\underline{\mathbf{S}}_{(2)} = \begin{bmatrix} \underline{\mathbf{S}}^*[0] & \underline{\mathbf{S}}[1] \end{bmatrix}$$

where $\underline{\mathbf{S}}[\cdot]$ denotes the OFDM symbol index and $\underline{\mathbf{S}}_{(\cdot)}$ denotes the antenna index. The

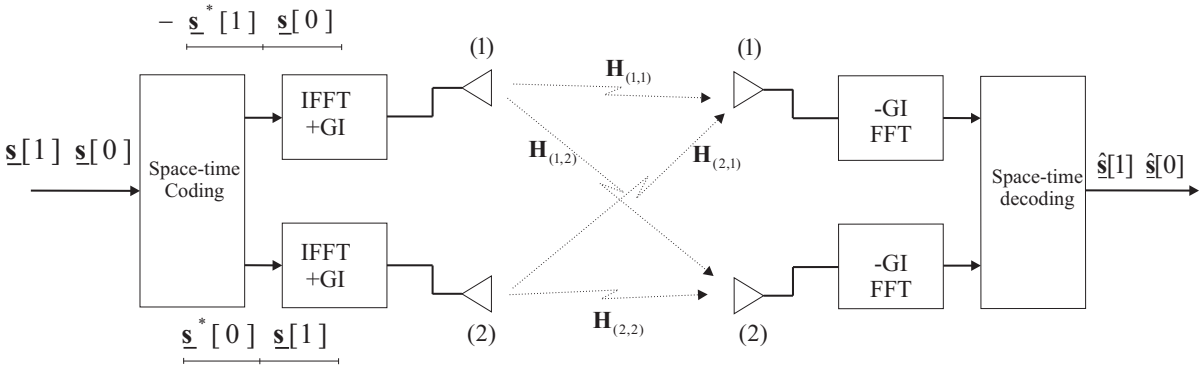

Figure 3.3: A block diagram of a 2× 2 OFDM-MIMO system with space-time block Alamouti encoder.

LMMSE equalizer output for 2X2 MIMO-OFDM system at the first receive antenna can be written as

$$\begin{bmatrix} \widehat{\underline{\mathbf{S}}}[0] \\ \widehat{\underline{\mathbf{S}}}[1] \end{bmatrix} = \begin{bmatrix} \mathbf{H}_{(1,1)}[0] & \mathbf{H}_{(2,1)}[0] \\ \mathbf{H}^*_{(2,1)}[1] & -\mathbf{H}^*_{(1,1)}[1] \end{bmatrix}^H \left(\begin{bmatrix} \mathbf{H}_{(1,1)}[0] & \mathbf{H}_{(2,1)}[0] \\ \mathbf{H}^*_{(2,1)}[1] & -\mathbf{H}^*_{(1,1)}[1] \end{bmatrix}$$

$$\left[\begin{array}{cc} \mathbf{H}_{(1,1)}[0] & \mathbf{H}_{(2,1)}[0] \\ \mathbf{H}^*_{(2,1)}[1] & -\mathbf{H}^*_{(1,1)}[1] \end{array} \right]^H + \mathbb{I}\sigma_v^2 \Bigg)^{-1} \left[\begin{array}{c} \underline{\mathbf{Y}}_{(1)}[0] \\ \underline{\mathbf{Y}}^*_{(1)}[1] \end{array} \right] \tag{3.21}$$

and at the second receive antenna

$$\left[\begin{array}{c} \widehat{\underline{\mathbf{S}}}[0] \\ \widehat{\underline{\mathbf{S}}}[1] \end{array} \right] = \left[\begin{array}{cc} \mathbf{H}_{(1,2)}[0] & \mathbf{H}_{(2,2)}[0] \\ \mathbf{H}^*_{(2,2)}[1] & -\mathbf{H}^*_{(1,2)}[1] \end{array} \right]^H \Bigg(\left[\begin{array}{cc} \mathbf{H}_{(1,2)}[0] & \mathbf{H}_{(2,2)}[0] \\ \mathbf{H}^*_{(2,2)}[1] & -\mathbf{H}^*_{(1,2)}[1] \end{array} \right]$$

$$\left[\begin{array}{cc} \mathbf{H}_{(1,2)}[0] & \mathbf{H}_{(2,2)}[0] \\ \mathbf{H}^*_{(2,2)}[1] & -\mathbf{H}^*_{(1,2)}[1] \end{array} \right]^H + \mathbb{I}\sigma_v^2 \Bigg)^{-1} \left[\begin{array}{c} \underline{\mathbf{Y}}_{(2)}[0] \\ \underline{\mathbf{Y}}^*_{(2)}[1] \\ . \end{array} \right] \tag{3.22}$$

Where $[\cdot]$ represents the OFDM symbol index, i.e. $\mathbf{H}_{(.,.)}[0]$ and $\mathbf{H}_{(.,.)}[1]$ are the channel matrices for the first symbol and the subsequent one, respectively, and $\mathbb{I}$ is the $NM_r \times NM_t$ identity matrix. The output signal is detected using likelihood estimation method or by simply averaging the value of the two outputs of the LMMSE equalizer.

3.3 Simulation Results

In this section, we present the numerical results to illustrate the performance of the combined channel estimation, which is a Matrix-pencil delay estimation algorithm followed by Winer filtering scheme. The considered OFDM system is the DRM system. For this simulation, a DRM system with robustness mode "B" and spectral occupancy "0" has been considered, which has the parameters shown in Table 3.1. We have simulated three

Table 3.1: System parameters

Parameter	Value
Modulation schemes	QPSK, 16QAM, and 64QAM
Number of Carriers	91
FFT length	1024
Guard interval	256
Bandwidth	4.5 KHz
Sampling rate	48 KHz
Carrier frequency	30 MHz
Number of symbols per frame	15
Maximum number of pilots	16

channels for DRM, which are standardized according to the European telecommunications standards institute (ETSI). Channel #1 is an AWGN time invariant (TI) channel with single path, channel #2, which is a very slow time-variant channel with two taps and maximum delay spread of 1 ms, and finally channel #3, which is a time-variant (TV) channel with four taps, maximum delay of 2.2 ms, and maximum Doppler spread of 2 Hz. This Doppler spread value is equivalent to a mobile speed of 78 Km/h. In these channels the WSSUS model is assumed and the channel taps are generated as random processes filtered with a Doppler filter that has a Gaussian shape, which is suitable for propagation

through the ionospheric and the earth-reflection paths. For simulation, only the main diagonal of the channel matrix is estimated according to the Winer filtering method described in Section 3.1.2. The knowledge of the channel statistics such as Doppler spread, delay spread, and noise variance has been assumed. The integration in (3.9) and (3.10) has been implemented as a numerical integration in MATLAB using adaptive Lobatto quadrature approximation method [73]. Fig. 3.2 shows the effect of the AWGN noise

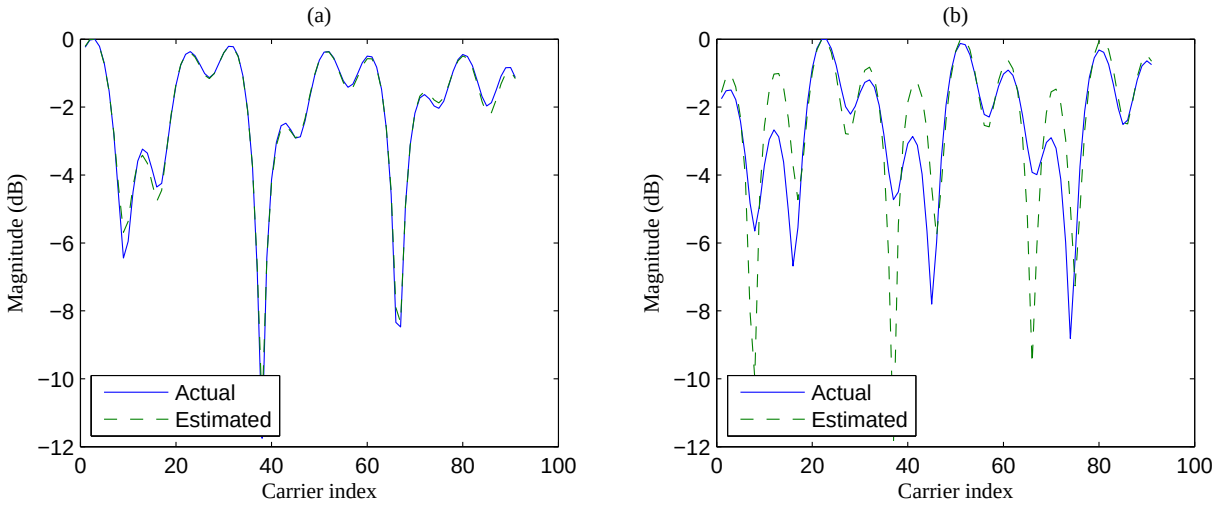

Figure 3.4: Comparison between the actual and estimated channel frequency response at: (a): SNR=40 dB; (b): SNR=0 dB.

on the estimated channel frequency response for channel #3 with different SNRs using 64QAM modulation scheme. Thr number of pilots used for the channel estimation is very

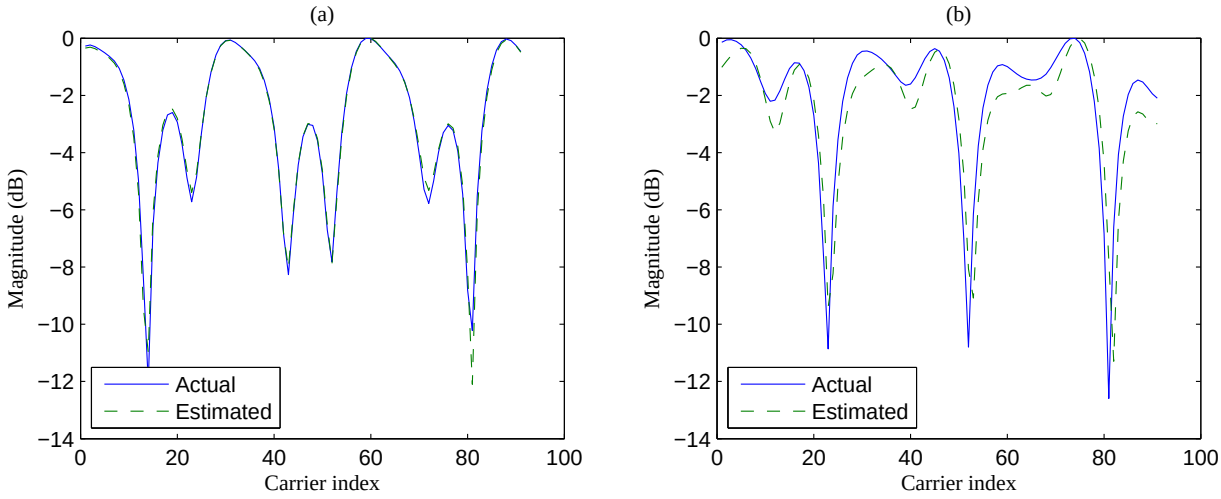

Figure 3.5: Comparison between the actual and estimated channel frequency response for two different pilot spacings; (a): $D_f = 6$; (b): $D_f = 12$.

critical parameter, since more pilots give more accurate channel estimation, but at the same time reduces the bandwidth efficiency of the system by introducing an overhead to

the signal. The effect of the pilot spacing on the estimated channel frequency response for channel #3 is illustrated in Fig. 3.5. The estimator performance by means of MSE is

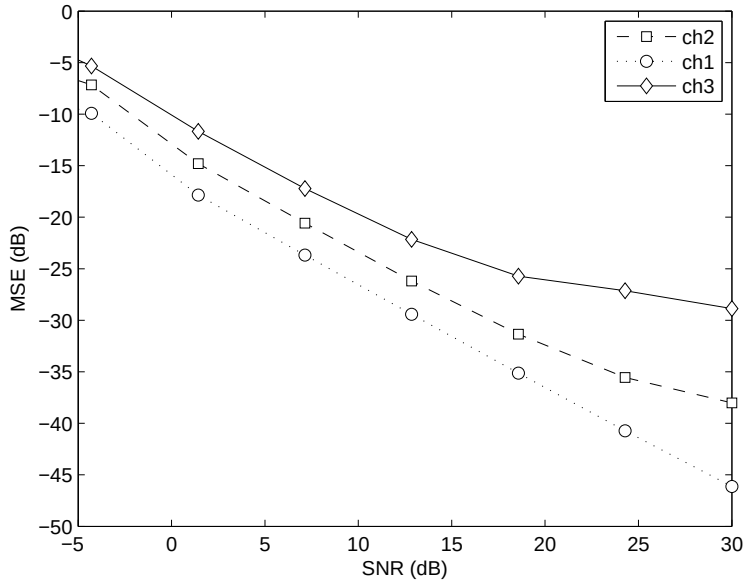

Figure 3.6: The averaged MSE of the estimated channel.

shown in Fig. 3.6. The figure shows the averaged MSE between the estimated and the actual channel over 30,000 OFDM channel realizations, which is calculated as follows

$$\text{MSE} = E\left\{\left|\text{diag}(\mathbf{H}) - \text{diag}(\hat{\mathbf{H}})\right|^2\right\} \tag{3.23}$$

The MSE has been evaluated for the three channels over variable SNR using 64QAM modulation scheme. The results show that the estimation error increases as the frequency and time selectivity increase. Fig. 3.7 illustrates the CIR estimation using Matrix-pencil algorithm used for optimizing the Wiener filter. The figure shows the algorithm capability of detecting very closed multipaths. Fig. 3.8 demonstrates the BER performance of the system for all considered channels. The BER has been averaged over 30,000 OFDM channel realizations, and a 64QAM modulation scheme was used. It is obvious that the system performance degrades because of the frequency selectivity (channel #2 , channel #3) and becomes more worse due to the time selectivity (channel #3). It can be seen that estimating only the main diagonal of the channel matrix in case of time selective channel #3, the error floor caused by ICI effect can not be eliminated. To reduce this effect, the whole channel matrix coefficients should be estimated, which will be the subject of the subsequent chapter. Fig. 3.9 illustrates the BER performance of the channel #3 for different modulation schemes, which are QPSK, 16QAM and 64QAM. In practical systems, a channel coding stage is combined with the OFDM system in order to utilize the frequency diversity of the multiple carriers. Fig. 3.10 shows the effect of the FEC coding on the system performance. A convolutional encoder has been applied on 64QAM symbols with code rate, $R = 0.5$. At the receiver side, a Viterbi decoder [80] with hard detection is applied. The performance enhancement is obvious at moderate and high

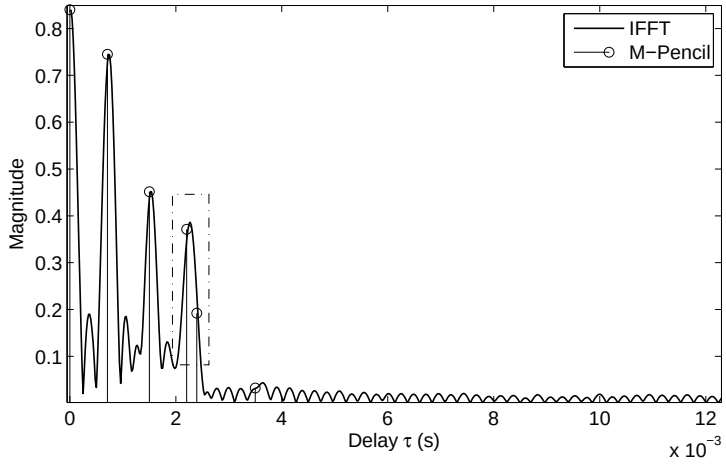

Figure 3.7: A comparison between the CIR estimation using DFT and using Matrix-pencil for a channel with 6 paths.

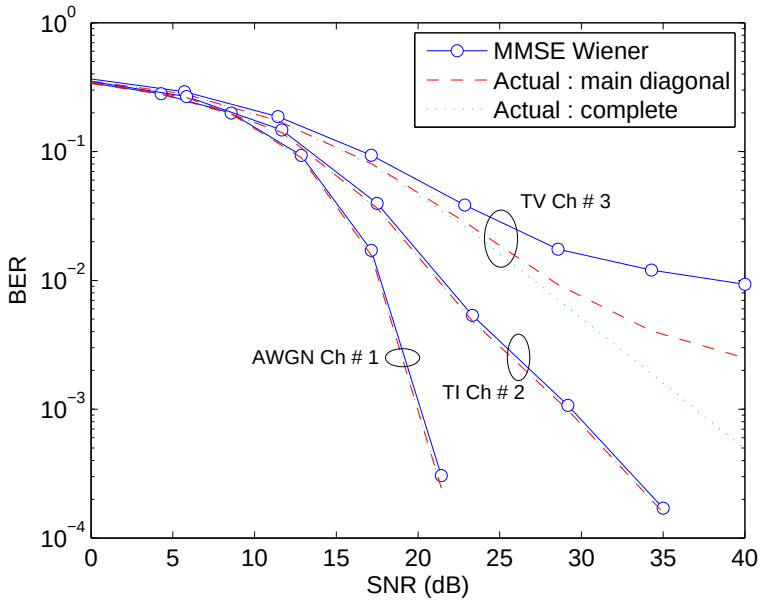

Figure 3.8: BER performance for different DRM channels.

SNR, while for low SNR, the performance suffers from extra errors. In order to cope with this drawback, an interleaving stage is required prior to the encoding stage to randomize the error on the code words. Fig. 3.11 shows the performance of the DRM system when combined with MIMO technology considering channel #2. The maximum number of the used transmit antennas is $M_t = 2$ and of the receive antennas is $M_r = 3$. To show the benefit of the multiple antennas, the total transmit power is kept constant and divided into the transmit antennas. An Alamouti space-time encoder was applied. For equalization, an MMSE equalizer represented by (3.21) and (3.22) was utilized. It can be seen from the figure that an improvement of about 10 dB can be achieved in case of (2×3) system at BER of 10^{-3}.

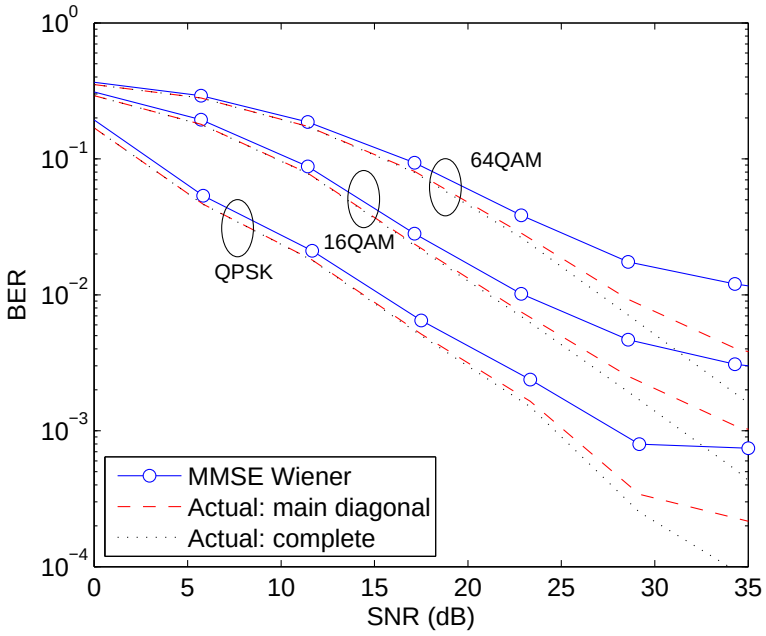

Figure 3.9: BER performance for DRM with different modulation schemes.

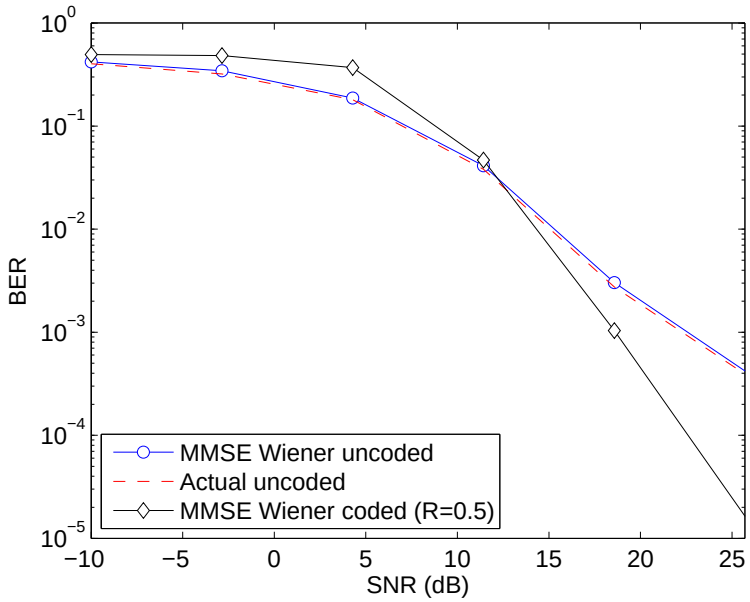

Figure 3.10: The effect of FEC on the BER performance.

3.4 Experimental Investigation of OFDM Systems in Wireless Multipath Channels

The channel estimation methods of the multipath time-variant channel have been detailed in the previous sections. Simulation has been made on the transmission and the reception of the OFDM signal in wireless channels with different characteristics. In order

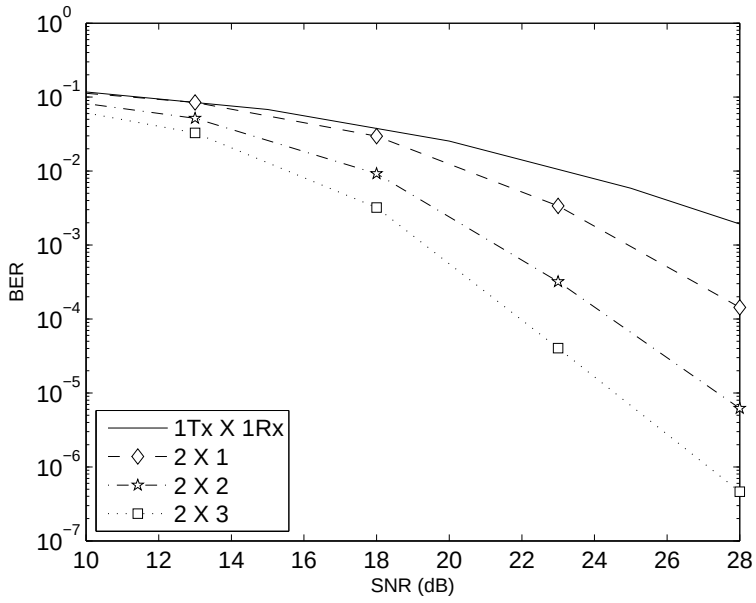

Figure 3.11: BER performance of the MIMO-OFDM system.

to have a practical real-time perspective, we discuss some measurements that have been established for transmitting, receiving and equalizing of the OFDM signal in multipath indoor environment. The goal is to better understand the effects of the multipath channel as well as the RF components on the system performance and verify the capability of the channel estimation algorithm described in Section 3.1.2.

3.4.1 Measurement Setup

This section discusses the measurement system used for channel characterization and the OFDM system performance evaluation. The measurement setup is shown in Fig. 3.12. As shown from the figure, the measurement system is a combination of software and hardware components.

3.4.1.1 Software setup

At an external PC, the baseband IQ OFDM signal based on IEEE802.11g standard is generated using Matlab code. The OFDM symbols are arranged in a few frames to be transmitted. At the beginning of each frame, some training symbols (preambles) are inserted, which are used for packet detection and frequency and time offset estimation. The time domain baseband signal is sent via LAN connection to the transmitter, in order to be upconverted and transmitted through the wireless channel. The commands for controlling the power and the carrier frequency are sent to the transmitter before sending the baseband signal. On the other hand, the IQ data from the captured signal at the receiver is sent back to the external PC via the LAN for processing. Packet detection, frequency and time offset estimation and pilot based channel estimation are all accomplished using Matlab.

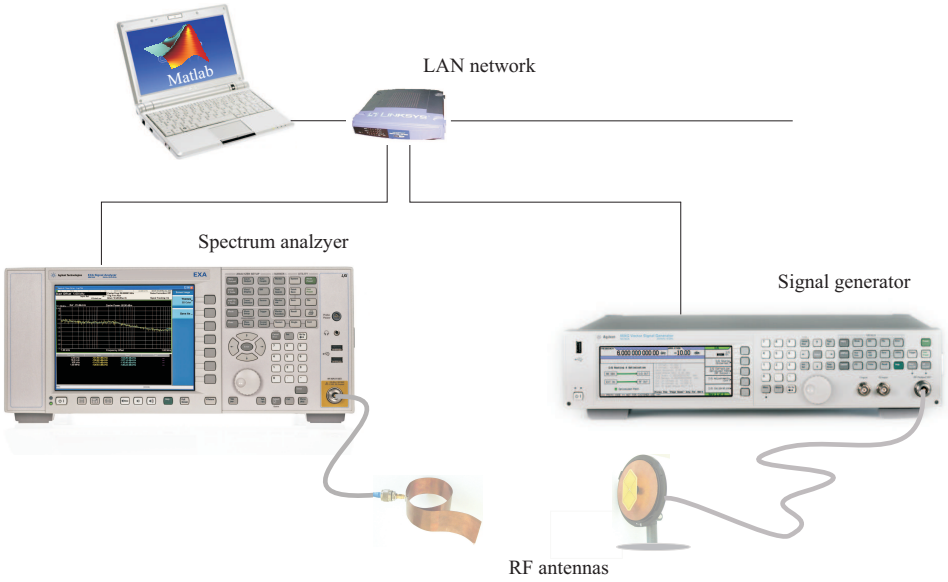

Figure 3.12: The measurement system setup.

3.4.1.2 Hardware setup

The transmitter

For transmitting the real time multicarrier signal, an MXG signal generator N5182A [81] has been used. This signal generator works on a frequency range between 100 KHz to 6 GHz and transmission power up to 17 dBm. The baseband IQ data is generated using Matlab and sent to the signal generator via LAN connection. The signal generator saves the IQ data, applies the IF modulation and RF upconversion and then transmits the signal with predefined power and carrier frequency. In order to have a continuous transmission, the signal generator sends the same signal repeatedly.

The antennas

The transmit antenna works between 2.4 GHz and 2.6 GHz with gain 9 dBi at the resonance frequency [82], while the receive antenna has an ultra-wideband characteristics in the frequency range from 800 MHz to 18 GHz [83]. Both antennas have been designed and fabricated in the IESK institute.

The receiver

The EXA spectrum analyzer from Agilent [84] has been used as a receiver. This device has an absolute sensitivity of -79.4 dBm, a dynamic range of 93.1 dB, and a maximum input power of +30 dBm. The reviver downconverts the RF signal and generates the IQ baseband data which is sent back to the external PC for processing.

3.4.2 Wireless Channel Characterization

Characterizing of the wireless communication channels is one of the most important parts for the design and implementation of any wireless communication system. Estimating the channel parameters such as the number of multipaths, the delay spread, and the Doppler spread allows for suitable design and robust behavior of the system. In this section some measurements have been made in order to estimate the channel taps and the delay spread of the channel. A multicarrier signal has been sent through the channel, captured at the receiver and then processed in order to calculate the CTF and the CIR. The measurements have been conducted in Lab312, which is one of the IESK laboratories. The lab was cluttered with furniture, test and measurement equipments. The topology of the lab and the test scenario is shown in Fig. 3.13

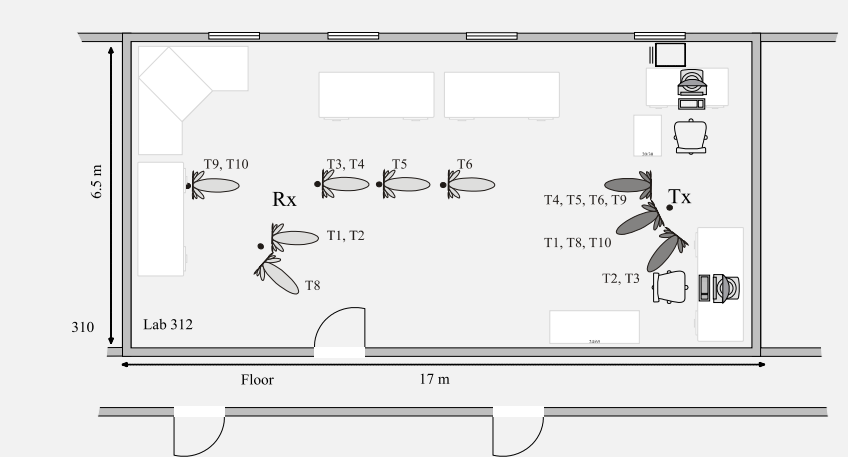

Figure 3.13: The floor plan of the measurement location.

During the measurements, the transmit antenna remained fixed at the same place with different orientations, while the receive antenna was moved to different places and orientations. The signal used for measurement was a WLAN signal with 20 MHz bandwidth and carrier frequency of 2.412 GHz. The channel transfer function was calculated as the ratio between the transmitted frequency domain OFDM symbols by the received frequency domain symbols. The channel impulse response h was calculated by simply applying an IFFT on the CTF.
One of the important parameters required for the characterization of any wireless channel is the RMS delay spread τ_{rms}, which is calculated from the CIR [85] as

$$\tau_{rms} = \sqrt{\frac{\sum_{l=0}^{L-1} h_l^2 \tau_l^2}{\sum_{l=0}^{L-1} h_l^2} - \left(\frac{\sum_{l=0}^{L-1} h_l^2 \tau_l}{\sum_{l=0}^{L-1} h_l^2} \right)^2}, \tag{3.24}$$

where h_l and τ_l are the complex magnitude and the delay of the l^{th} path, respectively. In order to get a clear idea about the multipath channel, the Ricean K-factor of the channel has been measured and calculated by taking the ratio between the signal power in the

main path to the power in the scattered paths as follows

$$K = \frac{h_{LOS}^2}{\sum_{l=0}^{L-1} h_l^2 - h_{LOS}^2} \tag{3.25}$$

Basically, the Ricean K factor lies between 0, in case of Rayleigh channel, and ∞ in the case of single path transmission. The measured channel parameters are summarized in Table. 3.2. In addition, the coherence bandwidth of the channel has been approximately calculated according to the 50% of the frequency correlation function [85] as

$$C_f \approx \frac{1}{5\tau_{rms}} \tag{3.26}$$

The measured parameters show that τ_{rms} lies between 306 ns and 58 ns for different

Table 3.2: The measured channel characteristics

Test	RMS delay (ns)	K factor (dB)	Coherence bandwidth (KHz)
T1	306.3	8.8195	653
T2	236	5.7749	847
T3	138	10.5308	1449
T4	97	10.8814	2062
T5	61	11.2222	3279
T6	58	11.3988	3448
T7	143	9.0309	1399
T8	233	10.2531	858
T9	151	10.8991	1325
T10	183	10.5308	1093

locations. Fig. 3.14 shows the CTF and the CIR of the experiment T1, which represents a multipath channel with $\tau_{rms} = 306$ ns, while Fig. 3.15 represents the experiment T5, which exhibits a strong LOS transmission.

3.4.3 Measurement and Equalization of OFDM Signals in Multipath Indoor Channels

3.4.3.1 Implementation considerations

In Section 3.2, time and frequency synchronization of the OFDM symbols were assumed for simulation. However, the time and frequency synchronization play an important role in designing and implementing the practical systems. In WLAN system, the signal is headed with a preamble at the beginning of each frame. This preamble is basically used for time synchronization, frequency offset estimation and for the initial channel estimation. The preamble contains two parts, the first one is called short training symbols (STS), which contains 10 short symbols occupy 8 μs. The STS are used for time synchronization and course frequency offset (CFO) estimation. The second part is called long training symbols (LTS), which contains two long symbols each with time duration of 3.2 μs as well as a GI with time duration of 1.6 μs. The LTS are used for further enhancing the time

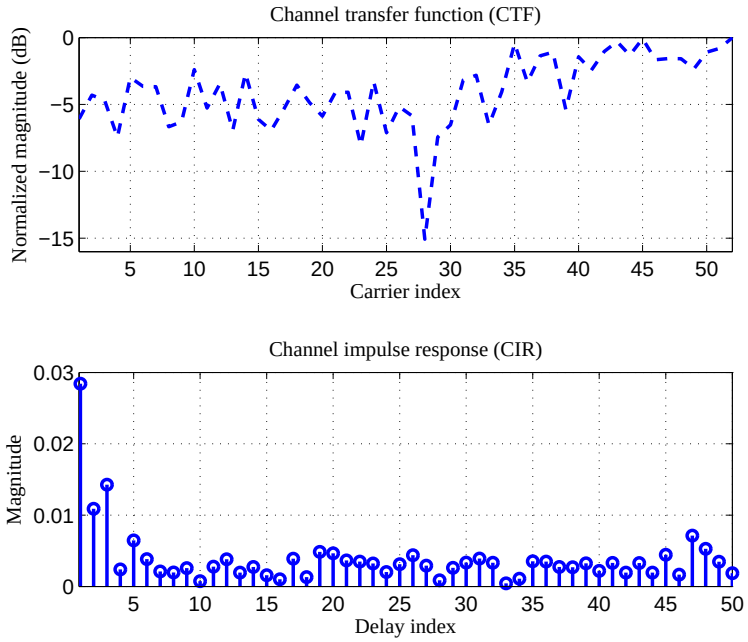

Figure 3.14: The CTF and the CIR of a multipath channel (T1).

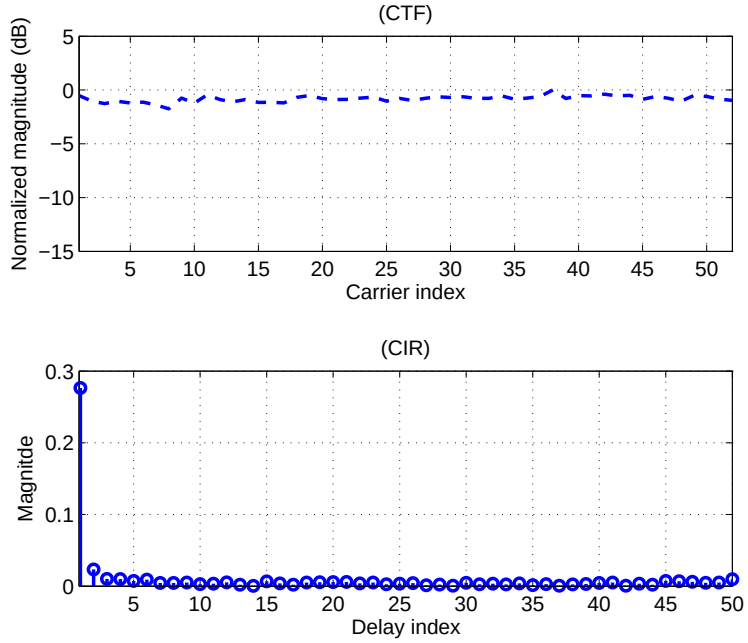

Figure 3.15: The CTF and the CIR of a flat fading channel (T5).

synchronization and for fine frequency offset (FFO) estimation as well as initial channel estimation. Fig. 3.16 shows the frame structure of the OFDM-based WLAN system including the preamble. The OFDM symbol of the WLAN system contains 64 carriers,

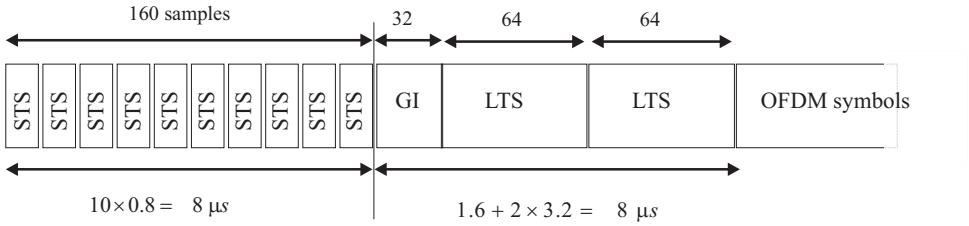

Figure 3.16: The frame structure of the OFDM-based WLAN system.

52 of them are active carriers, while the other 12 carriers work as frequency guard at both sides of the spectrum. For channel estimation and equalization purposes, 4 carriers out of the 52 are booked for pilots. Fig. 3.17 illustrates the time domain transmitted signal, which contains the STS and LTS. Fig. 3.18 shows the spectrum of the transmitted

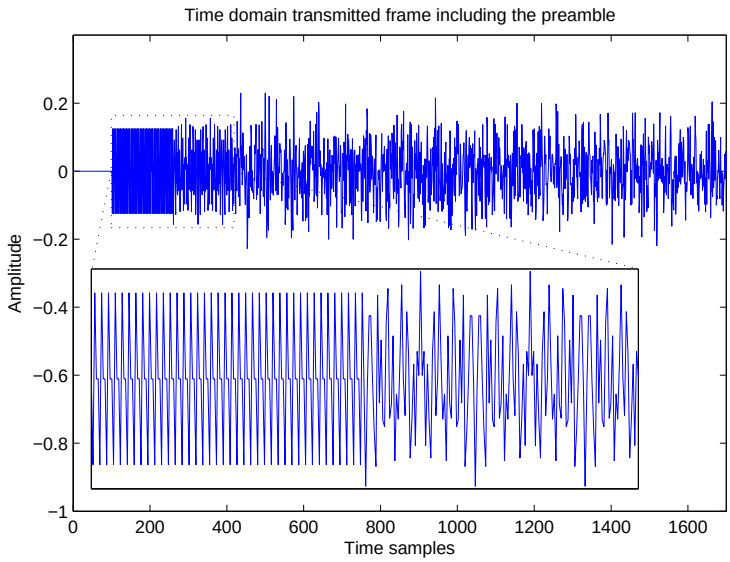

Figure 3.17: The transmitted OFDM signal including the short and long training symbols.

OFDM signal. The DC carrier is shown in the middle of the spectrum.

3.4.3.2 Packet detection

In order to start processing the received OFDM signal, the signal packets need to be detected first and the first sample of the OFDM symbols needs to be indicated in order to apply the FFT operation on the right symbol samples. One method for detecting the packets can be based on the power level of the baseband received signal [86]. The packet is said to be detected if the signal power exceeds a specific power threshold. However, in wireless channels, the variance of the signal power as well as the additive noise make this method unpractical. A suitable method for detecting the packet is based on the autocorrelation of the received preamble [86], which contains short and long training

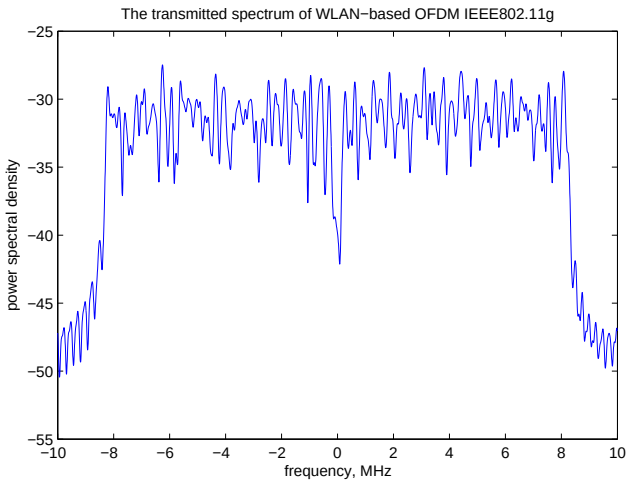

Figure 3.18: The spectrum of the transmitted OFDM signal.

symbols. The auto correlation is written in the following form

$$Z(n) = \sum_{c=0}^{N_{TS}-1} y^*(n+c)y(n+c+N_{TS}), \tag{3.27}$$

where $y(n)$ represents the n^{th} incoming sample of the baseband signal, $y^*(n)$ represents the conjugate of $y(n)$ and $N_{TS} = 16$ samples in case of short training symbols. In order to avoid the expected variance of the incoming signal power, the autocorrelation needs to be normalized by a moving sum of the received signal power [87]. The moving sum of the received power can be written as

$$P(n) = \sum_{c=0}^{N_{TS}-1} |y(n+c+N_{TS})|^2. \tag{3.28}$$

The normalized autocorrelation used for packet detection reads

$$M(n) = \frac{|Z(n)|^2}{P(n)}. \tag{3.29}$$

The packet is detected at the first peak of $M(n)$ after a predefined threshold, which should be chosen to minimize the possibility of false alarm. Using only the short training symbols in packet detection gives a reasonable performance in case of good conditions of the channel, however, because of the expected time offsets at bad channel conditions, it is better to use both short and long training symbols for this purpose. Fig. 3.19 shows the autocorrelation function $M(n)$, whose first peak indicates the beginning of the packet (the first sample of the short training symbols), while the second peak indicates the first sample of the GI of the long training symbols. By taking the difference between the two peaks, the time offset, if found, can be estimated and then the start of the packet is corrected. Also there are other methods for detecting the packet such as Likelihood-based packet estimation and MMSE packet detection [88], however, these methods have higher

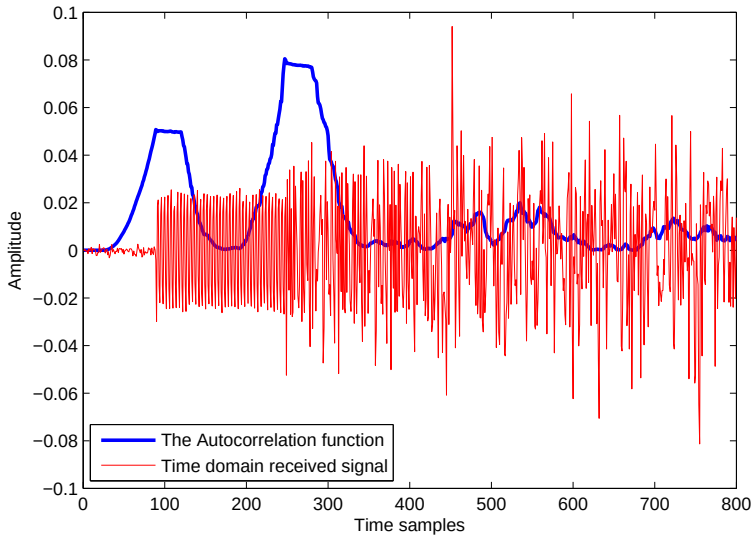

Figure 3.19: The packet detection based on autocorrelation of the preamble.

complexity than the autocorrelation one. For our measurement test, the autocorrelation method has given a reasonable performance with low complexity in detecting the OFDM packets for different channel and transmission power conditions. Fig. 3.20 shows a comparison between the spectrum of the transmitted and the received OFDM signals. The figure shows the effect of the widowing at the receiver side, which reduces the side loops of the spectrum.

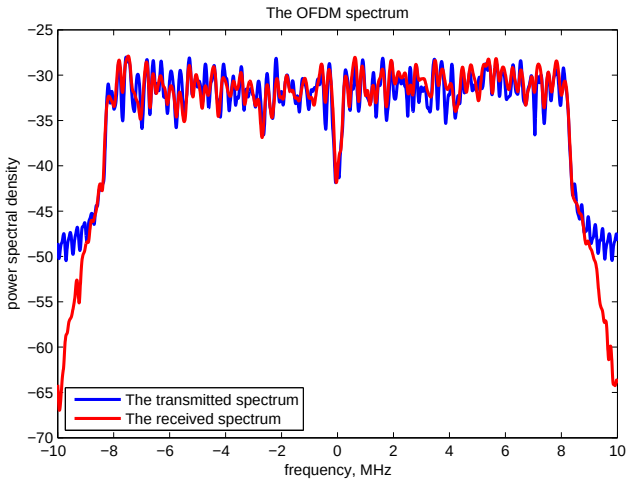

Figure 3.20: A comparision between the transmitted and measured spectrum of the OFDM signal.

3.4.3.3 A combined frequency offset estimation and pilot-based Wiener channel estimation

Here we discuss a joint scheme for the frequency offset and pilot-based channel estimation in which the frequency offset is first estimated using the autocorrelation function, and then is fined further by applying an iterative phase correction, using pilot-based Wiener filtering method.

Frequency offset estimation

As a consequence of the frequency offsets between the oscillators of the transmitter and the receiver, phase errors and ICI occur on the received signal and lead to degrading the OFDM system performance. The frequency offset can be estimated from the autocorrelation of the training symbols in the preamble. If there is a frequency offset f_e, the autocorrelation function will be modified by the phase error as

$$Z(n) = e^{-j2\pi f_e N_{TS}} \sum_{c=0}^{N_{TS}-1} |y(n+c)|^2. \tag{3.30}$$

The phase introduced by the frequency offset is calculated as

$$\phi = \angle Z(n)$$

The course frequency offset CFO is calculated in case of the short symbols as

$$f_e = \frac{\phi}{2\pi 16T}, \tag{3.31}$$

where T is the sampling time which is (50 ns) for WLAN system. The expected frequency offset values lies between -625 KHz and 625 KHz [89]. For fine frequency offset FFO estimation, the long symbols are used, which gives a fine estimation lies between -156.25 KHz and 156.25 KHz. For better frequency offset estimation, the estimation is accomplished in two stages CFO and then FFO estimations.

Phase correction using Wiener filtering

After the compensation of the frequency offset, the Wiener filtering method described in Section 3.1.2 is applied to further fining the frequency offset and correcting for the phase rotation, and at the same time equalizing the OFDM symbols. An iterative scheme is applied to find the phase error that minimizes the following cost function

$$MSE = E\{|\underline{\mathbf{S}}_p - \hat{\underline{\mathbf{S}}}_p|^2\} \tag{3.32}$$

where $\underline{\mathbf{S}}_p$ and $\hat{\underline{\mathbf{S}}}_p$ are vectors contain the transmitted and equalized pilots. $\hat{\underline{\mathbf{S}}}_p$ is estimated using LS criterion as follows

$$\hat{\underline{\mathbf{S}}}_p = \mathcal{D}(\hat{\underline{\mathbf{H}}}_p)^{-1}\underline{\mathbf{Y}}_p \tag{3.33}$$

where $\underline{\mathbf{Y}}_p$ is the received pilots and $\hat{\underline{\mathbf{H}}}_p$ is the estimated CTF, which is estimated by Wiener filtering of the received signal as follows

$$\hat{H}_p = (\mathbf{R}_p^{-1}\underline{\mathbf{P}}_p)^H \underline{\mathbf{Y}}_p \tag{3.34}$$

According to (3.9) and (3.10), the autocorrelation $\mathbf{R}_p$ and the cross-correlation $\underline{\mathbf{P}}_p$ contain the delay τ_l of each channel tap. In order to correct the phase rotation, the scheme is searching for τ_0 that minimizes (3.32). Fig. 3.21 illustrates the constellation of the equalized 16 QAM modulated OFDM symbols with different transmitted power. For simplicity, we used pilot carriers with same magnitude. Fig. 3.22 shows an example of

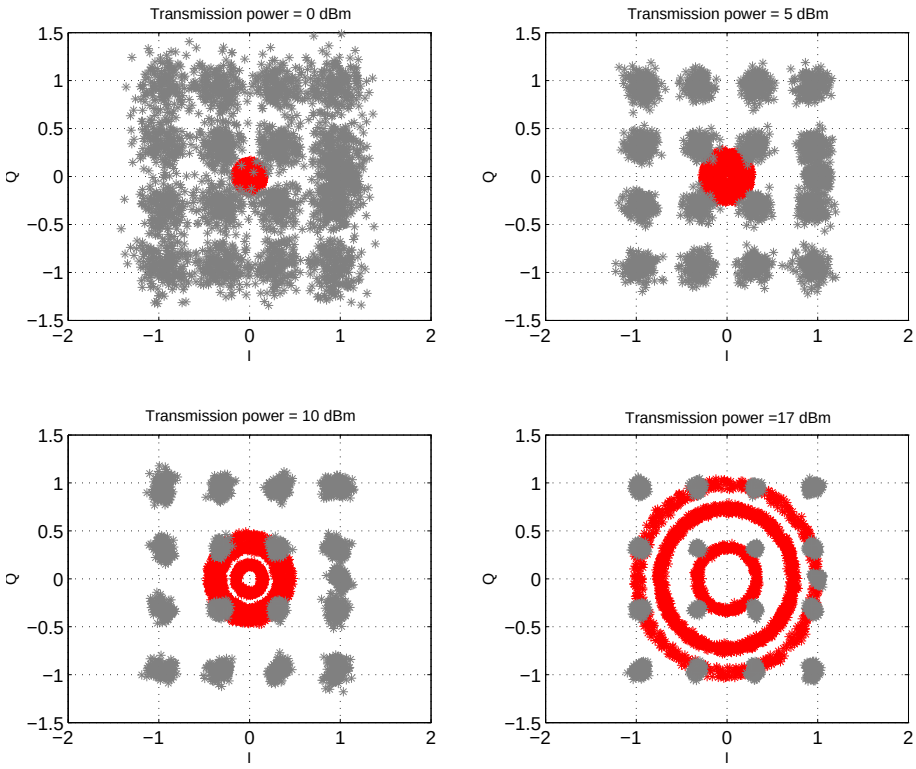

Figure 3.21: The constellation of the equalized 16 QAM modulated OFDM symbols with different transmission power at distance (d = 2 m). Red: Received symbols, Gray: Equalized symbols.

transmitting and receiving a gray scaled image through the wireless channel. The size of the image was 5.4 KB, which required 756 OFDM symbols coded by a convolutional encoder with coding rate of $R = 0.5$. Table 3.3 and Fig. 3.23 represent the measured BER and MSE for different transmission power using 16 QAM modulation scheme for antenna separation of 2 m. Table 3.4 and Fig. 3.24 represent the measured BER and MSE for different transmission power using 4 QAM modulation scheme for antenna separation of 2 m. Fig. 3.25 illustrates the measured MSE of the received OFDM symbols for 16 QAM at transmission power of 17 dBm and variant distance between the transmitter and the receiver. It can be seen from the figure that in addition to the path loss, the signal gets attenuated (shadowed) at certain distances because of the multipath effect.

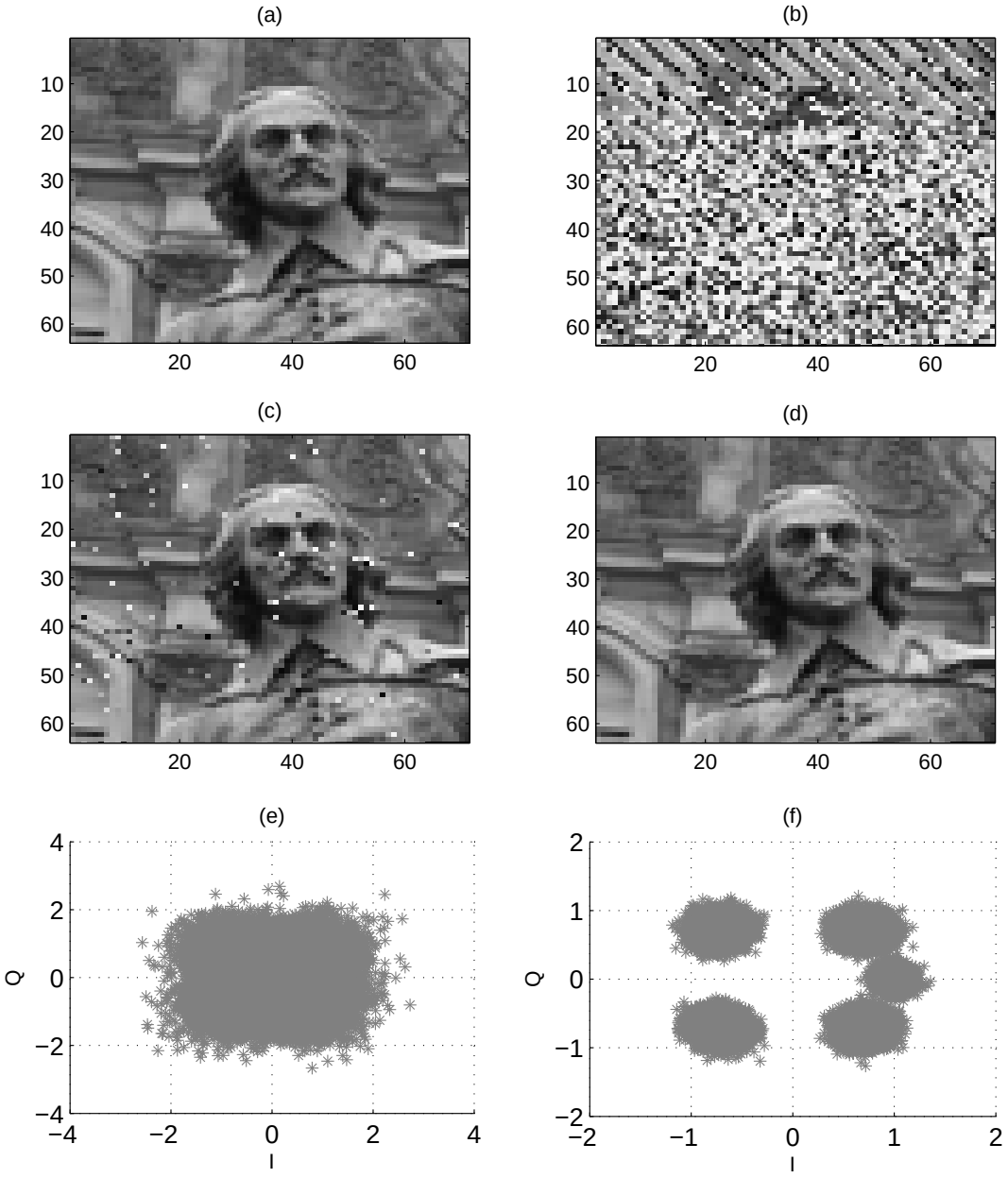

Figure 3.22: An example of transmitting a gray scaled image through the wireless channel; (a): The transmitted image, (b): The received un-equalized image, (c): The equalized image with a transmission power -10 dBm, (d): The equalized image with a transmission power 0 dBm, (e): The constellation of the equalized image with -10 dBm power, (f): The constellation of the equalized image with 0 dBm power.

Table 3.3: The measured system performance with 16 QAM modulation scheme

Transmission power (dBm)	MSE (dB)	BER
-10	-5.5000	.213
-5	-10.0000	.0771
0	-14.5000	.0093
5	-18.9500	2.5431e-5
10	-23.5000	0

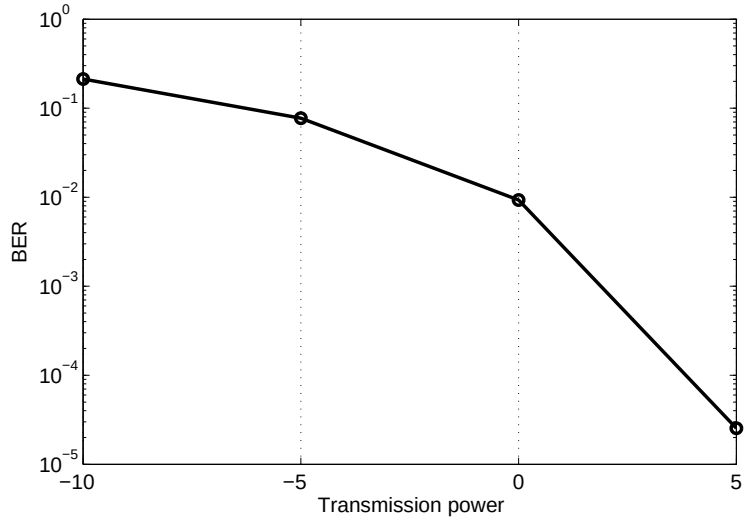

Figure 3.23: The measured BER versus the transmission power with modulation scheme 16 QAM at distance (d = 2 m).

Table 3.4: The measured system performance with 4 QAM modulation scheme

Transmission power (dBm)	MSE (dB)	BER
-5	-11.5	2.84e-4
0	-16	0
5	-21.2	0
7	-22.772	0
10	-26.5	0

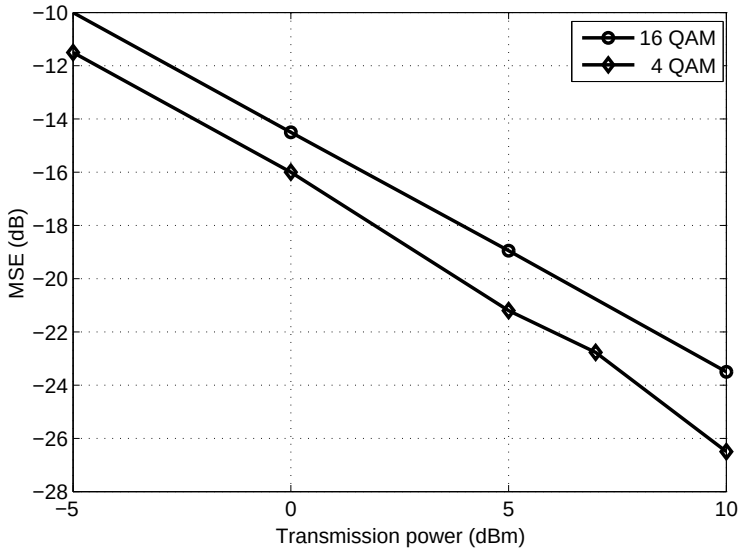

Figure 3.24: The measured MSE of the OFDM symbols versus the transmission power with modulation scheme 16 QAM and 4 QAM at distance (d = 2 m).

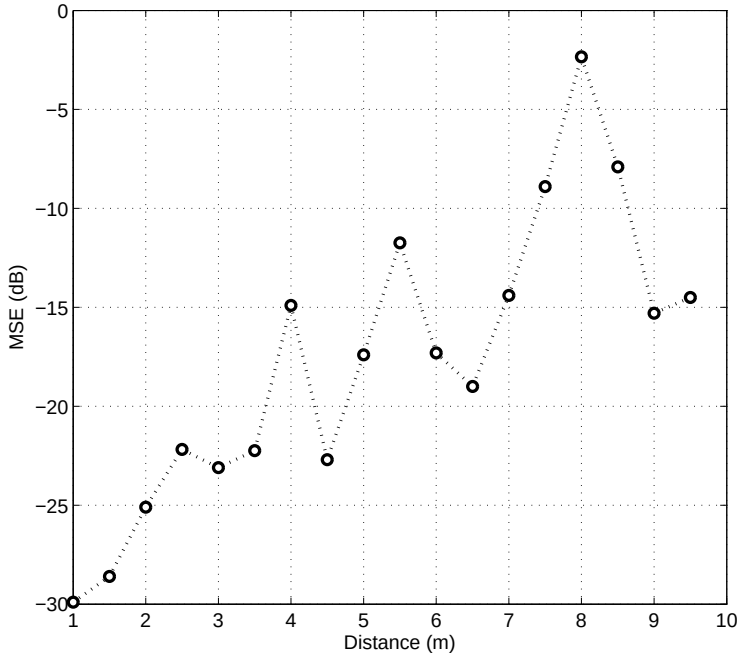

Figure 3.25: The measured MSE of the OFDM symbols versus the distance between the transmitter and the receiver with modulation scheme 16 QAM and transmission power 17 dBm.

Chapter 4

Low Complexity ICI Reduction for OFDM Systems

During the last decade, ICI cancellation in OFDM systems has gained a great interest in the literature motivated by the need for transmitting high data rates at high mobility scenarios. Several algorithms [90–101] have been proposed to reduce the effect of ICI in OFDM systems in case of slowly and rabidly time-variant channels. Authors in [91] used the autocorrelation of the weighting ICI function to estimate the phase noise in OFDM systems. In [93] a linear approximation method has been introduced for canceling the effect of ICI. In [94] a self-cancellation scheme for ICI caused by frequency offset has been developed. In general, ICI can be introduced either by the frequency offsets between the local oscillators of the transmitter and the receiver, the phase noise of these oscillators due to the thermal effects, or the Doppler frequency shift due to the mobility. In this thesis, only the ICI caused by Doppler shifts due to the dynamic nature of the communication channel is studied.

This chapter is organized as follows: Section 4.1 and Section 4.2 explain the time variation of the channel, and it also discusses and analyzes the ICI generation for DRM system and its influence on the channel matrix and the system performance. Section 4.3 introduces a new scheme for cancelling the ICI coefficients in rapidly time-variant channels using numerical approximation. The proposed scheme makes use of Taylor, Lagrange, and Newton polynomial approximation methods. The results of this algorithm is presented in Section 4.4. Section 4.5 introduces a method to reduce the complexity of the ICI reduction process. The complexity reduction is achieved by windowing the received time domain signal of the DRM system and thereby squeezing the channel matrix.

4.1 The Generation Mechanism of ICI

As it has been described earlier, the ICI phenomenon complicates the reception process by destroying the diagonality of the frequency domain channel matrix $\mathbf{H}$. As a consequence of ICI, the time domain channel matrix $\mathbf{h}$ loses its circularity. The relation between the channel matrix in time domain $\mathbf{h}$ and in frequency domain $\mathbf{H}$ has been discussed in Chapter 2, which reads

$$\mathbf{H} = \mathbf{F}\mathbf{h}\mathbf{F}^{H}, \tag{4.1}$$

where the element (l, n) of $\mathbf{h}$ is given by

$$h_{l,n} = h(< n - l >_N, n) \tag{4.2}$$

where $< \cdot >$ denotes the modulo operator. In principle, $h(l, n)$ is defined as the channel response at time n of an impulse applied at time $n - l$. In the frequency domain, the

off-diagonals of the frequency domain channel matrix **H** represent the ICI coefficients. To understand the ICI phenomenon, we introduce the diagonal index d so that $H_{k,d}$ represents the channel matrix coefficient at carrier k and diagonal d, where $-N+1 < d < N-1$. Note that $d = 0$ denotes the main diagonal of the matrix. The element (k, d) of the matrix can be written as

$$H_{k,d} = T(k, d-k) \tag{4.3}$$

$T(k, d)$ is interpreted as the frequency response at carrier $k+d$ to a frequency impulse centered at carrier k. It can be seen that $T(k, d)$ is the digital form of the Doppler-variant transfer function discussed in Chapter 2, i.e. $T(k, d) \equiv T(f, \mathrm{v})$, which can be obtained by applying the 2-D DFT on the time-variant channel impulse response $h(l, n)$

$$T(k, d) = \frac{1}{N} \sum_{n=0}^{N-1} \sum_{l=0}^{N-1} h(l, n) e^{-j\frac{2\pi}{N}(dn+lk)} \tag{4.4}$$

Notice that $h(l, n) = 0$ for $l > L$, where L is the number of channel paths. According to the WSSUS assumption, the autocorrelation of the channel impulse response $h(l, n)$ is given by

$$E\big\{h(l, n)h^*(l-l', n-n')\big\} = a(n')\sigma_l^2\delta(l'), \tag{4.5}$$

where $\delta(l')$ is the Kronecker delta and $a(n')$ is the channel autocorrelation function. For DRM channel models, this function has the following form

$$a(n') = e^{-\pi^2 f_D^2 n'^2/2} \tag{4.6}$$

where f_D is the normalized Doppler spread ($f_d T_s$). The distribution of ICI can be obtained by calculating the variance of $H_{k,d}$ [102]

$$\begin{aligned} E\{|H_{k,d}|^2\} &= \tfrac{1}{N^2} \textstyle\sum_{n,l,n',l'} w_n w_{n-n'} E\big\{h(l, n)h^*(l-l', n-n')\big\} e^{-j\frac{2\pi}{N}(kl'+n'd)} \\ &= \tfrac{\alpha^2}{N^2} \textstyle\sum_{n'} \Big(\sum_n w_n w_{n-n'}\Big) a(n')\delta(l') e^{-j\frac{2\pi}{N}(kl'+n'd)} \\ &= \tfrac{\alpha^2}{N^2} \textstyle\sum_{n'} \Big(\sum_n w_n w_{n-n'}\Big) a(n') e^{-j\frac{2\pi}{N}n'd} \end{aligned} \tag{4.7}$$

where

$$\delta(l') = \begin{cases} 1 & \text{for} \quad l' = 0 \\ 0 & \quad\ \text{else} \end{cases}$$

Both w_n and $w_{n-n'}$ are rectangular time domain windows that determine the useful part of the channel response and α^2 is the summation of the variances for all paths

$$\alpha^2 = \sum_{l=0}^{L-1} \sigma_l^2.$$

It can also be seen from (4.7) that ICI is independent of the carrier index k. The convolution in (4.7) between two rectangular windows w_n and $w_{n-n'}$ produces a triangular window $b_{n'}$, which is defined as

$$b_{n'} = \begin{cases} N - |n'|, & -N < n' < N \\ 0, & \text{else} \end{cases}$$

thus, (4.7) is rewritten as follows

$$E\{|H_{k,d}|^2\} = \frac{\alpha^2}{N^2}\sum_{n'} b_{n'}a(n')e^{-j\frac{2\pi}{N}n'd} \tag{4.8}$$

$$= \alpha^2 D(\frac{2\pi}{N}d) * B(\frac{2\pi}{N}d) \tag{4.9}$$

where $D(\frac{2\pi}{N}d)$ denotes the Doppler spectrum, which is the discrete time Fourier transform (DTFT) of the autocorrelation function. For $\phi = \frac{2\pi d}{N}$, one can write

$$D(\phi) = \sum_{n'} a(n')e^{-j\phi n'} = \sum_{n'} e^{-\pi^2 f_D^2 n'^2/2}e^{-j\phi n'} = \frac{1}{\sqrt{2\pi f_D^2}}e^{\frac{-\phi^2}{2f_D^2}}.$$

While $B(\frac{2\pi}{N}d)$ denotes the so called Dirichlet sinc [103], which is the DTFT of $\frac{b_{n'}}{N^2}$

$$B(\phi) = \frac{1}{N^2}\sum_{n'} b_{n'}e^{-j\phi n'} = \Big(\frac{\sin(\frac{\phi N}{2})}{N\sin(\frac{\phi}{2})}\Big)^2.$$

We notice that ICI is a result of a convolution between Doppler spectral density $D(\phi)$ and Dirichlet sinc $B(\phi)$.

$$E\{|H_{k,d}|^2\} = \frac{\alpha^2}{\sqrt{2\pi f_D^2}}e^{\frac{-\phi^2}{2f_D^2}} * \Big(\frac{\sin(\frac{\phi N}{2})}{N\sin(\frac{\phi}{2})}\Big)^2\Big|_{\phi=\frac{2\pi}{N}d} \tag{4.10}$$

Fig. 4.1 sketches the two functions that are responsible for ICI generation. Fig. 4.2 shows

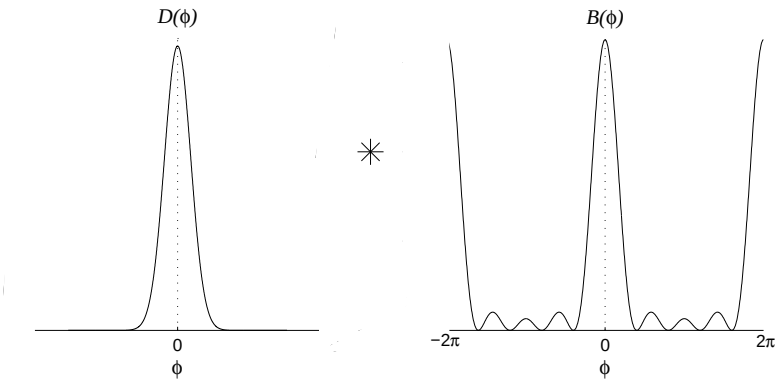

Figure 4.1: The convolution between Doppler spectral density and Dirichlet sinc.

the calculated variance of the channel matrix for different Doppler spread values. It can be shown that, the span (the width) of the channel matrix around the main diagonal is related to the Doppler spread. Fig. 4.3 illustrates the channel matrix coefficients calculated according to (4.10) at a normalized Doppler spread ($f_D = 0.08$), while Fig. 4.4 shows the channel matrix at ($f_D = 0.4$). From the previous figures, one can observe that the carrier of interest is strongly interfered by the adjacent carriers, whereas this

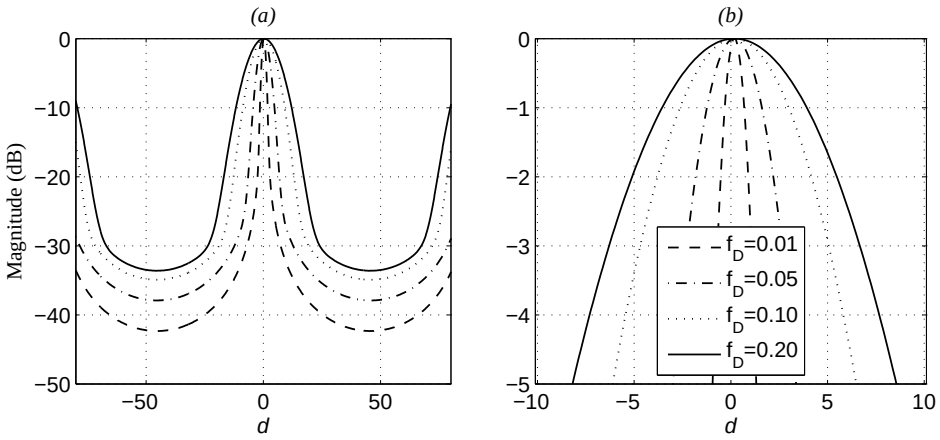

Figure 4.2: The calculated variance of $H_{.,d}$ for different Doppler spreads, (b): Zoomed version of (a).

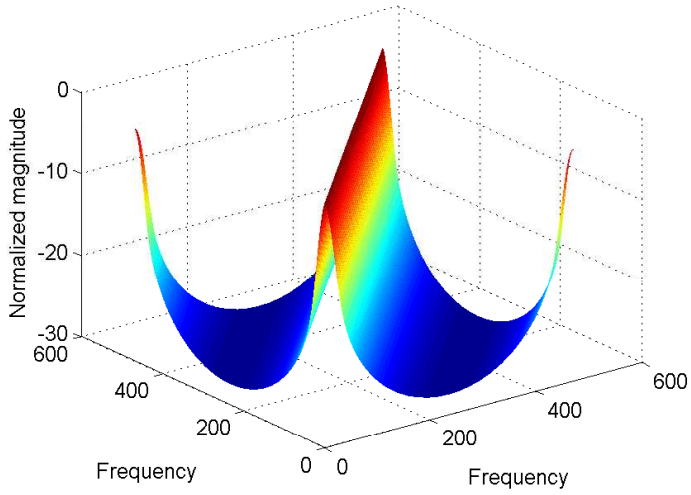

Figure 4.3: The calculated variance of $\mathbf{H}$ at Doppler spread $f_D = 0.08$.

interference is less from the far carriers. Also as a consequence of Dirichlet sinc, last carriers are affected by the first ones, which appears at the upper right and lower left corners of the channel matrix. In practical systems, a frequency guard interval is required for masking purposes, which is usually inserted as padded zeros on both sides of the signal spectrum. This guard interval also reduces the values of the ICI coefficients at the corners. Fig. 4.5 compares between a simulated channel matrix in the presence and absence of the padded zeros. The simulated system is a DRM system with robustness mode "B", which has 1024 carriers including 932 virtual carriers (zeros).

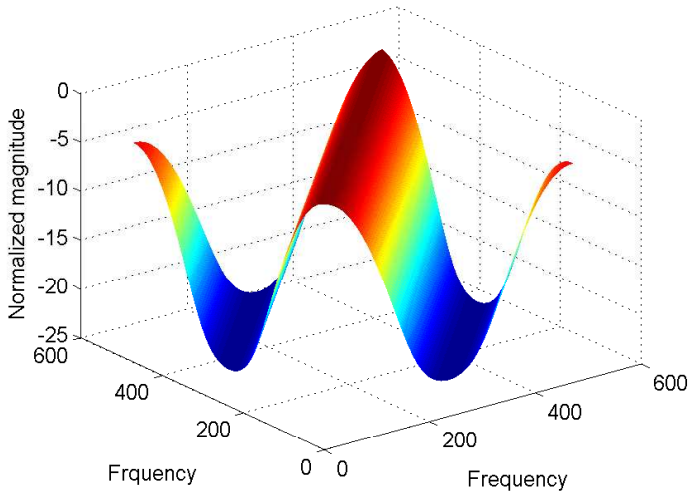

Figure 4.4: The calculated variance of $\mathbf{H}$ at Doppler spread $f_D = 0.4$.

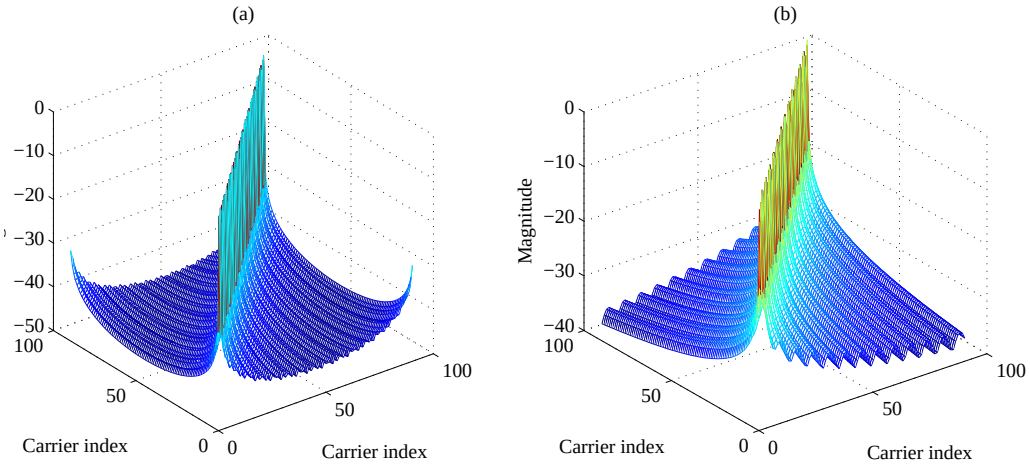

Figure 4.5: The effect of zero padding on the simulated channel matrix; (a): No padding, (b): 466 zeros at each side.

4.2 Effect of ICI on System Performance

Basically, ICI can be treated as an additional source of noise in OFDM systems, which modifies the SNR at the receiver. By including the interference effect, the SNR at the receiver is called SINR (signal-to-noise plus interference ratio) which reads

$$\text{SINR} = \frac{\text{Signal power}}{\text{Noise power} + \text{Interference power}} \tag{4.11}$$

As the input SNR increases the output SNR gets saturated according to the level of the ICI power, since the ICI dominates the noise. This introduces an error floor in the BER performance. In the presence of frequency offset, the resulting SNR can be written [15]

as

$$\mathrm{SINR} = \mathrm{SNR}\frac{\mathrm{sinc}^2(f_e T_s)}{1 + \mathrm{SNR}\sum_{k=0,k\neq m}^{N-1}\mathrm{sinc}^2(k-m+f_e T_s)} \tag{4.12}$$

where f_e is the frequency offset from the carrier frequency. Fig. 4.6 shows the calculated distortion in the SNR resulting from frequency offset according to (4.12) in case of using the WLAN system parameters. The effect of ICI on the simulated DRM system due to

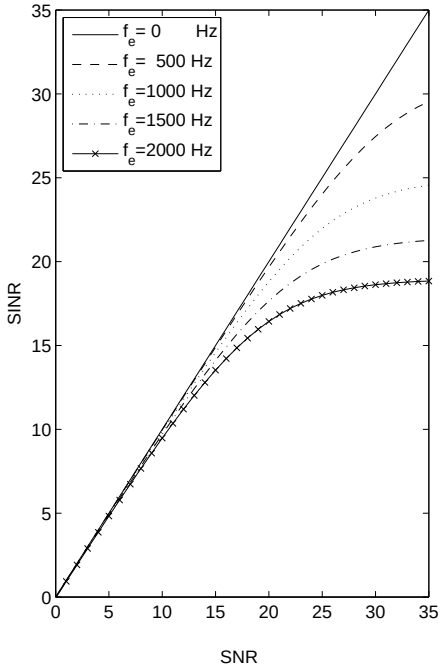

Figure 4.6: SNR vs. SINR of WLAN system for different Doppler spreads.

Doppler shifts is depicted in Fig. 4.7, which shows the significant loss in the SNR. SINR has been calculated from the channel matrix $\mathbf{H}$ as follows

$$\mathrm{SINR} = \frac{\|\mathbf{H}_{di}\|_F^2}{\|\mathbf{H}_{\bar{di}}\|_F^2 + \sigma_v^2}, \tag{4.13}$$

where $\mathbf{H}_{di}$ and $\mathbf{H}_{\bar{di}}$ are the diagonal matrix that contains only the main diagonal and the complementary matrix [1], respectively. $\|\cdot\|_F$ is the Frobenius norm of a matrix. The system performance for different Doppler spread values appears in Fig. 4.8.
Since the exact time-domain correlation or the power spectrum is not available at the receiver, the ICI power can be approximated by its upper and lower bounds. It has been proven in [104] that the ICI power is bounded by the following values

$$P_{ICI} \geq \frac{1}{12}(2\pi f_d T_s)^2 - \frac{1}{360}(2\pi f_d T_s)^4 \tag{4.14}$$

$$P_{ICI} \leq \frac{1}{12}(2\pi f_d T_s)^2 \tag{4.15}$$

[1] A matrix contains only the off-diagonals of the channel matrix.

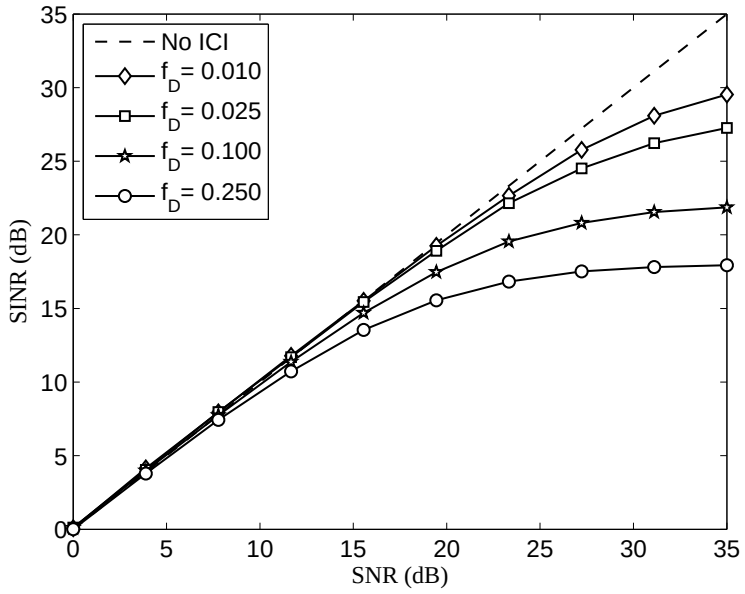

Figure 4.7: SNR vs. SINR of a simulated DRM system for different Doppler spreads.

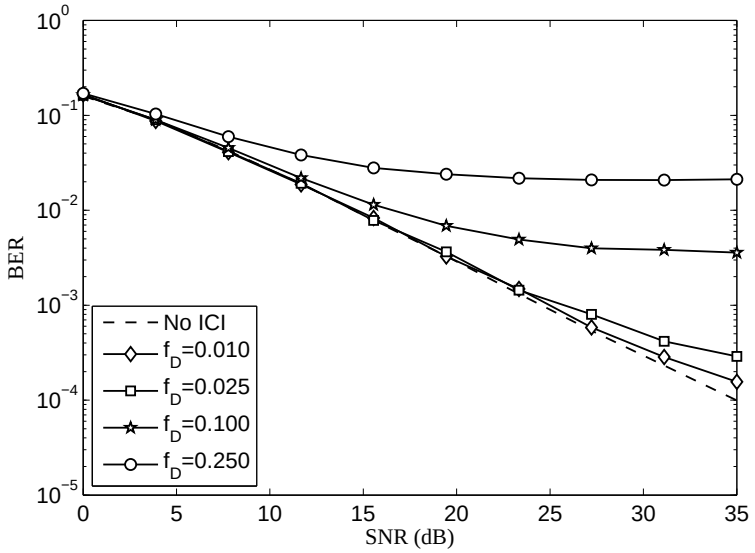

Figure 4.8: The effect of ICI on the BER performance for different Doppler spreads.

These bounds can be used directly to roughly estimate the Doppler spread at the receiver by having the ICI power.

4.3 Channel Matrix Estimation

Time-variant channels degrade the performance of OFDM systems because they collapse the orthogonality between the sub-carriers. This problem necessitates estimating the whole channel matrix in order to cancel the effect of ICI and to properly equalize the

received signal. The channel elements can be estimated efficiently using a pilot-based two-dimensional Wiener filter [75]. However, estimating the whole channel matrix requires high computational effort specially for large number of sub-carriers, therefor lower complexity methods are required for systems with large number of carriers, which is the case for most digital broadcasting systems in which the number of carriers can exceed 8000 carriers. In this section, we present some numerical methods to estimate the channel matrix for OFDM systems in rapidly time-variant channels, making advantage of approximating the time variation of the channel $U(k,n)$ over a few successive OFDM symbols. The main diagonal of $\mathbf{H}$ can be estimated and interpolated using one-dimensional Wiener filter [75], which reads

$$\hat{H}_{k,k} = \underline{\mathbf{W}}^{\mathtt{H}}_{k,k}\underline{\mathbf{Y}},$$

where $\underline{\mathbf{W}}_{k,k}$ is a Wiener filter vector related to the k^{th} element at the main diagonal of $\mathbf{H}$. From (2.31), it is obvious that $H_{k,k}$ is the averaged value of $U(k,n)$ over n index (time direction), and can be

$$H_{k,k} = \frac{1}{N}\sum_{n=0}^{N-1} U(k,n) = \overline{U}(k). \tag{4.16}$$

The off-diagonals of $\mathbf{H}$ can be estimated using an approximation of $U(k,n)$ between Q saved main diagonals corresponding to Q successive OFDM symbols. Fig. 4.9 sketches the approximation of the time-variant channel over few OFDM symbols. The positions

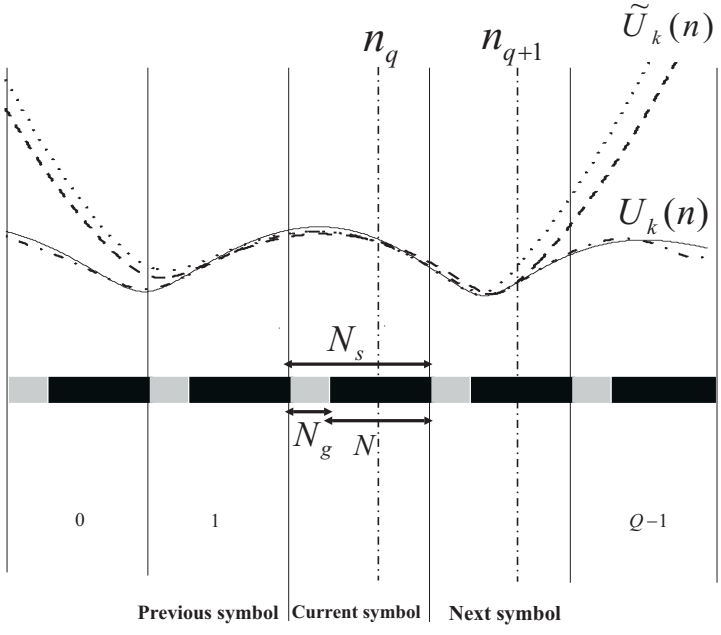

Figure 4.9: Channel approximation over Q symbols.

of n_q are chosen at the middle of the useful part of each symbol as

$$n_q = qN_s + \frac{N}{2} + N_g. \tag{4.17}$$

Where N, N_g, and N_s are the useful part length, guard interval length, and the total length of the OFDM symbol, respectively. Basically, any approximation method can be

used for estimating the channel matrix. However, they differ in the accuracy and the complexity. Here, we discuss three of the common polynomial approximation methods.

Taylor polynomial approximation

Taylor polynomial approximation is widely used for the numerical approximation making use of knowing a few samples of the function at certain distances. By considering a Taylor expansion one can write

$$U(k,n) = \overline{U}(k) + \frac{(n-\frac{N-1}{2})\overline{U}(k)'}{1!} + \frac{(n-\frac{N-1}{2})^2\overline{U}(k)''}{2!} + ... \\ + \frac{(n-\frac{N-1}{2})^Q\overline{U}(k)^{(Q)}}{Q!} + ... \tag{4.18}$$

where $\overline{U}(k)^{(Q)}$ is the Q^{th} derivative of $\overline{U}(k)$ at the central point of the approximation period. If we define $\overline{U}(k)^{[0]}$ and $\overline{U}(k)^{[\pm i]}$ as $\overline{U}(k)$ at the current symbol and the next and the previous symbols respectively, these derivatives can be expressed using the central difference formulas for $Q = 3$ as

$$\overline{U}(k)' \approx \frac{\overline{U}(k)^{[+1]} - \overline{U}(k)^{[-1]}}{2N_s}, \tag{4.19}$$

$$\overline{U}(k)'' \approx \frac{\overline{U}(k)^{[-1]} - 2\overline{U}(k)^{[0]} + \overline{U}(k)^{[+1]}}{N_s^2}. \tag{4.20}$$

And for $Q = 5$ as

$$\overline{U}(k)' \approx \frac{\overline{U}(k)^{[-2]} - 8\overline{U}(k)^{[-1]} + 8\overline{U}(k)^{[+1]} - \overline{U}(k)^{[+2]}}{12N_s}, \tag{4.21}$$

$$\overline{U}(k)'' \approx \frac{-\overline{U}(k)^{[+2]} + 16\overline{U}(k)^{[+1]} - 30\overline{U}(k)^{[0]} + 16\overline{U}(k)^{[-1]} - \overline{U}(k)^{[-2]}}{12N_s^2} \tag{4.22}$$

$$\overline{U}(k)^{(3)} \approx \frac{\overline{U}(k)^{[+2]} - 2\overline{U}(k)^{[+1]} + 2\overline{U}(k)^{[-1]} - \overline{U}(k)^{[-2]}}{2N_s^3} \tag{4.23}$$

$$\overline{U}(k)^{(4)} \approx \frac{\overline{U}(k)^{[+2]} - 4\overline{U}(k)^{[+1]} + 6\overline{U}(k)^{[0]} - 4\overline{U}(k)^{[-1]} + \overline{U}(k)^{[-2]}}{N_s^4} \tag{4.24}$$

N_s is the total OFDM symbol duration. The more terms of Taylor equation are considered in the approximation, the more accurate approximation is obtained. Once the approximated $U(k,n)$ is calculated, the channel matrix $\mathbf{H}$ is estimated relying on (2.31). The remainder term of the Taylor approximation method can be expressed as follows

$$R_Q = \frac{U^{(Q+1)}(c)}{(Q+1)!}(n-n_Q)^{Q+1}, \tag{4.25}$$

where c is a point belongs to the approximation period, $c \in [0,(Q-1)N_s]$. It can be concluded that the error of an approximation up to the Q^{th} derivative is bounded by the $(Q+1)^{th}$ derivative.

Newton polynomial approximation

According to Newton interpolation [73], the time varying channel weights $U(k,n)$ can be expressed as

$$U(k,n) = P(k,n) + R(k,n), \tag{4.26}$$

where $P(k,n)$ is a Newton polynomial that can be used to approximate $U(k,n)$, and $R(k,n)$ is the remainder term. The approximated time-varying channel by considering only $P(k,n)$ is written as

$$\begin{gathered}\tilde{U}(k,n) = P(k,n) = \\ A_{-\frac{(Q-1)}{2}} + A_{-\frac{(Q-1)}{2}+1}(n - n_{-\frac{(Q-1)}{2}})+ \\ A_{-\frac{(Q-1)}{2}+2}(n - n_{-\frac{(Q-1)}{2}})(n - n_{-\frac{(Q-1)}{2}+1})+ \\ A_{-\frac{(Q-1)}{2}+3}(n - n_{-\frac{(Q-1)}{2}})(n - n_{-\frac{(Q-1)}{2}+1}) \\ (n - n_{-\frac{(Q-1)}{2}+2}) + \cdots + A_{\frac{(Q-1)}{2}} \prod_{q=-\frac{(Q-1)}{2}}^{\frac{(Q-3)}{2}} (n - n_q)\end{gathered} \tag{4.27}$$

where $q = -\frac{(Q-1)}{2}, -\frac{(Q-1)}{2}+1, ..., \frac{(Q-1)}{2}$ is the index of the symbols used for the approximation, where $q = 0$ is the index of the current symbol, at which the channel matrix is estimated. Q represents the degree of the Newton polynomial. Notice that previous and next symbols are used for approximating the channel on the current symbol. The positions of the time points n_q are chosen at the middle of the useful part of each symbol. This reads $n_q = qN_s + \frac{N}{2}$ for previous symbols, where $q = 0, 1, ..., \frac{(Q-1)}{2}$, and $n_q = (q+1)N_s - (\frac{N}{2} + N_g)$ for next symbols, where $q = -\frac{(Q-1)}{2}, -\frac{(Q-1)}{2}+1, ..., -1$. N, N_g, and N_s denote the useful part length, guard interval length, and the total length of the OFDM symbol, respectively. Let $\overline{U}^{(n_q)}$ represent $\overline{U}(k)$ at the middle of the q^{th} OFDM symbol, with omitting k for simplicity. The terms A_q in (4.27) are given by

$$A_q = \overline{U}^{\left(n_{-\frac{(Q-1)}{2}}, n_{-\frac{(Q-1)}{2}+1}, \cdots, n_q\right)}. \tag{4.28}$$

The right-hand side of (4.28) is calculated in a recursive manner as

$$\overline{U}^{(n_{q-1},n_q)} = \frac{\overline{U}^{(n_q)} - \overline{U}^{(n_{q-1})}}{n_q - n_{q-1}},$$

$$\overline{U}^{(n_{q-2},n_{q-1},n_q)} = \frac{\overline{U}^{(n_{q-1},n_q)} - \overline{U}^{(n_{q-2},n_{q-1})}}{n_q - n_{q-2}},$$

$$\overline{U}^{(n_{q-3},n_{q-2},n_{q-1},n_q)} = \frac{\overline{U}^{(n_{q-2},n_{q-1},n_q)} - \overline{U}^{(n_{q-3},n_{q-2},n_{q-1})}}{n_q - n_{q-3}},$$

... ,

$$\overline{U}^{(n_{q-(Q-1)},n_{q-(Q-1)+1},...,n_q)} =$$

$$\frac{\overline{U}^{(n_{q-(Q-1)+1},\ldots,n_q)} - \overline{U}^{(n_{q-(Q-1)},\ldots,n_{q-1})}}{n_q - n_{q-(Q-1)}}.$$

Finally, $\tilde{U}(k,n)$ is used to estimate the off-diagonals of $\mathbf{H}$ relying on (2.31). Increasing the number of the considered Newton terms reduces the remainder term $R(k,n)$. This remainder term has the following form

$$R_Q = \frac{U^{(Q+1)}(c)}{(Q+1)!}(n-n_0)(n-n_1)(n-n_2)(n-n_3)...(n-n_Q), \tag{4.29}$$

The error term of Newton polynomial approximation is similar to that of Taylor approximation except that in Newton approximation, all points are considered, whereas for Taylor, only a central point is taken into account, at which all derivatives are calculated. Fig. 4.10 shows the error behavior for both Taylor and Newton approximations by assuming the knowledge of the derivative $U^{Q+1}(c)$ at an arbitrary point c. It can be seen

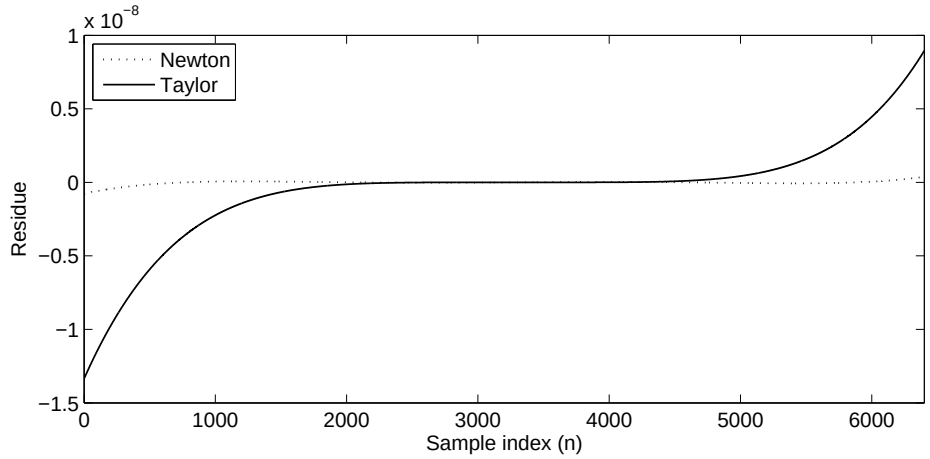

Figure 4.10: The remainder term of the channel approximation, Q=5.

from the figure that at the edges of the approximation duration, the error for Taylor polynomial is larger.

Lagrange polynomial approximation

According to Lagrange polynomial interpolation [73], the time varying channel $U(k,n)$ can be expressed as

$$U(k,n) = P(k,n) + R(k,n), \tag{4.30}$$

$$\widetilde{U}(k,n) = P(k,n) = \textstyle\sum_{q=0}^{Q-1} \overline{U}^{(n_q)} K_q, \tag{4.31}$$

where $\overline{U}^{[n_q]}$ represents $\overline{U}(k)$ at the middle of the q^{th} OFDM symbol with omitting k for simplicity. $q = 0, 1, ..., Q-1$, represents the symbol index of the symbols used for the approximation. K_q is calculated as follows

$$K_q = \prod_{i=0\, i\neq q}^{Q-1} \frac{n-n_q}{n_q-n_i}. \tag{4.32}$$

It is obvious that the accuracy is increased as we consider more OFDM symbols. However, increasing the number of the considered symbols increases the complexity of the system and requires saving more OFDM symbols which causes extra delay. Therefore, a trade-off between the required accuracy and the allowed delay must be taken into account.

Keeping the Processing Delay by Extrapolation

One possible way to increase the accuracy of the approximation without causing extra delay is by applying extrapolation method. This is done by adding extra virtual points at both sides of the approximation period QN_s. The channel at the extra points can be extrapolated by linear or higher order extrapolations making use of the known points as follows

$$\begin{pmatrix} l_1 \\ l_2 \\ \vdots \\ l_{p+1} \end{pmatrix} = \begin{pmatrix} n_{Q-p}^{p} & n_{Q-p}^{p-1} & \dots & 1 \\ n_{Q-p+1}^{p} & \dots & \dots & 1 \\ \vdots & \vdots & \vdots & 1 \\ n_{Q}^{p} & n_{Q}^{p-1} & \dots & 1 \end{pmatrix}^{-1} \begin{pmatrix} \overline{U}^{[Q-p]}(k) \\ \overline{U}^{[Q-p+1]}(k) \\ \vdots \\ \overline{U}^{[Q]}(k) \end{pmatrix} \tag{4.33}$$

$$\overline{U}^{[Q+1]}(k) = l_1 n_{Q+1}^{p} + l_2 n_{Q+1}^{p-1} + \ldots + l_{p+1} \tag{4.34}$$

where p is the extrapolation degree. The degree of the extrapolator must be chosen carefully, since using high degree polynomials may increase the estimation error. This related to the so called Runge's phenomenon [105], specially when the points are positioned at equidistance, which is the case here.

4.4 Simulation Results

In the simulation, a DRM system [36] with a robustness mode "B" and spectral occupancy "0" has been used. The system parameters are summarized in table 4.1. The

Table 4.1: System parameters: (mode B, spectral occupancy 0)

Parameter	Value
Modulation scheme	uncoded 64 QAM
Number of Carriers	91
FFT length	1024
Guard interval	256
Bandwidth	4.5 KHz

i.i.d OFDM symbols were transmitted through a 2-tap time-variant channel[2] with delay spread of 4 ms. Doppler spectrum has a Gaussian shape, which is suitable for radio propagation through the ionosphere. Doppler spread of both taps changes between 0 to 14 Hz which corresponds to mobile speeds from 0 to 252 Km/h at carrier frequency of 30 MHz. During the simulations, the knowledge of the main diagonal was assumed for

[2]This channel is the channel #5 of the European telecommunications standards institute (ETSI) for DRM system [36].

simplicity. Fig. 4.11 addresses the BER against the normalized Doppler spread (f_dT_s) for Taylor approximation method at SNR = 45 dB. In general, by using more Taylor terms, the system performance can be improved. However, increasing the number of the considered terms leads to higher computational complexity and the delay. Therefore, a trade-off between the required system performance and the computational complexity must be taken into account. It has been noticed that the approximation method is valid as long as Doppler spread is less than the frequency spacing between the sub-carriers Δf, which is according to the chosen system parameters (Δf= 46.8750 Hz). This method gives the maximum improvement when f_D varies between 0.1-0.2 (67-135 Km/h). It has

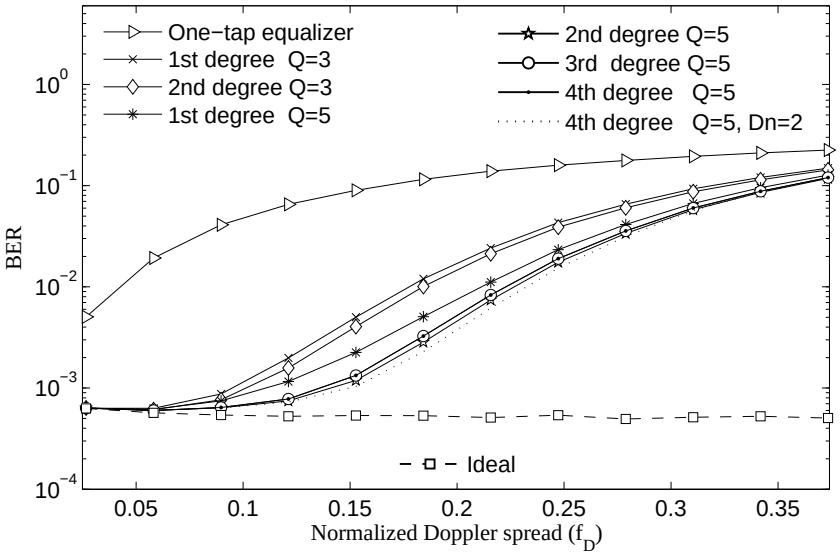

Figure 4.11: BER vs. Normalized Doppler spread for Taylor approximation at SNR=45 dB.

been noticed that the approximation using the second derivative with five symbols (Q=5) (4.22) outperforms the case of using the third and fourth derivatives, (4.23) and (4.24), respectively. The reason is that the truncation error of (4.22) is of order $O(T_s^4)$, i.e. the error goes to zero in the manner of T_s^4, while for (4.24), the error is of order $O(T_s^2)$. This means that at a certain symbol length, (4.22) can give better performance than (4.24) over the symbol of interest. However, (4.24) gives more accurate approximation if we consider the entire approximation period. Making use of the channel approximation at a number of the previous symbols Dn, the performance can be improved as depicted in the figure. Fig. 4.12 demonstrates the averaged MSE of the estimated channel. The MSE is calculated between the actual and approximated channel transfer function for all carriers and time samples as follows

$$MSE = E\Big\{||U(k,n) - \tilde{U}(k,n)||^2\Big\}.$$

The symbol length plays an important role in the approximation scheme. Fig. 4.13 shows the effect of the symbol duration on the MSE performance of the different approximation methods. It can be seen from the figure that the ICI effect increases and thereby the

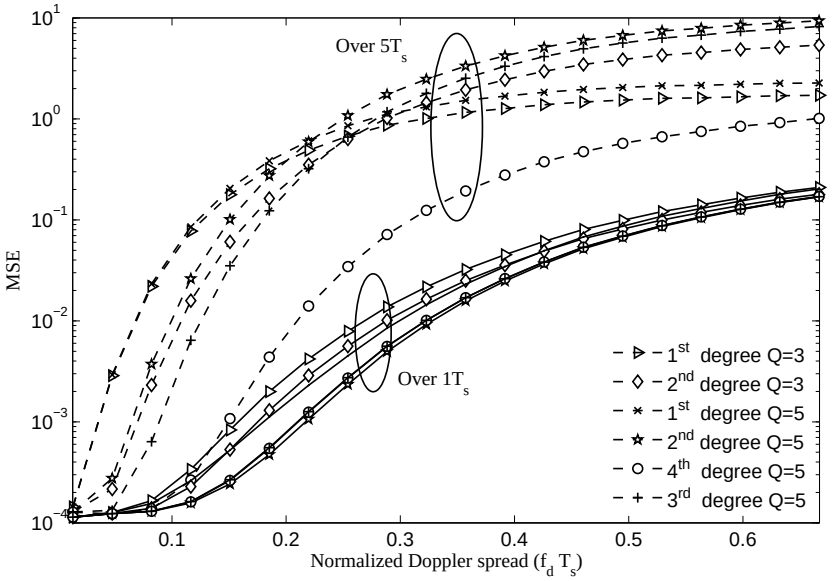

Figure 4.12: MSE vs. Normalized Doppler spread over $Q = 5$ and $Q = 1$ at SNR=45 dB.

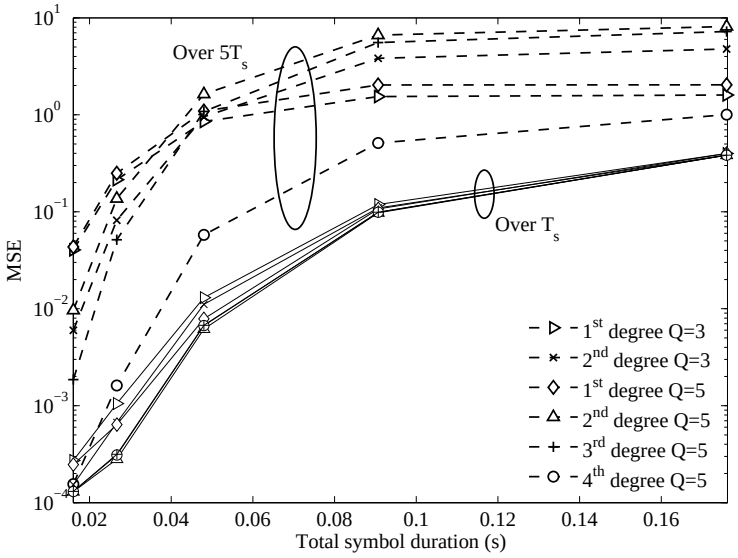

Figure 4.13: MSE vs symbol length in seconds at SNR =45 dB.

approximation accuracy decreases for longer symbol durations. Fig. 4.14 illustrates the MSE performance of Newton polynomial approximation for different Doppler spread values, considering 4 and 5 terms of Newton recursive function. In Fig. 4.15, the BER performance of Lagrange polynomial approximation is studied for varying Doppler spread values. The results show that the proposed method gives a considerable improvement to the BER performance comparing with the Linear model described in [21]. Fig. 4.16 presents the BER of the system for different SNR at Doppler spread of 6 Hz, which is

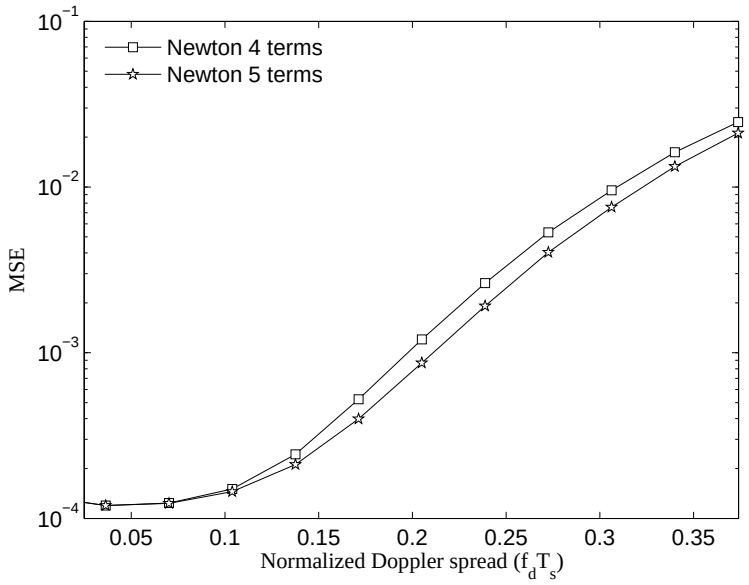

Figure 4.14: MSE vs. Normalized Doppler spread for Newton approximation.

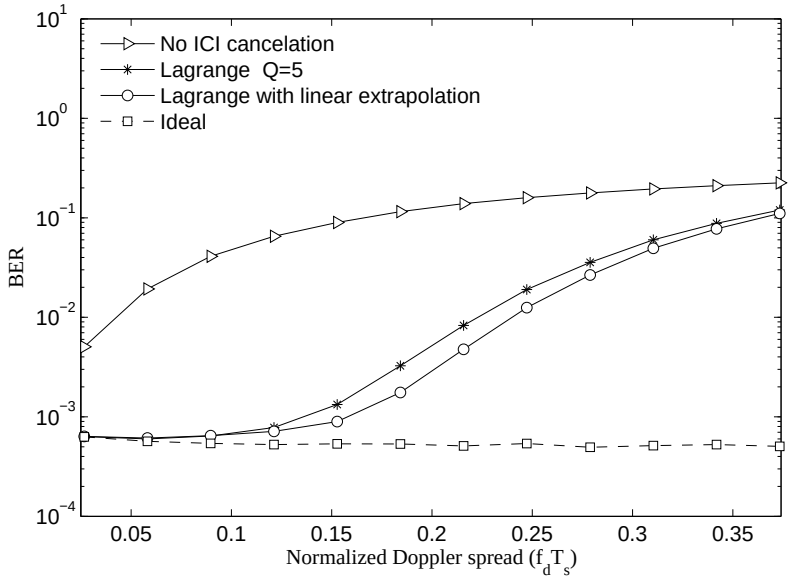

Figure 4.15: BER vs. Normalized Doppler spread for Lagrange approximation.

equivalent to a vehicular speed of 108 Km/h at carrier frequency of 30 MHz. It can be denoted that using only two linearly extrapolated points, a significant improvement can be achieved. Fig. 4.17 demonstrates the MSE comparison between the numerical methods described earlier for different Doppler spread values equivalent to mobile speed in range of $10-250$ Km/h. It can be shown that both Newton and Lagrange approximations schemes perform the same as expected, since they have the same error performance. Making use of the extrapolation, the performance can be further improved without causing extra delay. Fig. 4.18 shows a comparison of the BER. It is noticed that Taylor approximation

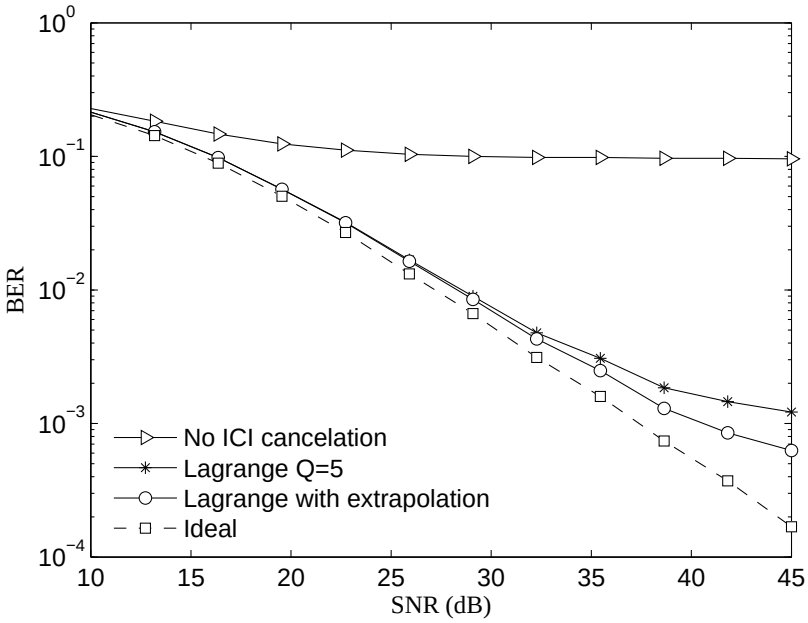

Figure 4.16: BER vs. SNR at Normalized Doppler spread = 0.16.

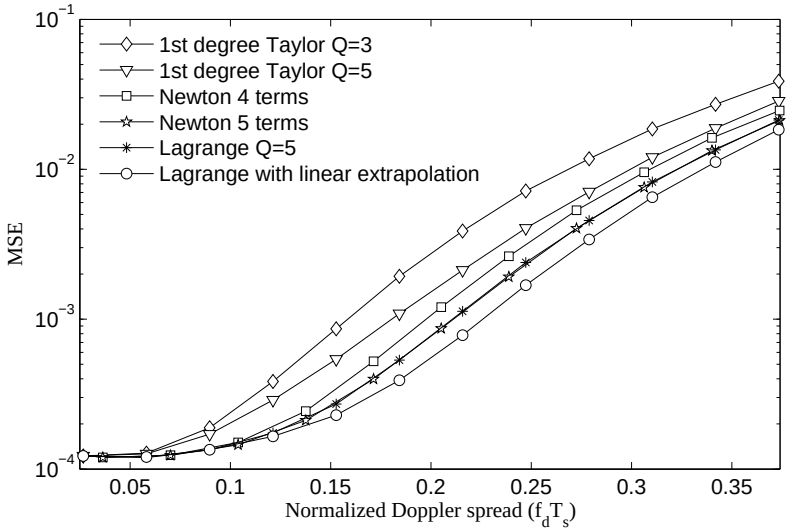

Figure 4.17: Comparison between different polynomial approximation methods.

with 4th derivative performs similar to both Newton and Lagrange for $Q = 5$. Although it is expected that Taylor is less accuracy than Newton and Lagrange. However, for the chosen system parameters, the difference can not be clearly seen. Fig. 4.19 illustrates the estimated channel matrix for different Doppler spreads. The effect of the increase of Doppler spread is clearly seen at the off-diagonals of the matrix. To clearly see the effect of the approximation, an application example has been considered, which is transmitting a gray scaled image through a time-variant channel. Fig. 4.20 shows the transmitted and the unequalized received pictures. Fig. 4.21 shows the equalized picture using different

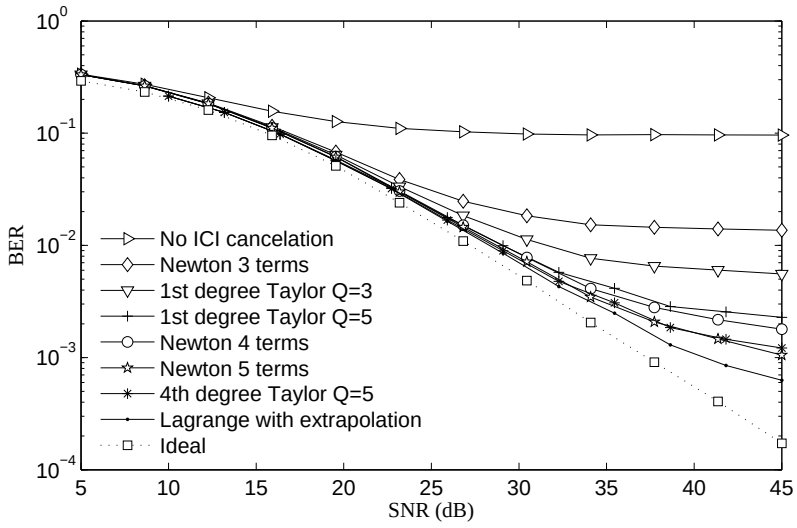

Figure 4.18: BER performance for different polynomial approximation methods.

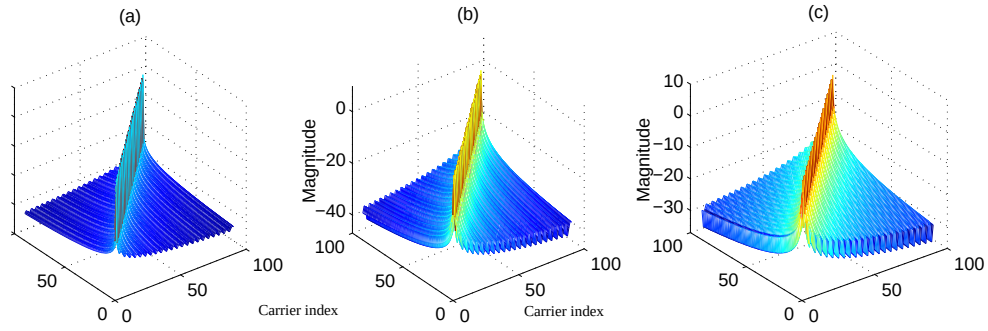

Figure 4.19: The estimated channel matrix for different Doppler spread values, (a): f_d=0.01 Hz ; (b): f_d=3 Hz, (c): f_d=34 Hz.

polynomial approximation schemes with different degrees. From the results, it can be concluded that the schemes were able to estimate the channel matrix at high values of Doppler. The approximation methods are valid as long as Doppler spread is less than the frequency spacing between the carriers, which is usually the case for wireless channels.

4.5 Low-Complexity Equalization for OFDM Systems

The equalization is simply detecting the transmitted OFDM symbols $\underline{\mathbf{S}}$ from the noisy and distorted received signal $\underline{\mathbf{Y}}$ making use of the estimated channel coefficients. In order to solve the system equation (2.29) for $\underline{\mathbf{S}}$ with including ICI effect, the channel matrix needs to be estimated first as described in the previous section and then calculating the

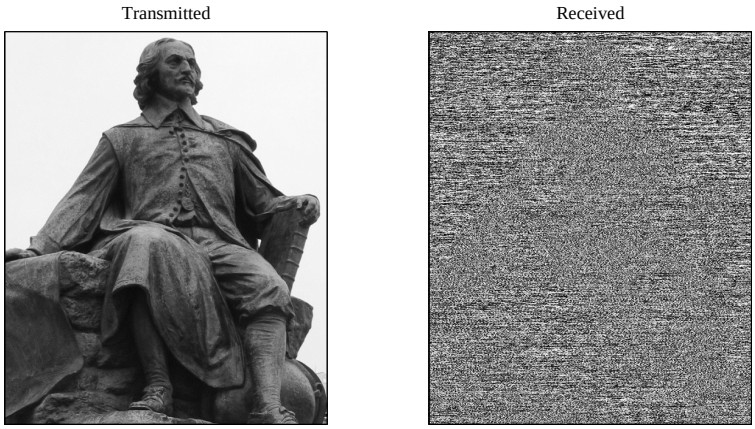

Figure 4.20: Transmitted and received images.

matrix inversion. Since the channel matrix can have a large size [3], the matrix inversion requires high computational effort, which makes it difficult to process in real time.

4.5.1 Exploiting Banded Structure of Channel Matrix

As has been shown previously, most of the ICI coefficients are concentrated at the neighborhood of the main diagonal of the matrix, since each carrier is strongly interfered by the adjacent carriers. For slowly varying channels, the equalization process can be greatly simplified by considering only the significant ICI components [19] and neglecting other small components by putting

$$H_{k,m} = 0 \qquad \text{for} \qquad |m-k| > D \tag{4.35}$$

where D denotes the number of the considered off-diagonals, which can be chosen according to the value of the expected Doppler spread. The resulting matrix is sparse which can be efficiently inverted by subdividing it into N small sub-matrices that are inverted separately making use of iterative equalization criteria. The iterative MMSE equalizer can be described as follows: The last element of $\underline{\mathbf{S}}$ is estimated using a sub-matrix $\mathbf{H}_{D+1}$ from $\mathbf{H}$, which consists the last $D+1$ rows and last $D+1$ columns of $\mathbf{H}$ as

$$S(N) = u\mathbf{H}_{D+1}^{H}(\mathbf{H}_{D+1}\mathbf{H}_{D+1}^{H} + \sigma_v^2\mathbf{I})^{-1}\underline{\mathbf{Y}}_{D+1} \tag{4.36}$$

where $u = [0, 0, ..., 1]$ is the unit vector and $\underline{\mathbf{Y}}_{D+1}$ is a vector contains the last $D+1$ elements of $\underline{\mathbf{Y}}$. This method is applied iteratively by shifting up the index until estimating the complete elements of $\underline{\mathbf{S}}$. This reduces the required multiplications from $\mathcal{O}(N^3)$ to $\mathcal{O}(N(D+1)^3)$, which is very useful when N is large. Fig. 4.22 shows the performance of the system with different D. The channel matrix has been estimated using 5-points Lagrange polynomial approximation and made sparse according to (4.35).

[3] Broadcasting systems in general use large number of carriers, e.g. DVB uses 8192 carriers for its 8K mode.

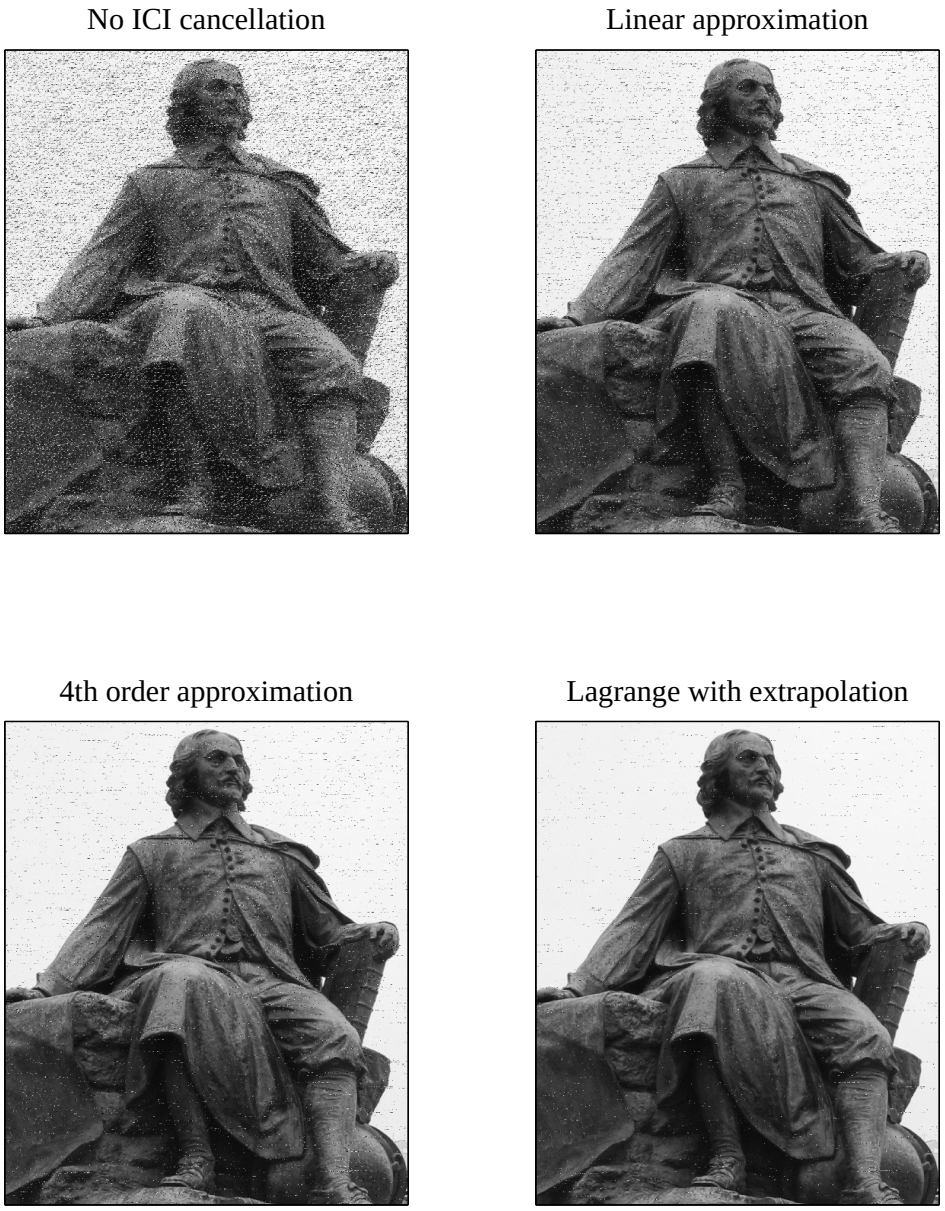

Figure 4.21: The equalized image using different approximation methods.

4.5.2 Low Complexity ICI Reduction for DRM Systems Using Windowing at the Receiver

In time fading channels, ICI complicates the equalization process. This complexity increases with increasing the number of carriers, where applying the classical methods that depend on the linear MMSE or ZF becomes infeasible. Windowing the received time

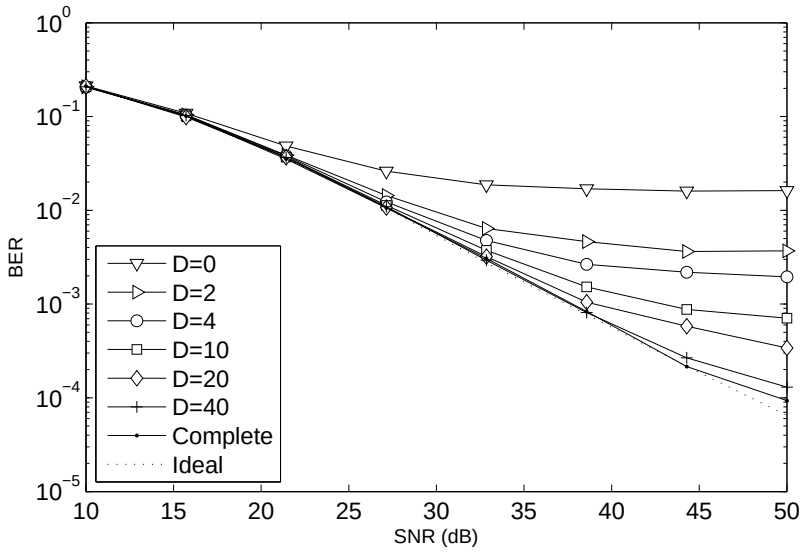

Figure 4.22: The BER performance of the sparse channel matrix for different D.

domain signal saves computations by squeezing the channel matrix into a desired banded structure, thereby reduces the out-of-band spectrum for each subcarrier, and hence ICI caused by far sub-carriers from the carrier of interest. In this section, a low-complexity pre-processing method for DRM system that maximizes the SINR is introduced. Instead of just ignoring the small-values of ICI as described in the previous subsection, ICI shortening can be reached by multiplying the time domain received symbols by a suitable N-point window (fast convolution) before FFT operation to decrease the effect of ICI caused by far sub-carriers, and at the same time squeeze the channel matrix into a small number of diagonals, which saves computation when N is large. This approach has been previously proposed in [102]. Another scheme has been introduced in [106]. The introduced algorithm differs from that of both schemes in some aspects. The first, we modify the window design according to the Gaussian shaped Doppler spectrum that is suitable for simulating DRM channels. Secondly, we show that ignoring the lower left and the upper right corners of the channel matrix does not affect the performance, since the large frequency guards in the DRM symbols make the coefficients in these corners negligible, as it has been described in Section 4.1. This leads to slightly reduce the complexity of the equalizer. On the other hand, we have introduced a modification on the conventional Hamming window to make it suitable for different Doppler spreads.

The Max-SNIR window is designed to maximize the SINR with considering the Gaussian shaped Doppler spectrum, which is suitable for DRM channel. The received time domain signal can be written as

$$\underline{\mathbf{y}} = \mathbf{h}\mathbf{F}^H\underline{\mathbf{S}} + \underline{\mathbf{v}} \tag{4.37}$$

where $\mathbf{h}$ is the time domain channel matrix, $\mathbf{F}^H$ is the N-IFFT operation, and $\underline{\mathbf{S}}$ is the frequency domain transmitted OFDM symbols. The frequency domain signal is calculated as

$$\underline{\mathbf{Y}} = \mathbf{F}\mathbf{h}\mathbf{F}^H\underline{\mathbf{S}} + \mathbf{F}\underline{\mathbf{v}} = \mathbf{H}\underline{\mathbf{S}} + \underline{\mathbf{V}} \tag{4.38}$$

In order to squeeze the channel matrix, the received time domain signal is multiplied

by a suitable window $\underline{\mathsf{w}}$. The window effect appears as an ICI-shaping process, which decreases the ICI coefficients caused by far carriers and increases the coefficients of the adjacent carriers [102]. This makes the channel matrix more sparse and allows for low complexity equalization. The received frequency domain windowed signal is given by

$$\breve{\underline{\mathbf{Y}}} = \mathbf{F}\,\mathcal{D}\{\underline{\mathsf{w}}\}\,\underline{\mathbf{y}} = \mathbf{F}\,\mathcal{D}\{\underline{\mathsf{w}}\}\,\mathbf{F}^H\mathbf{F}\underline{\mathbf{y}} \tag{4.39}$$

From the DFT property for any vector $\underline{\mathsf{w}}$

$$\mathbf{F}\,\mathcal{D}\{\underline{\mathsf{w}}\}\,\mathbf{F}^H = \frac{1}{\sqrt{N}}\,\mathcal{C}\{\mathbf{F}\underline{\mathsf{w}}\} \tag{4.40}$$

where $\mathcal{D}\{\cdot\}$ and $\mathcal{C}\{\cdot\}$ denote vector to diagonal matrix and to circulant matrix transformations respectively. Substituting in 4.39 gives

$$\breve{\underline{\mathbf{Y}}} = \frac{1}{\sqrt{N}}\,\mathcal{C}\{\underline{\mathsf{W}}\}\,\underline{\mathbf{Y}} = \frac{1}{\sqrt{N}}\,\mathcal{C}\{\underline{\mathsf{W}}\}\,(\mathbf{H}\underline{\mathbf{S}} + \underline{\mathbf{V}}) \tag{4.41}$$

where $\mathcal{C}\{\underline{\mathsf{W}}\}\mathbf{H}$ is the channel matrix including the windowing effect. To make the matrix sparse, Fig. 4.2 motivates us to mask the channel matrix by ignoring all ICI coefficients outside a desired region. This region considers only the ICI coefficient that matter as shown in Fig. 4.23 in case of no guard frequency bands. Where D changes according to Doppler spread. The designed window that maximizes the SINR can be written in the

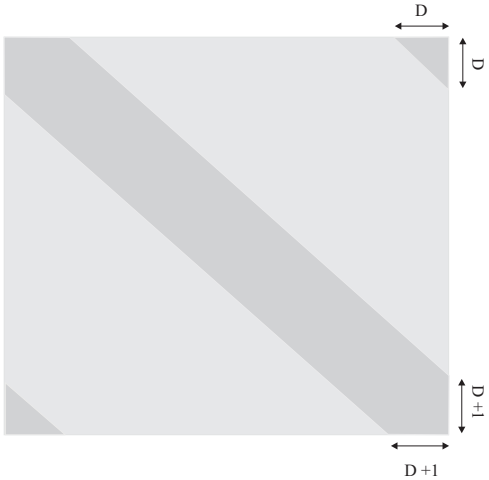

Figure 4.23: The desired structure of the channel matrix.

following form

$$\underline{\mathsf{w}}_{opt} = \arg \max_{\underline{\mathsf{w}}} (\text{SINR}) = \arg \max_{\underline{\mathsf{w}}} \left(\frac{\|\mathcal{M}\{\mathcal{C}(\underline{\mathsf{W}})\mathbf{H}\}\|_F^2}{\|\bar{\mathcal{M}}\{\mathcal{C}(\underline{\mathsf{W}})\mathbf{H}\}\|_F^2 + \sigma_v^2\|\mathcal{C}\{\underline{\mathsf{W}}\}\|_F^2} \right) \tag{4.42}$$

where $\|\cdot\|_F$ denotes the Frobenius norm, $\mathcal{M}\{\cdot\}$ denotes the mask operator that masks the windowed channel matrix to produce the desired structure of Fig. 4.23, and $\bar{\mathcal{M}}\{\cdot\}$ is the

complement mask. The window is constructed using the channel statistical parameters and can be simplified [102] to

$$\underline{\tilde{\mathsf{w}}}_{opt} = \arg \max_{\underline{\mathsf{w}}} (\underline{\tilde{\mathsf{w}}}^H \mathbf{A} \underline{\tilde{\mathsf{w}}}) \tag{4.43}$$

so that $\underline{\tilde{\mathsf{w}}}_{opt}$ is the principle eigenvector of $\mathbf{A}$. For more details, the derivation of (4.43) can be found in Appendix A. The matrix $\mathbf{A}$ is resulting from element-wise multiplication of two matrices as follows

$$\mathbf{A} = \mathbf{B} \odot \mathbf{D}, \tag{4.44}$$

where $\odot$ is the Hadamard product and $\mathbf{B}$ has a similar form of Dirichlet sinc, which is given by

$$[\mathbf{B}]_{k,m} = \frac{1}{N} \frac{\sin\left(\frac{\pi}{N}(2D+1)(m-k)\right)}{\sin\left(\frac{\pi}{N}(m-k)\right)}, \tag{4.45}$$

Considering the Gaussian shaped Doppler spectrum for DRM system, $\mathbf{D}$ is given by [107]

$$[\mathbf{D}]_{k,m} \approx \left(\frac{\alpha^2}{\sigma_v^2 + \alpha^2}\right) e^{-\pi^2 f_D^2 (m-k)^2/2}. \tag{4.46}$$

The resulting window can be calculated as follows

$$\underline{\mathsf{w}}_{opt} = \frac{\underline{\tilde{\mathsf{w}}}_{opt}}{\sqrt{\left(\sigma_v^2 + \alpha^2\right)}} \tag{4.47}$$

where σ_v^2 is the noise variance and α^2 is the summation of all the variances of the channel complex taps ($\alpha^2 = \sum_0^{L-1} \sigma_l^2$). Fig. 4.24 shows the channel estimation and equalization stages with time domain preprocessing, which require only the channel statistical parameters. In case of using the Wiener filter channel estimation described in Chapter 3, the auto and cross-correlation matrices used for Wiener filtering need to be modified by the designed window in order to have the windowing effect on the estimated channel matrix.

4.5.3 A Modified Hamming Window for ICI shortening

The hamming window is one among many other window types that used to reduce the out-of-band spectrum of the signal [108]. This window is written as

$$\mathsf{w}(n) = 0.53836 - 0.46164 \cos\left(\frac{2\pi n}{N-1}\right) \tag{4.48}$$

The window is used also to reduce the complexity of the equalization process in OFDM systems, since it concentrates the power of the ICI close to the main diagonal making the matrix sparse, and hence it allows low complexity equalization. However, the effect of the window on the channel matrix varies according to the Doppler spread and the

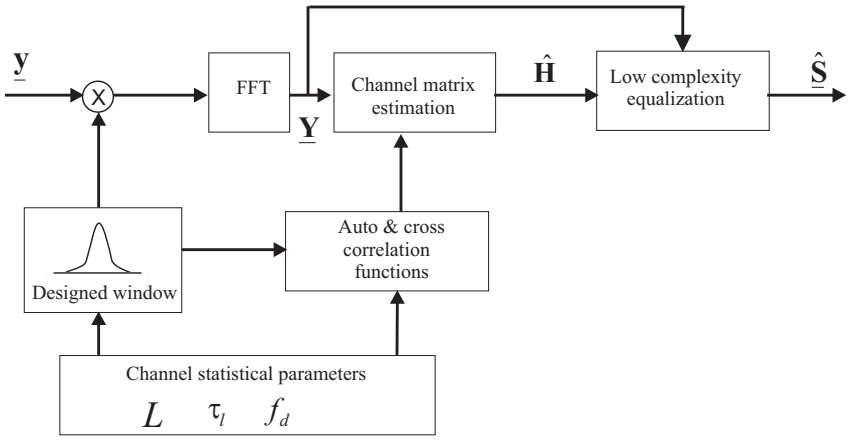

Figure 4.24: Channel estimation and equalization stages with time domain preprocessing.

required squeezing factor of the matrix. It is easy to see that for high Doppler spread and high squeezing factor the window needs to be narrower in order to span larger Doppler shifts, hence reducing the important ICI coefficients. We can achieve such an effect by modifying the Hamming window. A power operator is introduced in order to squeeze the window according to the expected Doppler spread values.

$$\underline{\mathrm{w}}_{mod} = \underline{\mathrm{w}}^{p} \tag{4.49}$$

where p is an operator proportional to the Doppler spread and the squeezing factor D, which tends to make the window narrower when D increases and wider for low values of D. Fig. 4.25 shows the shape of the window for different p. Using the role of thumb as

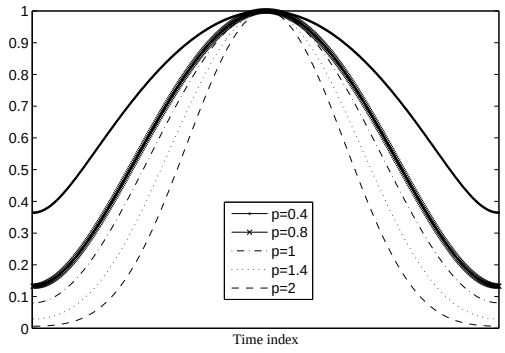

Figure 4.25: Modifying the Hamming window according to the Doppler spread.

well as the simulation results of the system performance, one can choose the suitable p value for a certain Doppler spread. We found that for DRM system with robustness mode "B" and spectrum occupancy "0", p value can be approximated as $p \approx \sqrt{D - 0.5} - 1$. However this approximation can vary according to the system parameters.

4.5.4 Iterative Equalization

The banded structure of the resulting windowed channel matrix allows us to use high performance low-complexity estimation using iterative algorithms by subdividing the matrix $\mathcal{C}\{\underline{\mathsf{W}}\}\mathbf{H}$ into small matrices so that the dimension of the inverted matrices is reduced to $((D+1)\times(D+1))$, and thereby the complexity is reduced to $\mathcal{O}(N(D+1)^3)$ multiplications. The system equation can be rewritten as following

$$\underline{\mathcal{Y}}_k = \mathcal{H}_k \underline{\mathcal{S}}_k + \mathcal{W}_k \underline{\mathbf{V}} \tag{4.50}$$

where $\mathcal{H}_k$ is a sub-matrix from $\mathbf{H}$ and written as

$$\mathcal{H}_k = \begin{pmatrix} H_{k-D,k-2D} & \dots & H_{k-D,k} & 0 & 0 \\ 0 & \ddots & \vdots & \ddots & 0 \\ 0 & 0 & H_{k+D,k} & \dots & H_{k+D,k+2D} \end{pmatrix}$$

Notice that the indexing taken here in this part is modulo-N indexing. $\underline{\mathcal{Y}}_k$ and $\underline{\mathcal{S}}_k$ are sub-vectors from $\underline{\mathbf{Y}}$ and $\underline{\mathbf{S}}$, respectively, and written as

$$\underline{\mathcal{Y}}_k = [Y_{k-D} Y_{k-D+1} \dots Y_{k+D}]$$

$$\underline{\mathcal{S}}_k = [S_{k-2D} S_{k-2D+1} \dots S_{k+2D}]$$

$\mathcal{W}_k$ is a sub-matrix from the frequency domain circulant window matrix $\mathcal{C}\{\underline{\mathsf{W}}\}$, which reads

$$\mathcal{W}_k = \begin{pmatrix} \mathsf{W}_{k-D} & \mathsf{W}_{k-D-1} & \dots & \mathsf{W}_{k-D-N+1} \\ \mathsf{W}_{k-D+1} & \mathsf{W}_{k-D} & \dots & \mathsf{W}_{k-D-N+2} \\ \vdots & \ddots & \ddots & \vdots \\ \mathsf{W}_{k+D} & \mathsf{W}_{k+D-1} & \dots & \mathsf{W}_{k+D-N+1} \end{pmatrix}$$

Under the assumption of zero mean Gaussian noise that uncorrelated with the transmitted symbols, we can write

$$E\{\underline{\mathbf{V}}\} = 0, \quad E\{\underline{\mathbf{V}}\underline{\mathbf{V}}^H\} = \sigma_v^2 \mathbf{I}, \quad \text{and} \quad E\{\underline{\mathbf{S}}\mathbf{V}^H\} = 0$$

The MMSE estimator can be written as

$$\tilde{S}_k = E\{S_k\} + \mathrm{Cov}(\underline{\mathcal{S}}_k, \underline{\mathcal{Y}}_k)\mathrm{Cov}(\underline{\mathcal{Y}}_k, \underline{\mathcal{Y}}_k)^{-1}(\underline{\mathcal{Y}}_k - E\{\underline{\mathcal{Y}}_k\}) \tag{4.51}$$

Utilizing the mean and the variance of the initially estimated symbols, we can apply an iterative equalization process. The iterative MMSE equalizer can be written [102] as

$$\tilde{S}_k = \bar{S}_k + \underline{\mathcal{F}}_k^H(\underline{\mathcal{Y}}_k - \mathcal{H}_k \underline{\mathcal{S}}_k) \tag{4.52}$$

where $\mathcal{F}_k$ is calculated as

$$\underline{\mathcal{F}}_k = (\sigma_v^2 \mathcal{W}_k \mathcal{W}_k^H + \mathcal{H}_k \mathcal{D}(\underline{\mathbf{b}}_k)\mathcal{H}_k^H)^{-1} \underline{\hbar}_k b_k \tag{4.53}$$

where $\underline{\hbar}_k$ is the last column of $\mathcal{H}_k$, b_k is the variance of the k^{th} subcarrier and $\bar{S}_k$ is the mean of this subcarrier over the possible values among the alphabet constellation. Notice that $\underline{\mathbf{b}}_k = [b_{k-2D} b_{k-2D+1} \dots b_{k+2D}]$. The scheme employs an iterative updating

of the estimated symbols either by estimating each subcarrier separately and use the estimated information to update the detected symbols sequentially, or by estimating all sub-carriers in parallel and immediately updating the estimation in blocks. For initializing the algorithm, b_k's and $\bar{S}_k$'s are used as prior information according to the type of data sent at each subcarrier. $\bar{S}_k = 0$ and $b_k = 1$ for data carriers that are assumed to have independent and identically distributed (iid) symbols with normal distribution and zero mean. While for pilot carriers, $\bar{S}_k = S_k$ and $b_k = 0$. The estimated symbols are updated using the previous estimates as prior information for the next iteration with hard decision feed back (HDF) or soft decision feed back (SDF) Equalization.

4.5.4.1 Hard decision feedback equalization HDF

For each S_k, a hard decision is done according to the alphabet of the transmitted constellation. For example, in case of BPSK, where $S_k \in (+1, -1)$, the updating values (posteriors) are calculated as follows $\bar{S}_{k,new} = \text{sgn}(\tilde{S}_k)$ and $b_{k,new} = 0$. The estimated posteriors are fed back to the equalizer for several iteration until achieving the required performance or until the saturation of the algorithm. Notice that, for higher QAM modulation schemes, $\tilde{S}_k$ must be hard decided to the nearest constellation symbol in both, I and Q channels.

4.5.4.2 Soft decision feedback equalizer SDF

Soft feedback is usually used to avoid the error propagation of hard decisions. The algorithm makes advantage of the log-likelihood ratios for estimating the updating values according to turbo principle [48, 109]. As an example, for QPSK modulation scheme, the values of the posteriors are calculated as following

$\bar{S}_{k,new} = \frac{1}{\sqrt{2}}\tanh\big(L(S_k/\tilde{S}_k)\big)/2$ for both, real and imaginary parts

$b_{k,new} = 0.5 - \bar{S}^2_{k,new}$ for both, real and imaginary parts

where $L(S_k/\tilde{S}_k)$ is the log-likelihood ratio of the transmitted and estimated carrier. For more details see Appendix B.

4.6 Simulation Results

Here we test the algorithm described above and study its effect on the system performance. A DRM system with different robustness modes and spectrum occupancies [36] has been considered. In order to test the effect of multipath channels, a two-path fading channel with different Doppler spreads was tested. ISI is assumed to be completely removed by having a suitable GI longer than the maximum delay of the channel. Un-coded QPSK symbols were used for the simulation.

We calculated the SINR for two different Doppler spreads (f_d=4 Hz & f_d=25 Hz) and compared the designed window with Hamming window for a DRM system with mode "B" and spectrum occupancy "0". Fig. 4.26 shows the improvement in the SINR using the windowing process. The figure shows that the designed window outperforms Hamming window for both cases. Fig. 4.27 shows the resulting windows for different D. It can be seen that the time domain window is getting narrower as D increases, which means

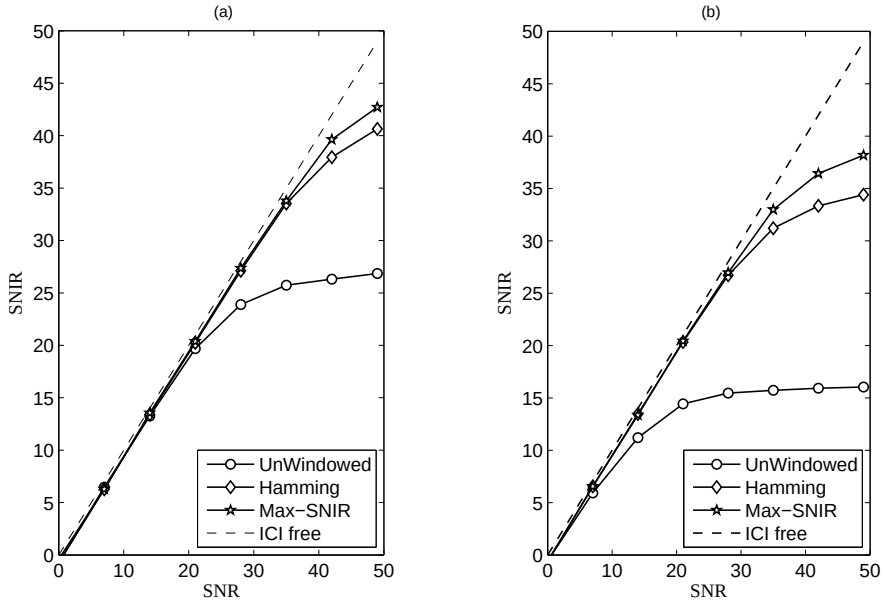

Figure 4.26: The improvement in the SINR for different windows at two different Doppler spread valuse, (a): f_d=4 Hz; (b): f_d=25 Hz.

that a wider ICI span from the frequency domain channel matrix is considered. It is obvious that if $D = 0$, the resulting window is equivalent to a rectangular window, while when $D = 1$, the resulting window is close in the shape to Hamming window. Fig. 4.28 describes the effect of the designed window on the channel matrix. One can recognize that the window has squeezed the channel matrix to a semi-sparse matrix according to the squeezing factor D. Fig. 4.29(a,b) show the improvement of the BER after a specific number of iterations for two cases, with sequential hard decision feed back HDF and SDF, which makes use of turbo principle. Two different Doppler scenarios have been tested, $f_d = 4$ Hz with $D = 1$ and $f_d = 25$ Hz with $D = 2$. As seen from Fig. 4.29(a) and Fig. 4.29(b), SDF performs better than HDF in the higher velocities (higher Doppler spreads). The reason is that for bad channel conditions, HDF suffers from the error propagation effect. For both schemes the estimation converges after 3 iterations with a good BER improvement. Fig. 4.30 demonstrates the BER vs. SNR with using SDF for different iterations compared to the linear estimation with masked and with a complete channel matrix[4]. Fig. 4.31 compares the BER for different windows after 2 iterations-SDF. Fig. 4.32 shows the BER performance of a DRM system with robust mode "D" and spectrum occupancy "3" with 180 virtual carriers at both sides. The figure shows a comparison of the Max-SNIR windowed symbols between the case of including the matrix corners at the upper right and lower left sides of the channel matrix and the case of discarding these corners. It can be seen that ignoring the corners leads to no change in the BER performance, since the coefficients are very small and can be neglected. This reduces further the complexity of the algorithm.

[4]The unwindowed channel matrix is masked in the same way of the windowed one to show the difference in the performance with the same complexity.

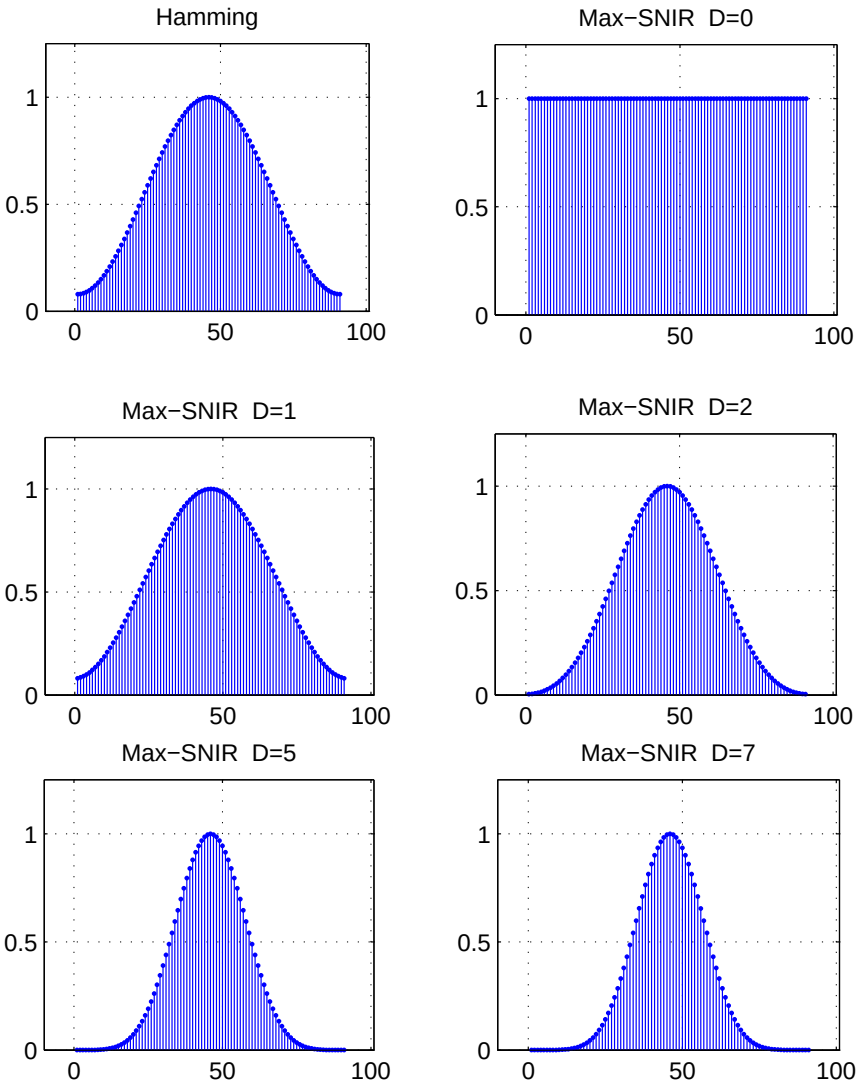

Figure 4.27: The resulting windows for different squeezing factor D.

As it has been described, simply modifying the Hamming window according to the channel conditions can enhance the performance at different Doppler spreads. Here we examine the modified window on a system with the following characteristics:
Number of carriers $N_c = 91$, the guard interval $N_g = 91$, the bandwidth $B = 4.5$ KHz, FFT length $N = N_c$. A 2-tab channel with gaussian shaped Doppler spread has been tested. Fig. 4.33 illustrates the variation in the MSE of the Hamming windowed symbols, with different values of the modification factor p compared to the conventional one ($p = 1$), after only one iteration with applying SDF iterative scheme. It can be observed that for different squeezing factors, the optimum value of p changes and varies from that of the conventional window. Fig. 4.34 illustrates the BER performance of the windowed system. Fig. 4.33(a) shows the BER comparison between the conventional Hamming window and the modified one with ($p = 0.1$) at Doppler spread ($f_d = 25$ Hz) and squeezing factor ($D = 2$). The performance was calculated using one iteration of the

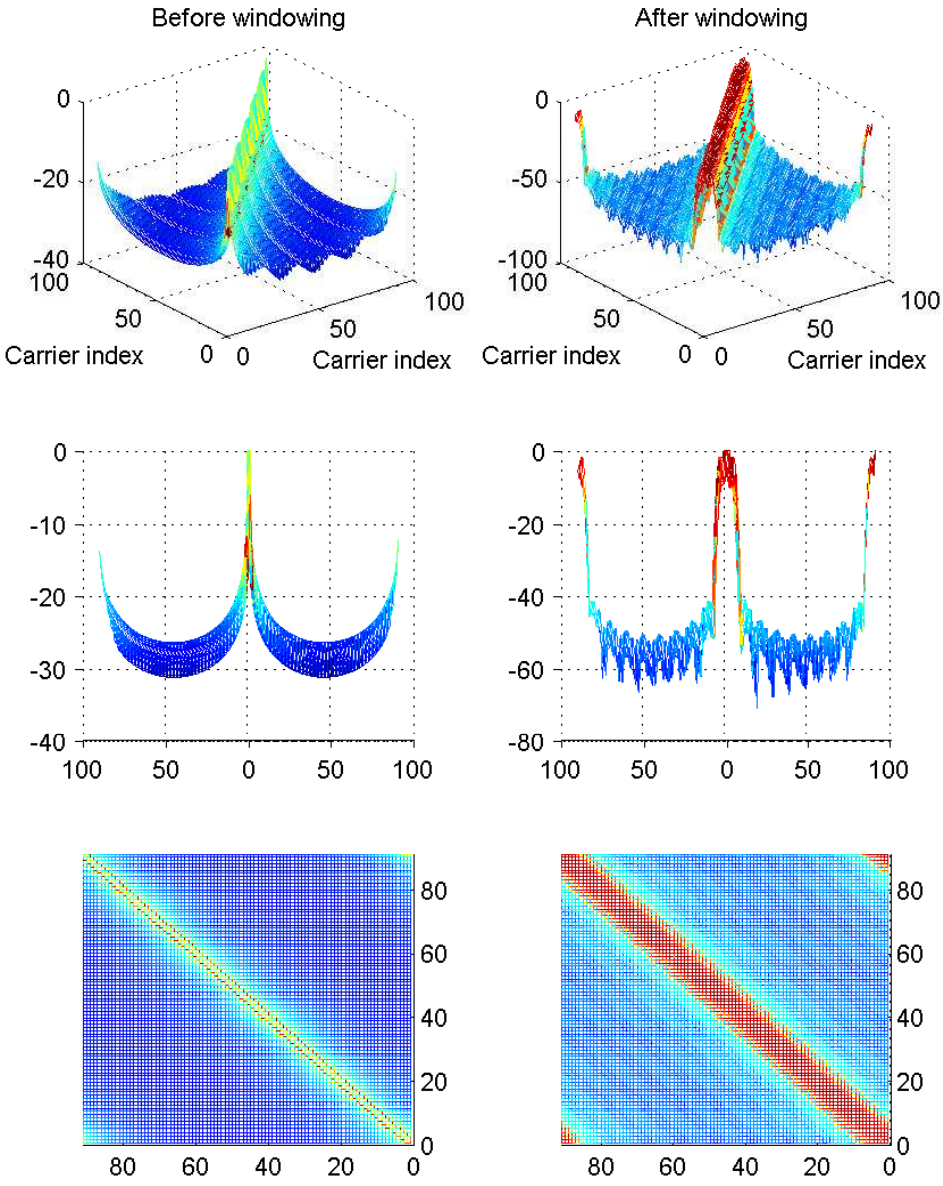

Figure 4.28: The windowing effect on the channel matrix (f_d=45, D=10).

SDF iterative scheme. Fig. 4.33(b) illustrates the comparison in case of (f_d = 65 Hz), ($D = 6$), and ($p = 2$), after 3 iterations of SDF.

It can be concluded that Max-SINR window has shown an increase in the SINR comparing with other common windows. Also the iterative algorithms give considerable improvements of the system performance after only 2 iterations. Using simple modification on the Hamming window, we can achieve a good performance at wide range of Doppler spread.

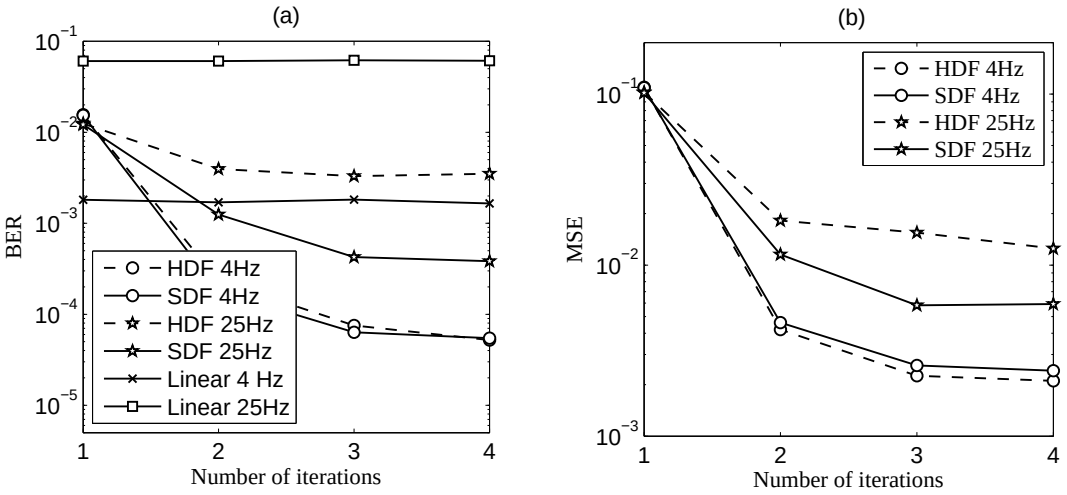

Figure 4.29: The improvement in the system performance of the Max-SINR window versus the number of iterations at SNR=35 dB; (a):BER, (b): MSE.

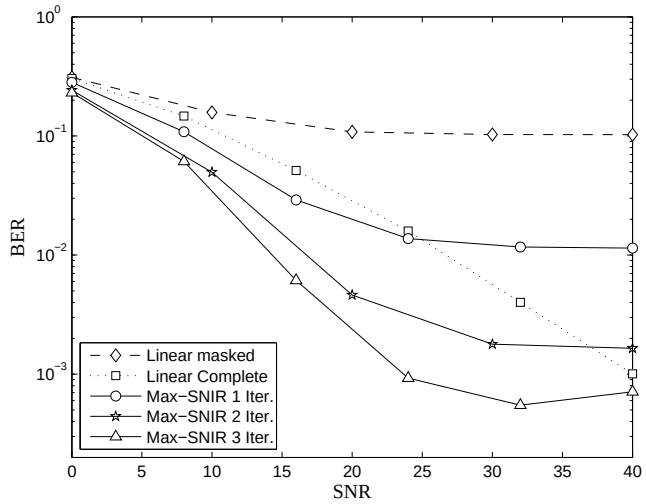

Figure 4.30: BER vs. SNR, f_d=35 Hz, D=2.

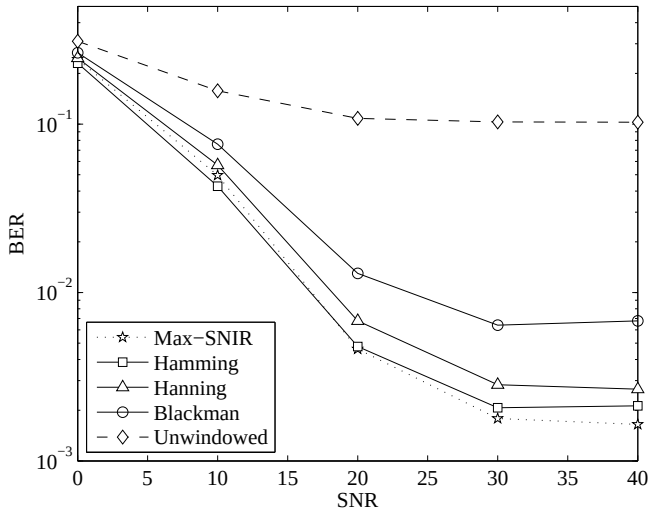

Figure 4.31: BER vs. SNR after 2 iterations-SDF for different windows, f_d=35 Hz, D=2.

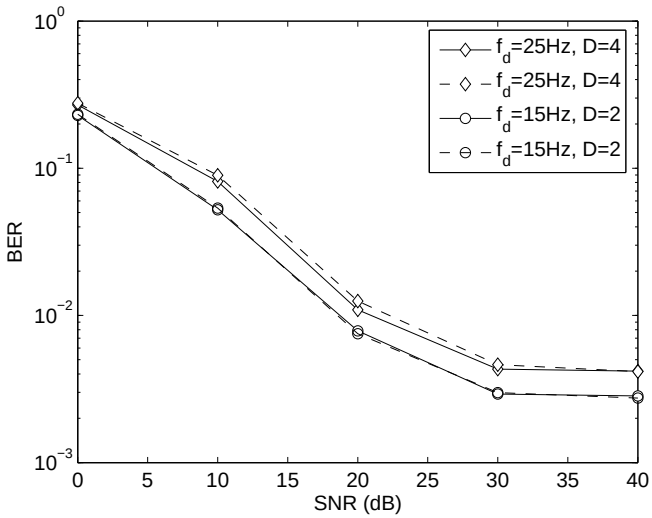

Figure 4.32: A comparison between including (solid) and discarding (dashed) of the matrix corners for windowed DRM symbols.

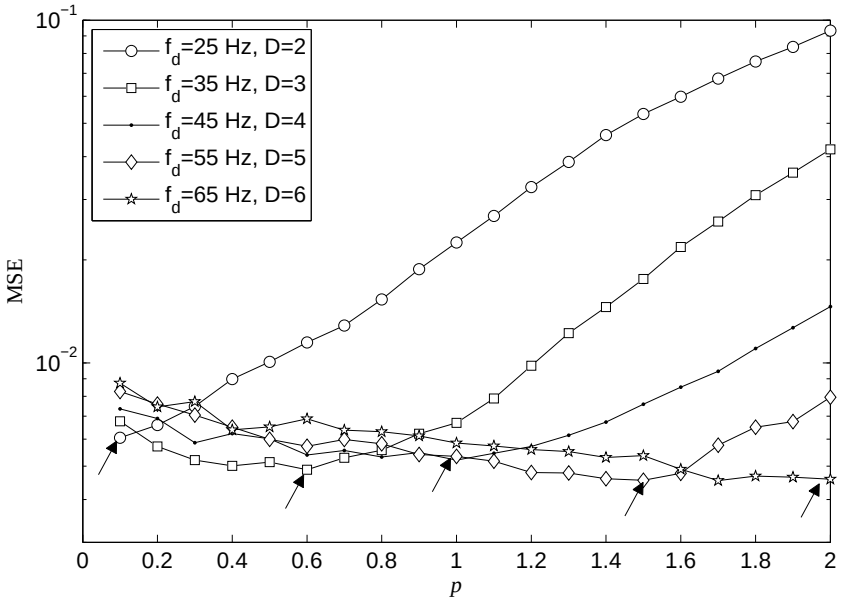

Figure 4.33: MSE versus the value of p for different Doppler spread values. The arrows indicate the minimum value of each curve.

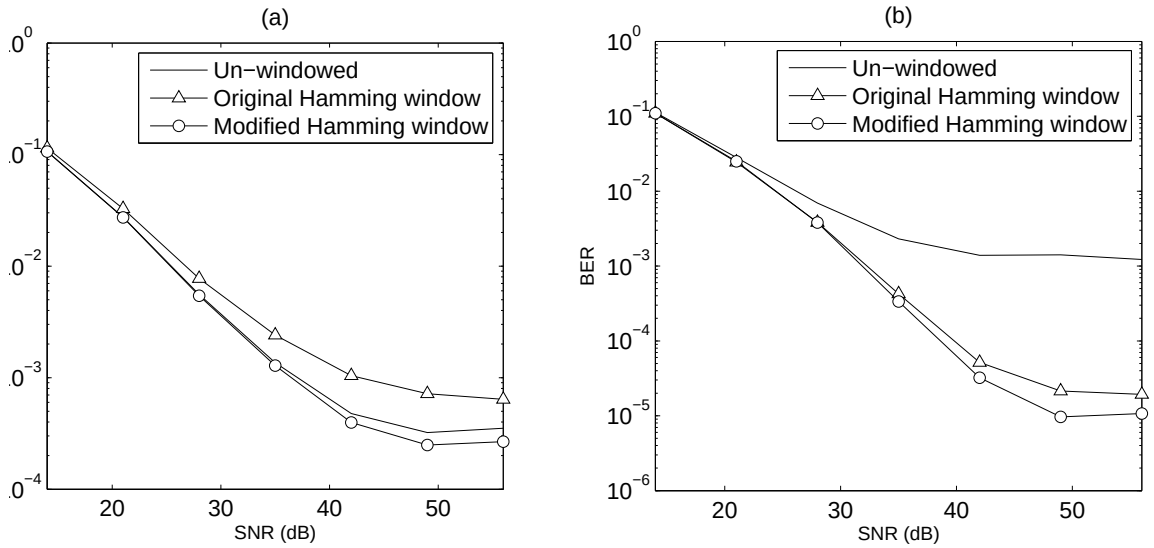

Figure 4.34: A comariosn of the BER performance of a windowed DRM system with applying Hamming window and the modified one; (a): The BER performance in case of $f_d = 25$ Hz, $D = 2$, and $p = 0.1$ after one iteration of SDF, (b): The BER performance in case of $f_d = 65$ Hz, $D = 6$, and $p = 2$ after 3 iterations of SDF.

Chapter 5

Adaptive Techniques for OFDM Systems

In order to have a reliable communication, OFDM systems should be capable to efficiently work in a wide range of channel conditions, such as different mobile speeds, different delay spread values, and at wide range of SNR values. Adaptive techniques allow for better reception behavior with less received signal quality to achieve the desired BER performance, and lead to improving the system performance, increasing the battery live, enlarging the coverage area, and enhancing the capacity of the system. The adaptive algorithms can also reduce the average computation complexity of the system, which reduces the required processing power [110]. In recent years, adaptive techniques have gained a significant interest for research, and have been widely studied in the literature in order to optimize the performance of the communication systems. One example of adaptive variable modulation rate for direct sequence code division multiple access (DS-CDMA) has been introduced in [111–113]. In [114–117], adaptive OFDM systems have been proposed. The digital adaptive filters have also found their applications for channel estimation and equalization in modern communication systems as in [118] and [119]. Some examples of adaptive power control techniques for cellular systems are studied in [120] and [121].
The adaptive strategy can be different depending on the applications and services to satisfy an acceptable quality-of-service (QoS). The goals for adaptation are to maximize the throughput with maintaining the BER below the target value or to improve the BER performance for a constant effective throughput. In general, the adaptive techniques for communication systems can be classified in two categories [110], receiver adaptation and link adaptation.

This chapter is divided into two sections. Section 5.1. introduces a new receiver adaptation scheme for the time interpolator used for estimating the channel and cancelling the ICI. Section 5.2. explains the link adaptation in OFDM systems and proposes two new adaptive schemes, adaptive GI length and adaptive pilot distribution.

5.1 Receiver Adaptation

In time-variant channels, the channel coefficients change during the transmission time according to the position and the velocity of the mobile station. Generally, a wireless channel with L taps can be modeled in time t and delay τ using the tapped delay line model as

$$h(t,\tau) = \sum_{l=0}^{L-1} \beta_l(t)\delta(\tau - \tau_l(t)) \tag{5.1}$$

where $\beta_l(t)$ and $\tau_l(t)$ are the time-variant channel coefficient and the time-variant delay of the l^{th} tap, respectively. The ability of a receiver to track the wireless channel depends on how fast the channel changes in time, space, and frequency. Adaptive algorithms provide means for extrapolating the channel state information from the received symbols. Kalmann filtering, e.g, is the most popular adaptive techniques for channel estimation. In non-adaptive communication systems, the filter is designed and optimized by assuming the knowledge of some channel statistics. These designs usually depend on the worst-case assumption of the channel conditions. However, for time-variant channels, these designs may lead to degrading the system performance and increasing the reception complexity because of the model-mismatch. Therefore, an adaptive filtering scheme can solve this problem. In this case, channel parameters like Doppler spread, delay spread, and noise variance are estimated continuously, and used as a priori information to optimize the channel tracker performance. The receiver can also choose between different equalization techniques such as LS, least mean square (LMS), MMSE, or recursive least square (RLS) according to the channel conditions. For bad conditions advanced algorithms can be used to efficiently extract the highly distorted symbols. Whereas for good conditions, lower complexity algorithms can be sufficient. Another example of receiver adaptation is the adaptive information generation for soft decoders, e.g, turbo decoder. The decoder performance is increased when a priori soft information is available for the encoded bits. This requires estimating of the varying noise covariance and updating this estimation during the transmission time. An example of a simple adaptive channel estimation scheme appears in Fig. 5.1.

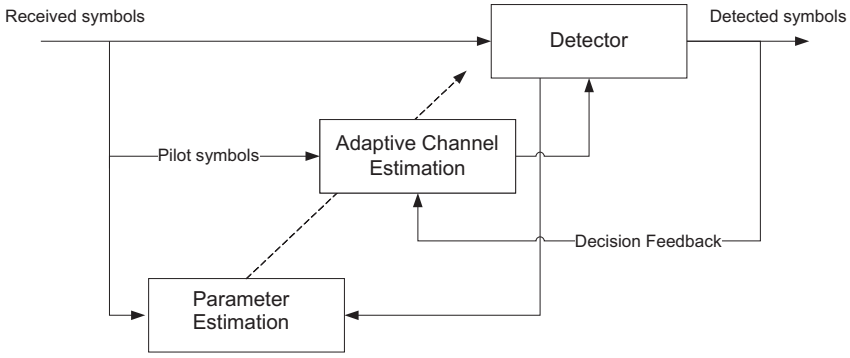

Figure 5.1: Adaptive channel estimation.

5.1.1 Newly Proposed Adaptive Time Interpolator for DRM Systems

In this section, we propose an adaptive time interpolator for OFDM systems in time-variant channels. The off-diagonals of the channel matrix, which represent the ICI coefficients, are estimated by approximating the channel over a few successive OFDM symbols making advantage of Taylor or Lagrange polynomial interpolation discussed in Section 4.3. The interpolation degree is adapted according to the estimated Doppler spread aiming at minimizing the BER performance as a subject to the processing delay. For short

term time variations, the channel can be assumed wide sense stationary uncorrelated scattering WSSUS [34], which means that the second order channel statistical parameters, such as Doppler and delay spreads, can be assumed constant. However, the long term variations of the channel lead to changes in the channel statistical parameters during the transmission time. This variations degrade the system performance, either by increasing the BER for rabidly time-varying channels, or by increasing the system complexity and the processing delay without achieving extra gain for slow varying channels. This motivates us to use an adaptive approximation method to choose the required order of the approximation according to: The required accuracy (BER), the speed of the vehicle, or the allowed delay and complexity. Adapting the time interpolator that makes use of Taylor and Lagrange polynomial approximation helps to track the long-term channel variations in order to, either minimize the BER as a subject to the delay and complexity or to minimize the delay and complexity as a subject to the BER performance. The required number of OFDM symbols and the degree of the interpolator is adapted according to the estimated Doppler spread. Since the off-diagonals of the channel matrix $\mathbf{H}$ represent the ICI coefficients, The ICI strength at an arbitrary sub-carrier (which is equal for all sub-carriers) can be calculated [122] as

$$P_{ICI} = \sum_{k \neq m} E\left[|\hat{H}_{k,m}|^2\right]. \tag{5.2}$$

Making use of the ICI power, Doppler spread can be roughly estimated exploiting the upper bound of the ICI described by (4.15) as

$$f_d \approx \frac{\sqrt{3P_{ICI}}}{\pi T_s}, \tag{5.3}$$

where T_s is the total symbol duration. Fig. 5.2 shows a block diagram of the adaptive interpolation in the OFDM receiver. For a given long-term BER target, some Doppler

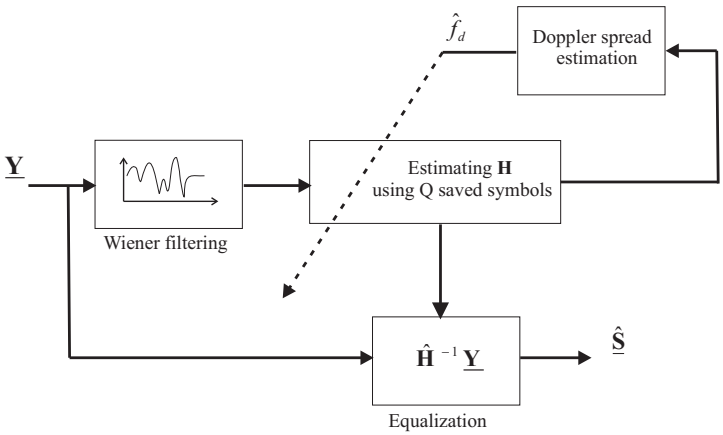

Figure 5.2: Adaptive channel interpolation.

spread thresholds are chosen to adapt the number of OFDM symbols Q and the polynomial degree. Doppler thresholds are chosen from the simulated system performance for different Doppler spread values and different approximation orders. Doppler spread can be estimated using the estimated channel matrix. This value is sent back to the channel estimator to estimate the channel matrix for the next received OFDM symbol.

5.1.2 Simulation Results

For simulation, a DRM system [36] has been considered. The robustness mode "B" and the spectrum occupancy "0" of DRM system have been considered. The system parameters are summarized in Table 5.1. OFDM symbols were transmitted through the

Table 5.1: Parameters of DRM system

Parameter	Value
Modulation scheme	64QAM
Number of Carriers	91
FFT length	1024
Guard interval	256
Bandwidth	4.5 KHz
Sampling frequency	48 KHz

channel # 5 of the ETSI for DRM, which is a 2-tap time-variant channel with delay spread of 4 ms. Fig. 5.3 illustrates the BER performance of the system for different Doppler spread at SNR=45 dB. It can be shown that increasing the polynomial degree increases the system performance. According to this results, five threshold levels of Doppler spread have been chosen to adapt the interpolator in order to guarantee that the BER does not exceed (10^{-3}). An arbitrary function of Doppler spread that changes

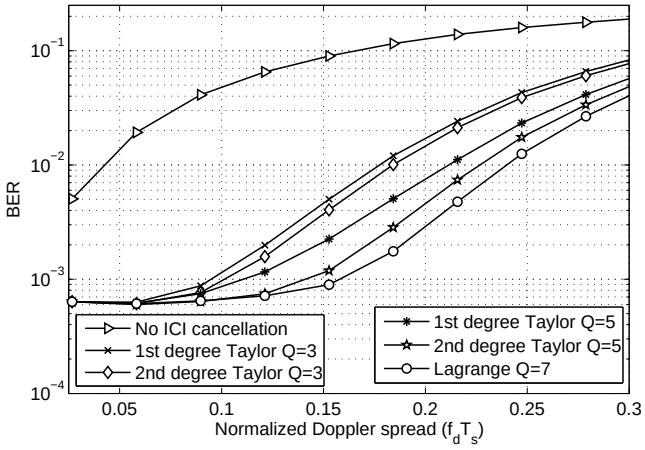

Figure 5.3: The performance evaluation (BER vs. Normalized Doppler spread).

during the transmission time has been used as shown in Fig. 5.4. This figure illustrates a comparison between the actual and the estimated Doppler spread. Although only the upper bound of ICI power is used for Doppler estimation, the estimated value can tracks the Doppler spread during the transmission time. Fig. 5.5 shows the adaptive behavior of the BER performance. It can be seen that the BER of the adaptive system stays almost constant and bellow the BER target during the transmission time [1] comparing with the non-adaptive cases. Fig. 5.6 shows the change in the processing delay, which is calculated

[1] For simulation, 150000 OFDM symbols have been transmitted.

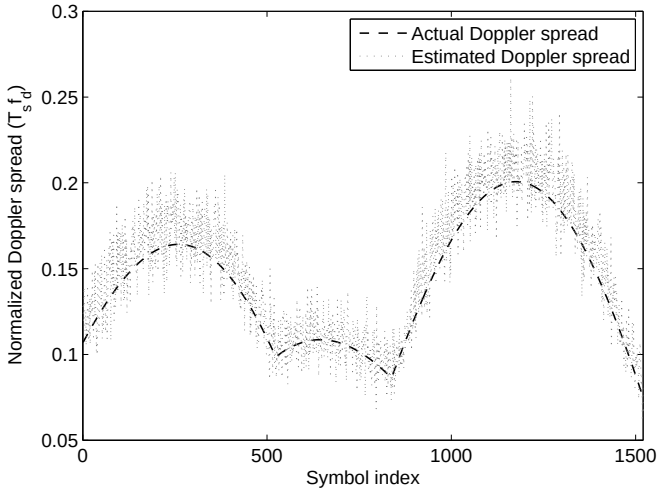

Figure 5.4: Doppler spread estimation.

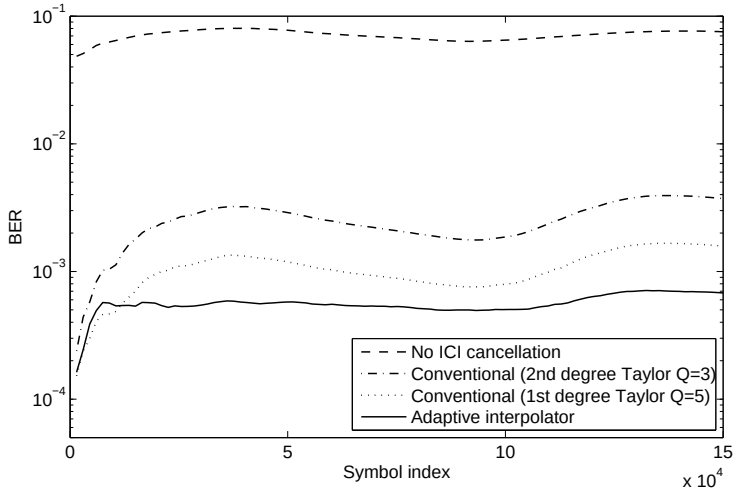

Figure 5.5: The adaptive behavior of the BER performance.

as the total time of only the saved future OFDM symbols $(\frac{Q-1}{2})T_s$. It is obvious that this change follows the change in Doppler spread. The total delay is comparable with that of $Q = 5$. In order to show the adaptive behavior, the delay has been averaged over each 1500 symbols. Furthermore, the results show that the BER performance is almost constant and bellow the target value and has less dependency on Doppler spread variations as shown in Fig. 5.7, which compares the adaptive system with the non-adaptive systems of $Q = 5$ and $Q = 3$ that exhibit bad performance as Doppler spread increases.

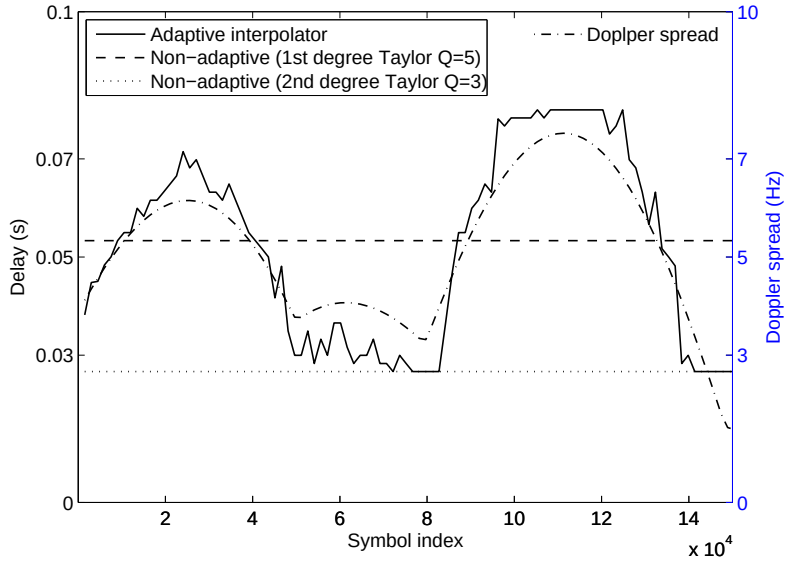

Figure 5.6: The change in the processing delay of the system.

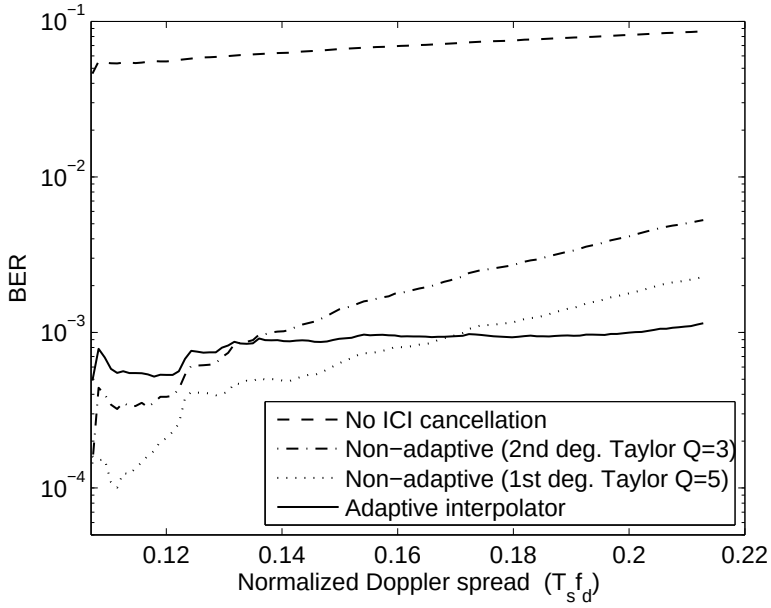

Figure 5.7: BER vs. Doppler spread.

5.2 Link Adaptation

The reliable communication between two terminals requires maintaining a target of QoS during the time of transmission. This can be accomplished by adapting the system parameters to gain the maximum system capacity with guaranteeing a certain BER target for different types of applications. For instance, transmitting voice signal requires BER performance different than transmitting Data. The transmitter adaptation is based on estimating the channel parameters at the receiver, and then a signal is fed back to the

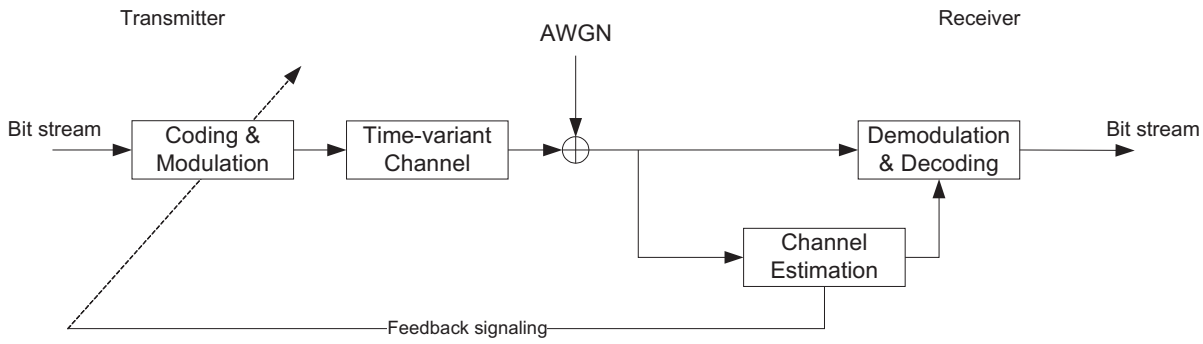

Figure 5.8: Adaptive transmission parameters.

transmitter in order to adapt its transmission modes as shown in Fig. 5.8.
Signaling the estimated parameters to the transmitter requires a reliable feedback link, and can be done in two different ways [123]:
-In reciprocal channels; The base station (BS) and the mobile station (MS) estimate the channel parameters, and decide the transmission mode for their local transmitters.
-In non-reciprocal channels; One station estimates the channel parameters, and signals the requested transmission mode to the transmitter of the other station. Fig. 5.9 shows the signaling strategy in case of a reciprocal channel. Different transmission parameters

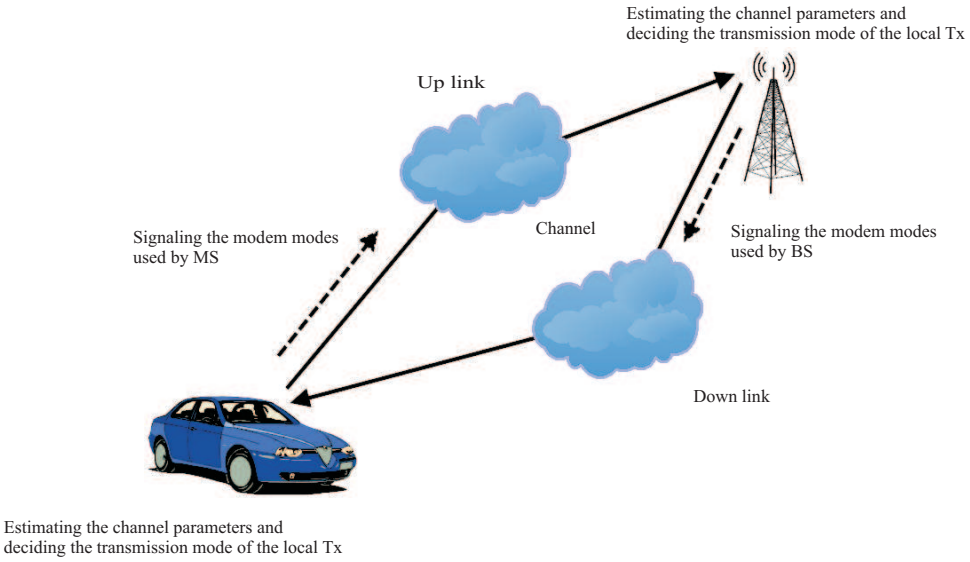

Figure 5.9: Signaling the estimated parameters of the adaptive OFDM system in reciprocal channels.

can be adapted according to the channel conditions like transmitted power, modulation scheme, code rate, interleaving depth [124], guard interval length, pilots distribution, cell and frequency assignment, etc., In the following points, we describe some of theses parameters:

Adaptive power control

If the transmitter increases the transmitted power, a significant interference from the near users can affect the user of interest. This is one of the most known problems in mobile cellular systems which is called near-far effect. Adaptive power control can handle this problem by controlling the transmitted power in such a way that the user benefits from the lowest possible transmission power that guarantees a certain QoS target. One application of the adaptive power control is found in CDMA systems [120, 121], since the achievable capacity in CDMA is significantly interference-limited.

Adaptive modulation

An efficient technique that provide a good link quality is by adapting the modulation levels or coding rate based on the channel quality. Adapting the modulation levels in response to the estimated SNR can provide a wide range of trade-offs between the required BER performance and the achievable throughput. Fig. 5.10 shows the different modulation levels for a varying received SNR. One example of the adaptive modulation

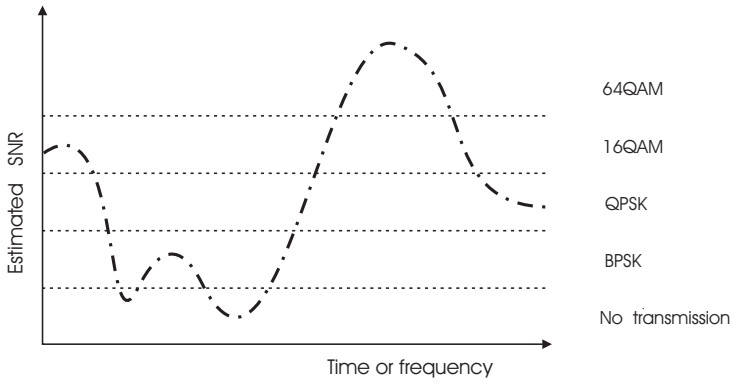

Figure 5.10: Adaptive modulation modes.

can be encountered in OFDM systems [114–117] in which the adaptation is accomplished by two different ways. The first one is done by adapting the modulation scheme for the entire OFDM symbol according to the average value of the estimated SNR. The other is done by adapting the modulation mode for each subcarrier separately. The later scheme is widely used, since the SNR is fluctuating in both time and frequency due to the frequency and time selectivity behaviors of the channel. Also the code rate of the Forward Error Correction (FEC) encoders can be adapted in conjunction with the adaptive modulation scheme as in WLAN system.

5.2.1 A Proposed Guard Interval Length Adaptation Method for OFDM-Based WLAN Systems

The long-term variation of the channel leads to changes in the delay spread during the transmission time. This variation degrades the performance of conventional OFDM systems that use fixed length of the guard interval by introducing ISI in highly frequency selective scenarios (high delay spread) or causes needless loss of capacity for small delay

spread values. In OFDM a so called cyclic prefix guard interval is used, which inserts the last portion of the time domain symbol in the beginning. Cyclic prefix extension maintains the orthogonality between the sub-carriers and allows for circular convolution with the channel. In order to avoid ISI, the guard interval is designed to be longer than the expected length of the CIR, which needs to be estimated at the receiver. In practice, the channel delay spread may change during the transmission time. In this case, the fixed length of the guard interval degrades the system performance, either by increasing the effect of ISI for large unexpected values of delay spread or by introducing unnecessary overhead without achieving extra gain for low delay spread values, which leads to loss in the power and capacity. Adapting the length of the guard interval can improve the system performance and allows for reliable communication as it has been recently studied in the literature as [125] and [126]. In this section, a method for adapting the guard interval length is proposed. The estimation of the delay spread at the receiver side is accomplished by means of root multiple signal classification (Root-MUSIC). Root-MUSIC performs eigenspace analysis of the channel's correlation matrix in order to efficiently estimate the channel's delay contents. A signal is fed back to the transmitter in order to change the guard interval aiming at maximizing the throughput without sacrificing the performance in terms of BER.

5.2.1.1 Time delay estimation

In order to properly estimate the time delays and the number of paths, pure training symbols (pilots) $\underline{\mathbf{S}}_p$ are first transmitted as a starting phase of the transmitted frame. The channel frequency response on pilots can be calculated using LS criterion as follows

$$\underline{\hat{\mathbf{H}}}_p = \mathcal{D}(\underline{\mathbf{S}}_p)^{-1}\underline{\mathbf{Y}}_p. \tag{5.4}$$

From the calculated channel frequency response and using the Root-MUSIC algorithm [127], the time delays can be estimated efficiently using the available limited bandwidth. The conventional FFT method on the other hand requires a much wider bandwidth, as to distinguish between two time delays τ_1 and τ_2, a bandwidth of $1/(\tau_2 - \tau_1)$ is required. Utilizing the estimated channel transfer function, one can write the covariance matrix of the noisy estimated channel as

$$\mathbf{R}_N = E\{\underline{\mathbf{H}}_p\underline{\mathbf{H}}_p^H\} = \mathbf{A}(\tau)\mathbf{R}_d\mathbf{A}^H(\tau) + \sigma_v^2\mathbf{I}, \tag{5.5}$$

where σ_v^2 denotes the noise variance and $\mathbf{R}_d$ represents the covariance matrix.

$$\mathbf{R}_d = E\{\underline{\mathbf{d}}\underline{\mathbf{d}}^H\}, \tag{5.6}$$

where $\underline{\mathbf{d}} = [\sigma_0, \sigma_1, ..., \sigma_{L-1}]^T$ consists of the complex amplitudes of the channel at different paths. $\mathbf{A}(\tau)$ is an $(N \times L)$ time delay matrix with columns

$$\underline{\mathbf{A}}(\tau_l) = \begin{pmatrix} 1 & 0 & 0 & \dots & 0 \\ 0 & e^{\frac{j2\pi\tau_l}{N}} & 0 & \dots & 0 \\ 0 & 0 & e^{\frac{2j2\pi\tau_l}{N}} & 0 & \vdots \\ \vdots & \vdots & 0 & \ddots & 0 \\ 0 & 0 & \dots & 0 & e^{\frac{(N-1)j2\pi\tau_l}{N}} \end{pmatrix} \begin{pmatrix} S_0 \\ S_1 \\ \\ \\ \vdots \\ S_N \end{pmatrix}.$$

The time delay contents can be obtained by solving the following eigensystem

$$\mathbf{R}_N\mathbf{E} = \mathbf{E}\Lambda, \tag{5.7}$$

where $\Lambda = \mathcal{D}(\lambda_0, \lambda_1, ..., \lambda_{N-1})$ is a diagonal matrix contains the eigenvalues of $\mathbf{R}_N$ and $\mathbf{E} = [\underline{\mathbf{E}}_0, \underline{\mathbf{E}}_1, ..., \underline{\mathbf{E}}_{N-1}]$ is a matrix contains the corresponding eigenvectors. The number of the dominant paths L can be estimated according to the fact that $\lambda_0 > \lambda_1 > ... > \lambda_{L-1} > \sigma_v^2$. By evaluating the following formula

$$\mathbf{e}(\tau) = \frac{1}{\underline{\mathbf{A}}^H(\tau)\Big(\sum_{k=L}^{N-1}\underline{\mathbf{E}}_k\underline{\mathbf{E}}_k^H\Big)\underline{\mathbf{A}}(\tau)}, \tag{5.8}$$

the time delays $\tau_0, \tau_1, ..., \tau_{L-1}$ can be estimated by finding the largest L peaks of $\mathbf{e}(\tau)$.

5.2.1.2 Channel matrix estimation

For the payload data, the main diagonal of $\mathbf{H}$ is estimated and interpolated using Wiener filter utilizing the scattered pilots,

$$\hat{H}_{k,k} = \underline{\mathbf{W}}_{k,k}^H\underline{\mathbf{Y}} \tag{5.9}$$

where $\underline{\mathbf{W}}_{k,k}$ is a Wiener filter vector related to the k^{th} element at the main diagonal of $\mathbf{H}$. The Wiener filter is designed using MMSE criterion [75], which requires a knowledge of the channel statistical parameters as the number of paths and their time delays that have been previously estimated. The off-diagonals of $\mathbf{H}$ are estimated by linearly approximating the time variation between three successive symbols [21]. By considering the first two terms of a Taylor expansion one can write

$$U(k,n) = \overline{U}(k) + (n - \frac{N-1}{2})\overline{U}(k)'. \tag{5.10}$$

$\overline{U}(k)'$ is the derivative of $\overline{U}(k)$ and can be expressed as

$$\overline{U}(k)' = \frac{\overline{U}(k)^{(next)} - \overline{U}(k)^{(prev.)}}{2N_s}, \tag{5.11}$$

where N_s is the total symbol length. The estimated channel matrix is then expressed as

$$\hat{\mathbf{H}} = \mathcal{D}(\underline{\mathbf{U}}) + \Gamma\mathcal{D}(\underline{\mathbf{U}}'), \tag{5.12}$$

where $\underline{\overline{\mathbf{U}}}$ and $\underline{\overline{\mathbf{U}}}'$ are vectors consist of $\overline{U}(k)$ and $\overline{U}(k)'$ for all k's, respectively. Γ is a precalculated matrix [16] which depends only on the OFDM parameters and is defined as

$$\Gamma = \begin{bmatrix} 0 & \gamma_1 & \cdots & \gamma_{N-1} \\ \gamma_{-1} & 0 & \cdots & \gamma_{N-2} \\ \vdots & \vdots & \ddots & \vdots \\ \gamma_{1-N} & \gamma_{2-N} & \cdots & 0 \end{bmatrix}$$

where

$$\gamma_n = \frac{1}{N}\sum_{k=0}^{N-1} k e^{j\frac{2\pi}{N}nk} = \begin{cases} \frac{N-1}{2} & n \bmod N = 0 \\ -\frac{1}{1-e^{j\frac{2\pi}{N}n}} & n \bmod N \neq 0 \end{cases}.$$

The estimated maximum time delay τ_{max} is used as CSI at the transmitter in order to adapt the GI length as

$$N_g \approx (\tau_{max} F_s) + 1),$$

where F_s is the sampling frequency. The adaptive OFDM system with the feedback signaling stage is diagrammed in Fig. 5.11.

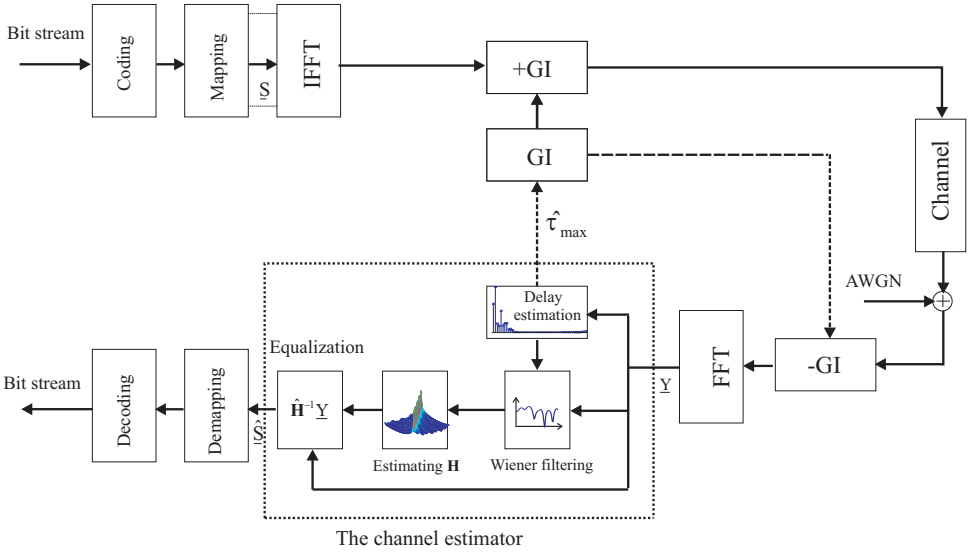

Figure 5.11: Baseband adaptive GI OFDM system.

5.2.2 Simulation Results

The adaptive scheme has been applied for OFDM-based WLAN [4] system. Uncoded QPSK scheme was used. The system parameters are summarized in Table 5.2.

Table 5.2: Parameters of WLAN system

Parameter	Value
Modulation scheme	QPSK
Number of Carriers	52
FFT length	64
Guard interval	16
Bandwidth	20 MHz

The OFDM symbols were transmitted through a 4-tap time-variant channel. We assume that the channel has a variant maximum delay between 150 ns to 750 ns during the transmission time. The channel taps were generated as random processes with common Doppler spread of 200 Hz. According to the estimated delay spread at the receiver, a

signal is fed back to the transmitter to change the cyclic prefix length with assuming an ideal feedback channel without errors. In order to evaluate the estimation algorithm, the MSE criterion has been used which is expressed as

$$MSE = E\{|\hat{\tau}_{max} - \tau_{max}|^2\} \tag{5.13}$$

where τ_{max} and $\hat{\tau}_{max}$ are the actual and the estimated maximum delay, respectively. The delay is normalized to the sampling time T, which is 50 ns for WLAN. Fig. 5.12 shows the MSE performance of the estimator at various SNR. The adaptive behavior of the

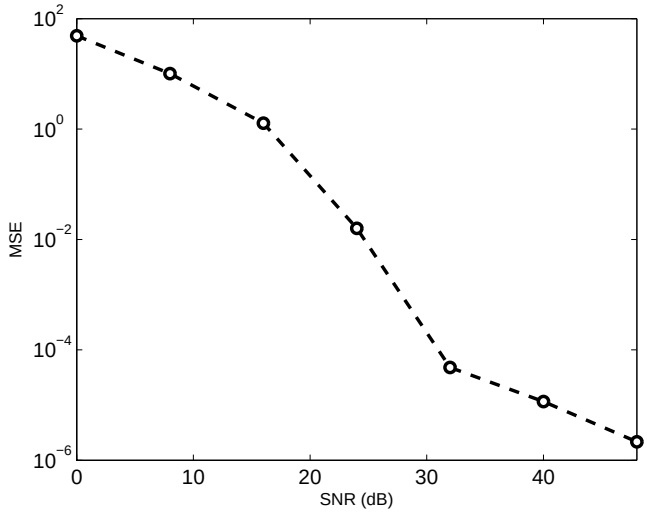

Figure 5.12: MSE of the estimated delay spread vs. SNR.

system is demonstrated in Fig. 5.13 by tracking the variation of the delay spread. The figure shows a considerable gain in the throughput for low dispersive scenarios. This gain decreases to the conventional one (24 Mbps) as the dispersion increases. In order to show the adaptive behavior, the bit rate has been averaged each $I' = 500$ symbols according to the following equation

$$b(i') = \frac{1}{I'} \sum_{i=i'+1}^{i'+I'} \frac{N\log2(M)}{T_u + T_g^i}, \quad i' = 0 : I' : I - 1. \tag{5.14}$$

where T_g^i is the guard interval of the i^{th} symbol, M is the modulation level, and I is the total transmitted symbols. Root-MUSIC is a noise-limited algorithm, therefore, some noise power is added to the estimated delay spread at low SNR, which results in increasing the guard interval more than required, thereby reduces the effective throughput. Nevertheless, some smoothing or de-noising algorithms can be used before applying root-Music. Fig. 5.14 and Fig. 5.15 show the effect of noise on the achievable throughput for different delay spreads and different SNR. The aim of the adaptive system was to gain the maximum throughput without sacrificing the BER performance. Fig. 5.16 compares between the BER performance of the conventional and the adaptive systems. Both systems are performing approximately the same for two cases: Firstly, by assuming the knowledge of

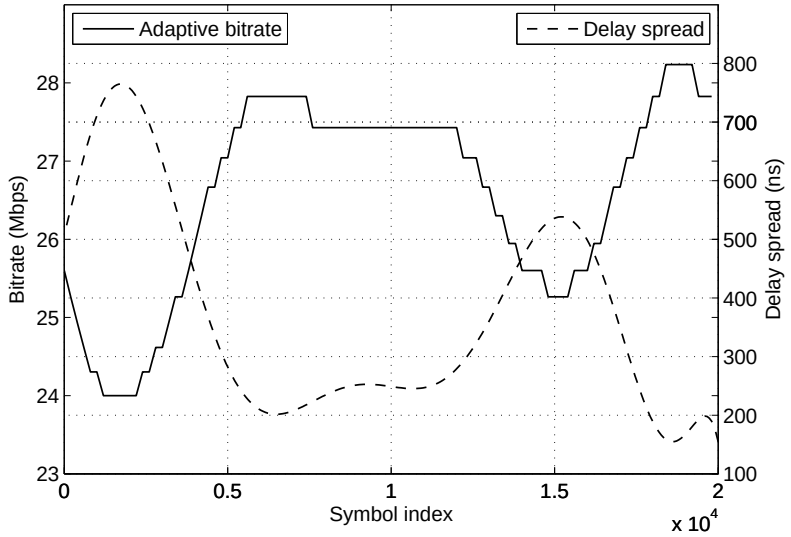

Figure 5.13: Bit rate vs. variant-delay spread , SNR=30 dB.

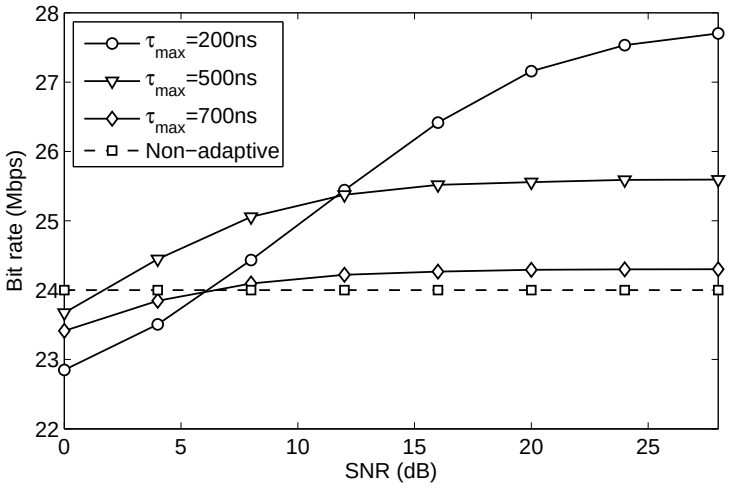

Figure 5.14: Bit rate vs. SNR.

the delay spreads for Wiener filtering (Optimal Wiener) and secondly, with estimating the time delays and using them to optimize Wiener filter. Further more, we can expect a slight improvement in the linear approximation algorithm described by (5.12). The reason behind that is that the distance between the averaged points at the three symbols that are used for approximating the channel matrix, decreases with decreasing the guard interval. This slightly improves the approximation at certain Doppler spread values. It has been shown from the simulation results that a considerable gain in the system throughput has been achieved without sacrificing the system performance in terms of BER. The results also showed that for improving the adaptation performance at very low SNR, de-noising algorithms for delay estimation are required.

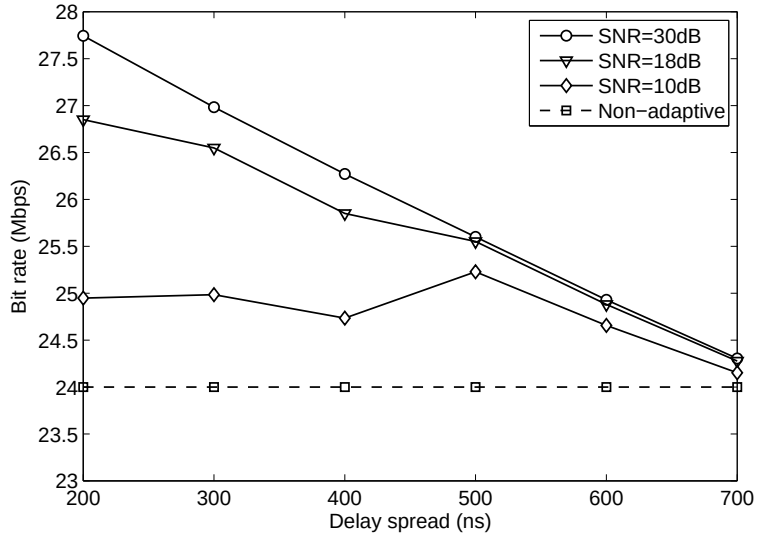

Figure 5.15: Bit rate vs. delay spread.

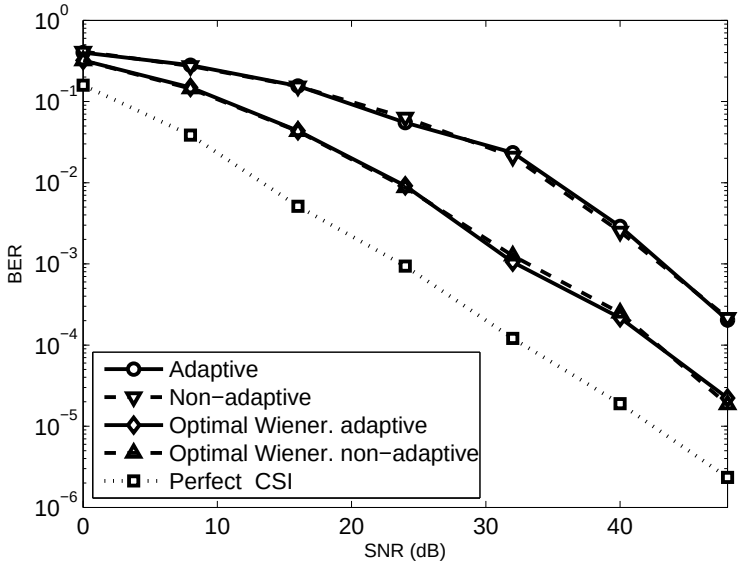

Figure 5.16: BER performance of the system.

5.2.3 Newly Proposed Adaptive Time and Frequency Pilot Distribution for OFDM-Based WLAN systems

The conventional fixed-pattern of pilot distribution in OFDM system may fail to track the highly dispersive channels, or causes unnecessary loss of capacity in flat and time-invariant channels.

5.2.3.1 Optimal number of pilots

As it has been described earlier, the number of pilots used for channel estimation is a trade of between the estimation accuracy and the bandwidth efficiency. To decide how many pilot symbols are required for channel estimation and where to locate the positions of these pilots, maximizing and minimizing methods are used, which require calculating some of the system metrics. During the last decade, many research works have been done for designing the optimal pilot distribution for channel estimation either by minimizing the MSE as described in [128] and [129], or by maximizing the capacity of the system as have been proposed in [130] and [131]. In [132], a method that minimizes the Cramer-Rao bound (CRB) of the MSE of the channel estimator was proposed. In [133], a design of the optimal (least) number of pilots needed at a required BER and a given SNR was proposed. Besides the number of the used pilots, the way of distributing these pilots affect the performance of the system that works in different channel conditions, therefore, the design of pilot structure also has received a significant attention. Since the previous works consider optimal but fixed-patterns of pilots, one design may not be optimal for all channel situations in the long-term sense. In order to come over this drawback, we are interested in this work in designing an adaptive pilot distribution that works in most of the channel conditions, such as frequency and time selectivity. The considered channel has a varying delay spread and varying Doppler spread. In OFDM system, different transmission parameters such as the modulation and coding rate are adapted to the channel quality. These parameters are chosen according to the estimated SNR [123]. According to the same concept, the distribution of pilots can also be adapted to the channel quality. To choose the required number of pilots in time and frequency directions, the estimation of Doppler spread and the delay spread must be exploited. The receiver controls the arrangement of the transmitted pilots according to the CSI in time and frequency. Delay spread and Doppler spread are estimated at the receiver and used to rearrange the pilot positions within the transmitted symbols in frequency and time directions, respectively. In relatively large coherence bandwidth or coherence time, the pilot-patterns can be managed with less pilot symbols, thereby reducing the overhead introduced by the pilots without significantly sacrificing the BER.

5.2.3.2 Delay spread estimation

At the beginning of each frame, the training symbols are used to estimate the Delay spread of the channel. The channel transfer function can be estimated using LS solution as

$$\underline{\hat{\mathbf{H}}}_p = \mathcal{D}(\underline{\mathbf{S}}_p)^{-1}\underline{\mathbf{Y}}_p. \tag{5.15}$$

The covariance matrix of the estimated channel $\mathbf{R}_N = E\{\hat{\mathbf{H}}_p\hat{\mathbf{H}}_p^H\}$ is used to efficiently estimate the delay contents using Root-MUSIC algorithm. This algorithm has a super resolution properties of decomposing the delay contributions in the covariance matrix based on eigenspace analysis as described in Section 5.2.1.

5.2.3.3 Doppler spread estimation

For the payload data, the channel matrix is estimated in the same procedure of Section 5.2.1, where the main diagonal is estimated using Wiener filtering method. The statistical channel parameters used for filter design are first estimated during the training stage [2], while other diagonals are estimated by linearly approximating the channel utilizing three successive OFDM symbols. The Doppler spread is estimated for the channel matrix making use of the upper bound of the ICI power described by (4.15)

$$f_d \approx \frac{\sqrt{3\sum_{k\neq m} E\left[|\hat{H}_{k,m}|^2\right]}}{\pi T_s} \tag{5.16}$$

After estimating Doppler and delay spreads, a signal is fed back to the transmitter to

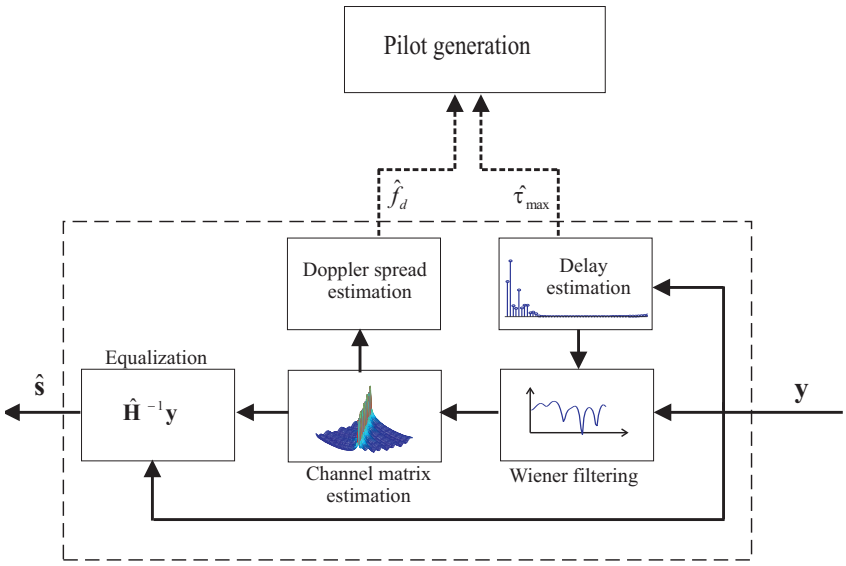

Figure 5.17: The estimator stages of the adaptive pilot distribution system.

adapt the pilot distribution as shown in Fig. 5.17.
For a given long-term BER target, some Doppler spread and delay spread thresholds must be chosen to adjust the pilot density in time and frequency directions. In the frequency direction, the number of pilots changes according to the estimated delay spread τ_{max}. Since the estimated Doppler spread itself depends on the pilot spacing, the pilots in time direction are inserted in groups of three symbols, and the distance between these groups changes according to the estimated Doppler spread in order to guarantee a robust estimation of Doppler spread as depicted in Fig. 5.18. Estimating Doppler spread using only three symbols allows near-instantaneous CSI for fast adaptation.

5.2.4 Simulation Results

In this section, we discuss the results of the simulation of OFDM-based WLAN system [4]. OFDM symbols modulated by uncoded QPSK scheme. These symbols were transmitted

[2]The estimated delays using Root-Music are used as prior information of the Wiener filter, while Doppler spread for each tap is neglected during estimating the main diagonal.

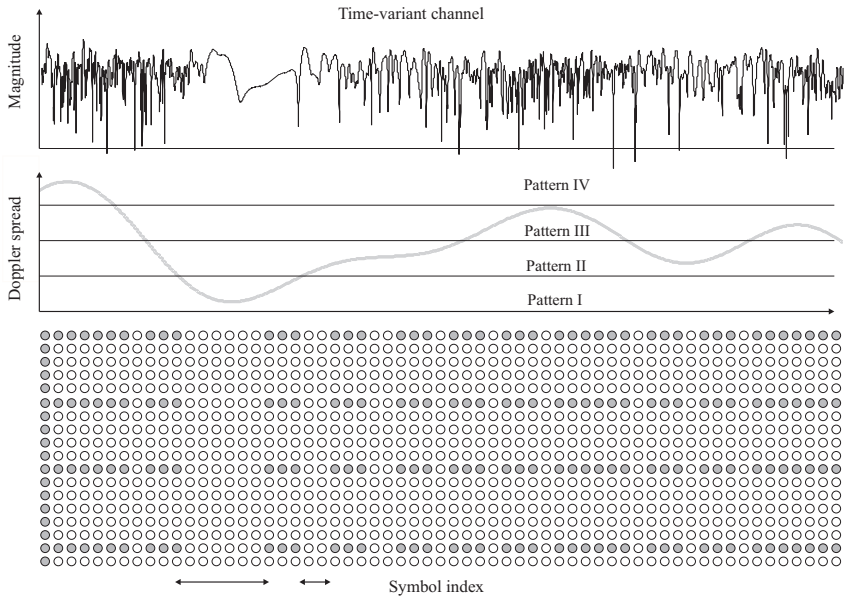

Figure 5.18: An example of adapting the time spacing between the pilots according to Doppler spread (The pilot symbols in time direction are gathered in groups of three pilots in order to guarantee a robust Doppler spread estimation).

through a 4-tap time-variant channel. A more realistic assumption is to let channel taps have variant maximum delay and Doppler spreads. The delay spread changes between 0 ns to 700 ns, and Doppler spread changes between 0 Hz to 3000 Hz during the transmission time. We chose to let the delay spread varying in steps each 100 OFDM symbols, while Doppler spread varies smoothly along the time. The channel taps amplitudes were generated as random processes with Rayleigh distribution, while the phases assumed uniformly distributed. Six threshold levels of the delay spread and four threshold levels of Doppler spread were chosen to change the number of pilots in frequency direction as (4, 5, 6, 7, 8, and 10) pilots and the distance between the pilot-symbols in time direction as (0, 4, 8, and 12) symbols, respectively. According to these levels, a signal is fed back to the transmitter with assuming an ideal feedback transmission without errors.

Three different scenarios have been tested in this simulation. In the first one, we consider a channel with variant Doppler spread and a constant delay spread of 500 ns. In this case the adaptive pilot distribution is done only in the time direction, while in the frequency direction, the number of pilots is set to 4 pilots. Fig. 5.19 shows the simulated pilot distribution. It can be seen that the pilots density changes in both time and frequency directions according to channel selectivity. In Fig. 5.20 it can be shown that the adaptive system gives an improvement in the achievable bit rate compared with the conventional one. In order to show the adaptive behavior, the bit rate has been averaged each $I' = 500$ symbols according to the following equation

$$b(i') = \frac{1}{I'} \sum_{i=i'+1}^{i'+I'} \frac{(N - N_p^i)\log2(M)}{T_s}, \quad i' = 0 : I' : I - 1. \tag{5.17}$$

where N_p^i is the number of pilots in the i^{th} symbol. It can be seen from Fig. 5.21 that the

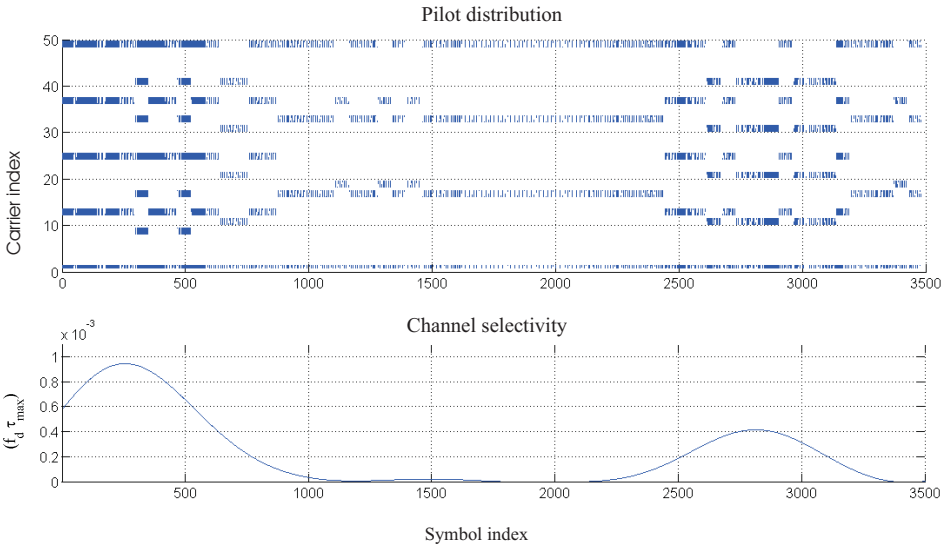

Figure 5.19: The simulated pilot distribution vs. channel selectivity.

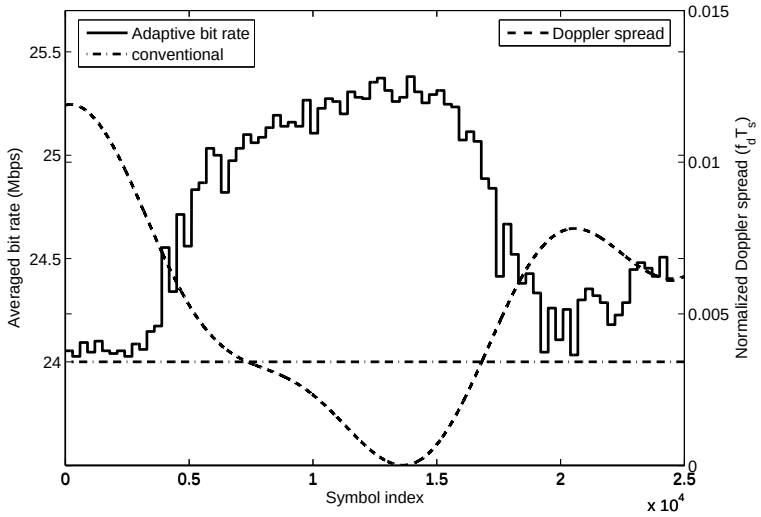

Figure 5.20: Averaged bit rate vs. Doppler spread (SNR = 36 dB).

adaptive system is slightly more erroneous than the conventional one. The second case is considering a channel with variant delay spread and a constant Doppler spread of 500 Hz. It can be seen from Fig. 5.22 that, the bit rate is reduced at high delay spreads, since more pilots are used comparing with the conventional one. While the BER performance is improved compered to the conventional one as depicted in Fig. 5.23. In the last case, the channel has variant Doppler spread and variant delay spread at the same time. A trade-off between the required BER performance and the required averaged bit rate has been taken into account in designing the pilot pattern. Fig. 5.24 demonstrates the adaptive behavior of the system. The averaged bit rate is reduced to 21 Mbps when the channel is highly dispersive, and increased to reach about 25 Mbps when the channel has

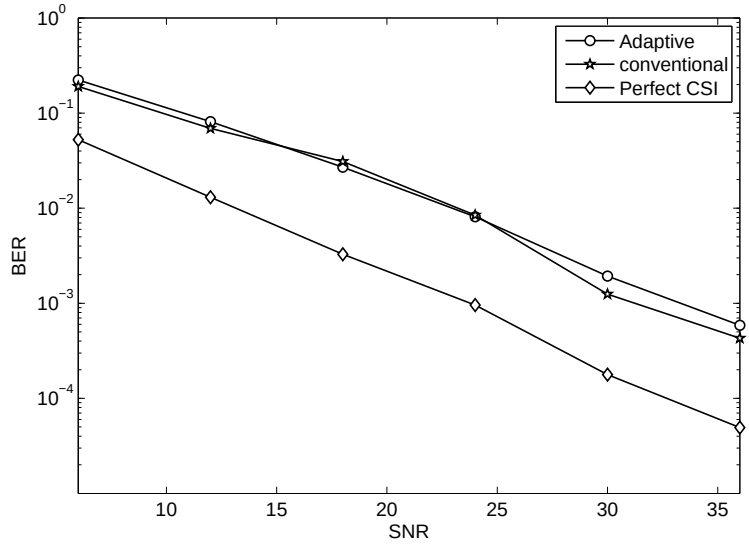

Figure 5.21: BER performance for Doppler spread-variant channel (Delay spread = 500 ns).

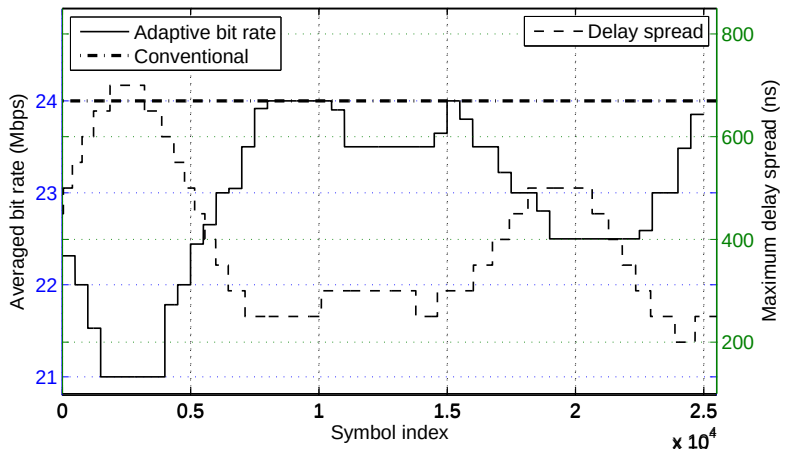

Figure 5.22: Averaged bit rate vs. delay spread (SNR = 36 dB).

low selectivity. It is easy to conclude that the performance in terms of BER is improved as shown in Fig. 5.25. It has been observed that with sacrificing a small value of the total throughput, a significant improvement in the BER performance has been achieved. In general, it has been shown that the adaptive method increases the total capacity of the system. The gain in the throughput is noticeable when the channel is static or slowly varying. The simulation results showed also a considerable improvement in the BER performance without significantly sacrificing the total throughput of the system. The noise affects the performance of both delay and Doppler estimation. Therefore, the total throughput is decreased for low SNR as is depicted in Fig. 5.26, Fig. 5.27, and Fig. 5.28, which demonstrate the throughput versus SNR in case of Doppler-variant channel. It can also be concluded that the complexity of the system is adaptively reduced compared to

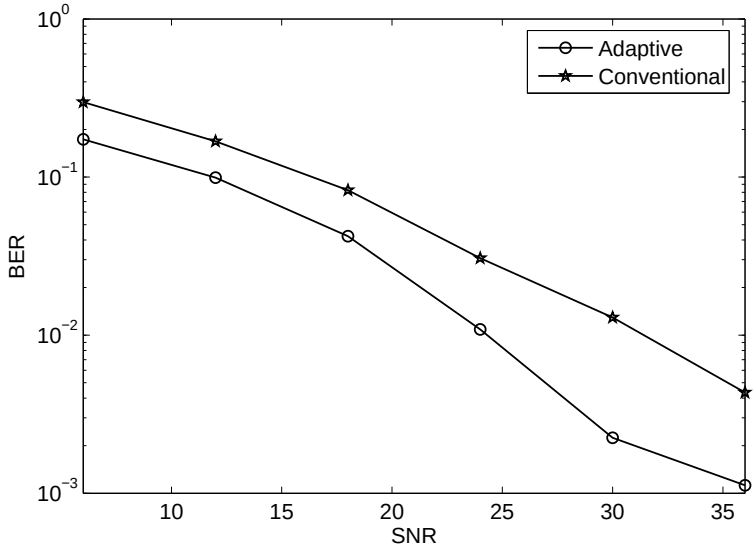

Figure 5.23: BER performance for delay spread-variant channel (Doppler spread = 500 Hz).

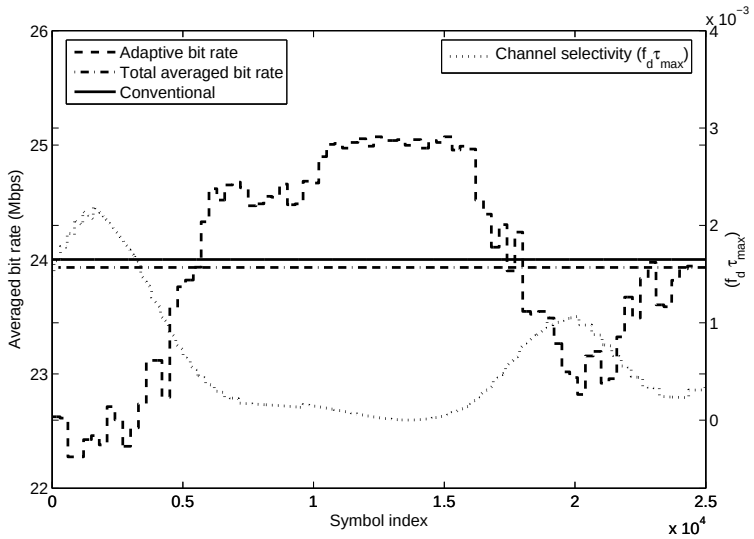

Figure 5.24: Averaged bit rate vs. channel selectivity ($f_d\tau_{max}$) SNR = 36 dB.

the conventional patterns, since for symbols that carry no pilots, estimating the channel is not applied, where a saved channel matrix from the last estimate is used.

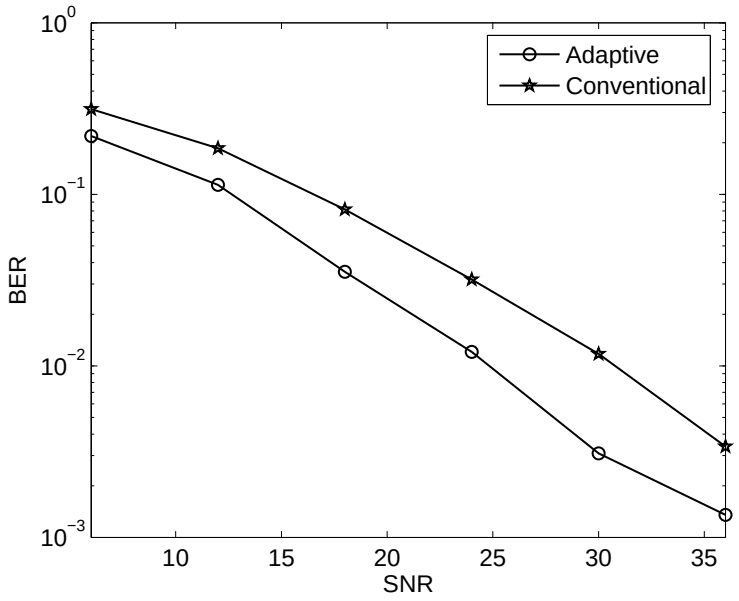

Figure 5.25: BER performance for variant delay and Doppler spreads.

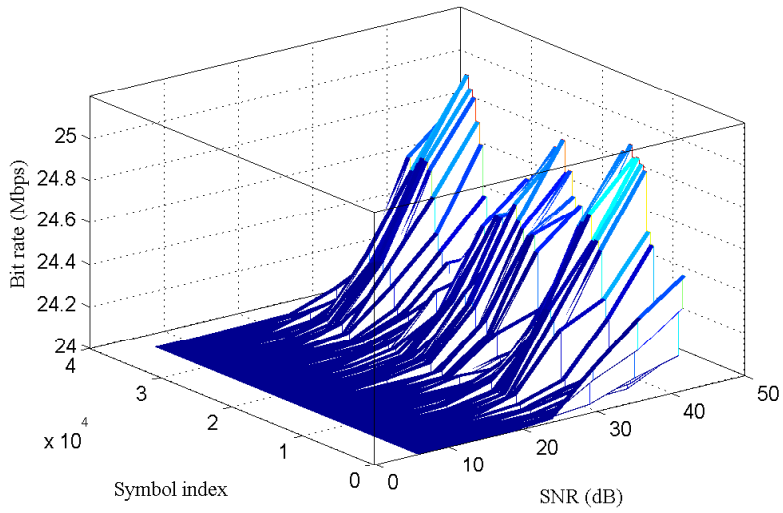

Figure 5.26: The effect of the noise on the throughput of the system for Doppler-variant channel.

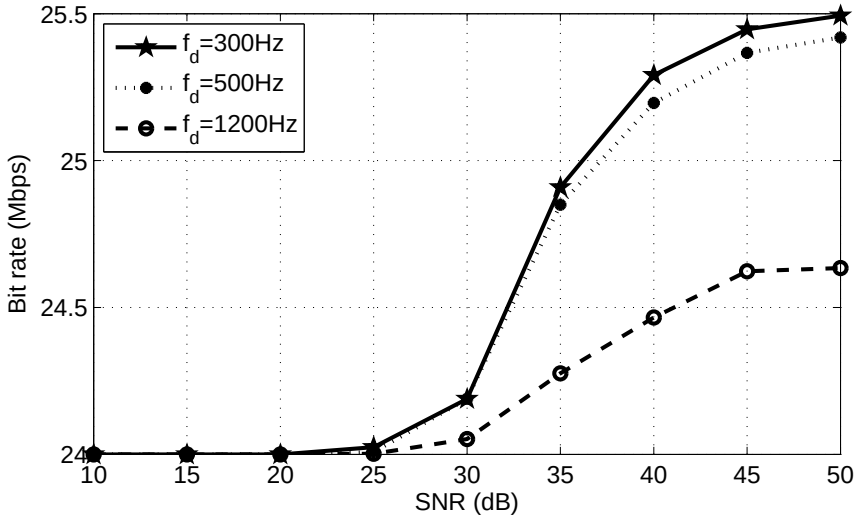

Figure 5.27: Bit rate vs. SNR for different Doppler spread values.

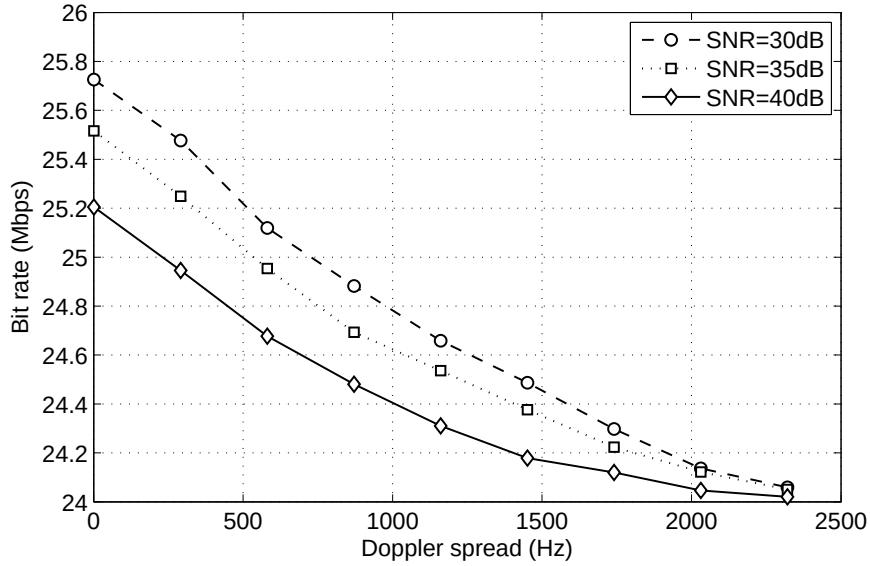

Figure 5.28: Bit rate vs. Doppler spread for different SNR values.

Chapter 6

Conclusions and Future Work

6.1 Thesis Summary

The aim of this work was to enable the OFDM system to efficiently work in time-variant channels, therefore the thesis has focused on developing low complexity reduction methods of the ICI resulting from Doppler effects, and introducing adaptive schemes that allow the reliable transmission and reception of the OFDM signal. A study of the OFDM system in multipath time-variant channels was carried out supported with mathematical analysis, simulation in MATLAB as well as real time testing of the OFDM signal, in order to find new and robust channel estimation and equalization algorithms able to enhance the performance and reduce the computational effort at the reviver side. As a result some ICI reduction, channel estimation, and adaptation algorithms have been proposed and verified. The thesis starts with a detailed introduction to the multipath time-variant channel and its statistical characteristics. The concept of the multicarrier OFDM system, its spectrum efficiency and its robustness against multipath channels have been explained. The OFDM system degradation due to the doubly dispersive channel has been studied. The study was supported through simulations according to the wide sense stationary uncorrelated scattering (WSSUS) assumption with different channel conditions. A discussion about the pilot-based channel estimation and equalization algorithms for OFDM systems such as LS and MMSE criteria have been overviewed.

In the thesis an MMSE Wiener filtering estimation scheme for digital radio mondiale (DRM) system is developed. The Wiener filter is designed according to the Gaussian shaped Doppler spectrum, and combined with Matrix pencil algorithm as a pre-stage in order to estimate the channel statistical parameters that are required for optimizing the Wiener filter. The effects of the number of pilots, the modulation level, the number of channel taps, and the number of transmit and receive antennas have been shown through the simulation results. Furthermore, the algorithm has been verified with some real experiments. The measurement system used for testing OFDM signal has been discussed. This system has been used to characterize the multipath channel and test the transmission, reception and channel estimation of the OFDM-based WLAN system. A method of joint channel and frequency offset estimation based on the signal preamble and Wiener filtering has been implemented.

A mathematical analysis of generating the ICI in OFDM-based DRM system has been studied. A New low complexity schemes used for reducing the ICI for OFDM in rapidly time-variant channels have been proposed. These schemes make use of approximating the time variation of the channel by means of numerical methods, such as Newton and Lagrange polynomial approximation. The simulation results showed that the proposed method gives a considerable improvement to the BER performance comparing with the Linear models. The schemes were able to estimate the channel matrix at high values

of Doppler spread. The approximation methods are valid as long as Doppler spread is less than the frequency spacing between the sub-carriers, which is usually the case for wireless channels. Making use of the extrapolation, the performance can be further improved without causing extra delay.

Another low complexity estimation method for DRM system has been developed. The method applies a time domain preprocessing at the received signal to maximize the signal-to-noise plus interference ratio (SNIR) and make the channel matrix sparse, thereby it allows for low complexity equalization from $\mathcal{O}(N^3)$ to $\mathcal{O}(N(D+1)^3)$. A gaussian shaped Doppler spectrum has been considered in implementing this algorithm. Further more, another window has been applied, which results from slight modification on the Hamming window, in order to make it suitable for different Doppler spread values. Some iterative detection schemes that depend on hard and soft feedback equalization have been implemented for equalizing the sparse matrix, and verified by the simulation results.

The thesis introduces and suggests some adaptive techniques for OFDM system for both, receiver and link adaptation that allow the system to work in a wide range of channel conditions. A new receiver adaptation scheme for OFDM system based on the long-term tracking of the channel has been proposed. The scheme adapt the polynomial degree of the channel approximation method discussed in Chapter 4, aiming at minimizing the bit-error rate (BER) as a subject to the processing delay. The simulation results showed that the proposed scheme gives a stable BER performance with an improvement comparing with the non-adaptive systems, and has less dependency on the Doppler spread variation. Adaptive GI length for OFDM-based WLAN systems has been proposed in which the delay spread is estimated using Root-Multiple Signal Classification Root-MUSIC algorithm, and used to adapt the GI length at the transmitter aiming at maximizing the system throughput with maintaining the BER performance. It has been shown from the simulation results that a considerable gain in the system throughput has been achieved without sacrificing the system performance in terms of BER. The results also showed that for improving the adaptation performance at very low SNR, de-noising algorithms for delay estimation are required. Another link adaptation method has been introduced, which is adapting the pilot distribution used for channel estimation. The pilot spacing in time and in frequency directions has been adapted according to the channel state information (CSI). Doppler spread used for adapting the time pilot spacing is estimated from the off-diagonals of the channel matrix. In order to guarantee a robust Doppler estimation process, the pilots are gathered in blocks of three symbols and used for estimating the channel matrix via linear channel approximation. The spacing between these blocks is adapted instead of adapting the spacing between the pilots. The delay spread used for adapting the frequency pilot spacing is estimated using Root-MUSIC algorithm. It has been shown that the adaptive method increases the total capacity of the system. The gain in the throughput is clear at static or slowly varying channels. The simulation results has also shown an improvement in the BER performance without significantly sacrificing the total throughput of the system. It has also been concluded that the AWGN noise affects the performance of both delay and Doppler estimation. Therefore, the total throughput is decreased for low SNR. It can also be concluded that the complexity of the system is adaptively reduced comparing with that of the conventional pilot distribution patterns, since for symbols that carry no pilots, estimating the channel is not applied and a saved channel matrix from the last estimate is used.

6.2 Future Work

In developing the link adaptive schemes, the feedback channel has been assumed ideal. However, for real systems, the effects of the feedback channel needs to be investigated, therefore more research work is required. Further more, in addition to simulation, measurements can be carried out to verify the capability of these schemes in a real time-variant channels. In addition to estimating Doppler from the off-diagonals of the channel matrix, a blind estimation of Doppler spread exploiting the padded zeros on the OFDM spectrum could be of interest in the future work. Finally, an interesting future work is to apply the algorithms discussed throughout this thesis on the downlink of the emerging 4G LTE system. Combining these algorithms with the MIMO technology used in LTE could give new perspectives and improvements to the system performance. In addition to the usual OFDM disadvantages such as ICI and high PAPR, another new challenge of using the OFDM in the downlink of the LTE mobile communication systems, is the inter-cellular interference, which needs to be studied to identify the best frequency, time, and power allocation schemes.

Appendices

Appendix A

Deriving The Max-SNIR Window for DRM System

The windowed frequency domain received signal is written as

$$\underline{\mathbf{Y}} = \frac{1}{\sqrt{N}}\mathcal{C}(\mathsf{W})\mathbf{H}\underline{\mathbf{S}} + \frac{1}{\sqrt{N}}\mathcal{C}(\mathsf{W})\underline{\mathbf{V}} \tag{A.1}$$

The relationship between the time and frequency domain of the first term at the right hand side is explained as follows

$$\mathcal{C}(\mathsf{W})\mathbf{H}\underline{\mathbf{S}} = \mathbf{F}\mathcal{D}(\mathsf{w})\mathbf{h}\underline{\mathbf{x}} = (\mathbf{F}\mathcal{D}(\mathsf{w})\mathbf{F}^H)(\mathbf{F}\mathbf{h}\mathbf{F}^H)\underline{\mathbf{S}} = \mathcal{C}(\mathsf{W})\mathbf{H}\underline{\mathbf{S}} \tag{A.2}$$

where $\underline{\mathbf{x}}$ is the transmitted time domain signal. With the same concept

$$\|\mathcal{M}\{\mathcal{C}(\underline{\mathsf{W}})\mathbf{H}\}\|_F^2 = \|\mathcal{M}\{\mathbf{F}\mathcal{D}(\underline{\mathsf{w}})\mathbf{h}\}\|_F^2 \tag{A.3}$$

The denominator of equation (4.42) is written as

$$\|\bar{\mathcal{M}}\{\mathcal{C}(\underline{\mathsf{W}})\mathbf{H}\}\|_F^2 + \sigma_v^2\|\mathcal{C}\{\underline{\mathsf{W}}\}\|_F^2 \tag{A.4}$$

The second term of (A.4) can be simplified making use of the energy saving between frequency and time domains as

$$\frac{\sigma_v^2}{N} = \sigma_v^2\sum_m |\mathsf{W}_m|^2 \equiv \sum_n |\mathsf{w}_n|^2 = \underline{\mathsf{w}}^H diag(\sigma_v^2\mathbf{I})\underline{\mathsf{w}} \tag{A.5}$$

Also, the second term is simplified further as follows

$$\|\bar{\mathcal{M}}\{\mathcal{C}(\underline{\mathsf{W}})\mathbf{H}\}\|_F^2 = \|\mathcal{C}(\underline{\mathsf{W}})\mathbf{H}\|_F^2 - \|\mathcal{M}\{\mathcal{C}(\underline{\mathsf{W}})\mathbf{H}\}\|_F^2 \tag{A.6}$$

So that, the denominator becomes

$$\underline{\mathsf{w}}^H diag(\sigma_v^2\mathbf{I} + \mathbf{h}\mathbf{h}^H)\underline{\mathsf{w}} - \|\mathcal{M}\{\mathbf{F}\mathcal{D}(\underline{\mathsf{w}})\mathbf{h}\}\|_F^2 \tag{A.7}$$

In order to maximize the SINR, we need to maximize the second term of (A.7) as

$$\underline{\mathsf{w}}_{opt} = \arg \quad \max \|\mathcal{M}\{\mathbf{F}\mathcal{D}(\underline{\mathsf{w}})\mathbf{h}\}\|_F^2 \tag{A.8}$$

Rewriting (A.8) in summation form gives

$$= \frac{1}{\sqrt{N}}\sum_{n,n'}\mathsf{w}_n\mathsf{w}_{n'}^*\sum_{|d|\le D} e^{-j\frac{2\pi(n-n')d}{N}}.\sum_{l=0}^{L-1} h(n,l)h^*(n',l) \tag{A.9}$$

Finally, by ordering (A.9), we get

$$= \underline{\mathsf{w}}^H \mathbf{A} \underline{\mathsf{w}} \tag{A.10}$$

The matrix $\mathbf{A}$ is resulting from element-wise multiplication of two matrices as follows

$$\mathbf{A} = \mathbf{B} \odot \mathbf{D}, \tag{A.11}$$

where $\mathbf{B}$ is given by

$$[\mathbf{B}]_{k,m} = \frac{1}{N} \frac{\sin\left(\frac{\pi}{N}(2D+1)(m-k)\right)}{\sin\left(\frac{\pi}{N}(m-k)\right)}, \tag{A.12}$$

Considering the Gaussian shaped Doppler spectrum of DRM system, $\mathbf{D}$ is given by

$$[\mathbf{D}]_{k,m} \approx \left(\frac{\alpha^2}{\sigma_v^2 + \alpha^2}\right) e^{-\pi^2 f_D^2 (m-k)^2/2}. \tag{A.13}$$

The resulting window can be calculated as follows

$$\underline{\mathsf{w}}_{opt} = \frac{\underline{\tilde{\mathsf{w}}}_{opt}}{\sqrt{\left(\sigma_v^2 + \alpha^2\right)}} \tag{A.14}$$

where σ_v^2 is the noise variance and α^2 is the summation of all the variances of channel complex taps ($\alpha^2 = \sum_0^{L-1} \sigma_l^2$).

Appendix B

Soft Decision Feedback Equalization (Turbo Principle)

The prior log-likelihood ratio in case of BPSK can be written as

$$L(S_k) = ln\frac{P(S_k = +1)}{P(S_k = -1)} \tag{B.1}$$

and the posterior

$$L(S_k|\tilde{S}_k) = ln\frac{P(S_k = +1|\tilde{S}_k)}{P(S_k = -1|\tilde{S}_k)} \tag{B.2}$$

By Assuming a gaussian distribution of the transmitted symbols, the probability density is written as follows

$$P(\tilde{S}_k|S_k = r) = \psi((\tilde{S}_k - \mu_k(r))/\sigma_k(r))/\sigma_k(r) \tag{B.3}$$

where r is the value of the transmitted carrier, $\psi(n) = \frac{e^{-n^2}}{\sqrt{\pi}}$, $\mu_k(r) = E\{\tilde{S}_k|S_k = r\}$, and $\sigma_k(r) = \mathrm{Cov}(\tilde{S}_k, \tilde{S}_k|S_k = r)$. Making use of (4.51) and (4.52), we can write

$$\mu_k(r) = \underline{\mathcal{F}}_k^H \underline{\hbar}_k r,$$

$$\sigma_k^2(r) = \underline{\mathcal{F}}_k^H \underline{\hbar}_k (1 - \underline{\hbar}_k^H \underline{\mathcal{F}}_k)$$

The difference between the prior and the posterior log-likelihood ratios is written as

$$\Delta L(\tilde{S}_k) = L(S_k|\tilde{S}_k) - L(S_k) \tag{B.4}$$

By the substitution in (B.3) we get

$$P(\tilde{S}_k|S_k = r) = \frac{1}{\sigma_k(r)} e^{-\frac{(\tilde{S}_k - \mu_k(r))^2}{\sigma_k^2(r)}}$$

$$= \frac{1}{\sqrt{\underline{\mathcal{F}}_k^H \underline{\hbar}_k (1 - \underline{\hbar}_k^H \underline{\mathcal{F}}_k)}} e^{-\frac{(\tilde{S}_k - \underline{\mathcal{F}}_k^H \underline{\hbar}_k . r)^2}{\underline{\mathcal{F}}_k^H \underline{\hbar}_k (1 - \underline{\hbar}_k^H \underline{\mathcal{F}}_k)}}$$

It can be shown that

$$P(\tilde{S}_k|S_k = +1) = \frac{1}{\sqrt{\underline{\mathcal{F}}_k^H \underline{\hbar}_k (1 - \underline{\hbar}_k^H \underline{\mathcal{F}}_k)}} e^{\frac{-\tilde{S}_k^2 + 2\tilde{S}_k \underline{\mathcal{F}}_k^H \underline{\hbar}_k - (\underline{\mathcal{F}}_k^H \underline{\hbar}_k)^2}{\underline{\mathcal{F}}_k^H \underline{\hbar}_k (1 - \underline{\hbar}_k^H \underline{\mathcal{F}}_k)}}$$

$$P(\tilde{S}_k|S_k=-1)=\frac{1}{\sqrt{\underline{\mathcal{F}}_k^H\underline{\hbar}_k(1-\underline{\hbar}_k^H\underline{\mathcal{F}}_k)}}e^{\frac{-\tilde{S}_k^2-2\tilde{S}_k\underline{\mathcal{F}}_k^H\underline{\hbar}_k-(\underline{\mathcal{F}}_k^H\underline{\hbar}_k)^2}{\underline{\mathcal{F}}_k^H\underline{\hbar}_k(1-\underline{\hbar}_k^H\underline{\mathcal{F}}_k)}}$$

and then

$$\frac{P(\tilde{S}_k|S_k=+1)}{P(\tilde{S}_k|S_k=-1)}=e^{\frac{4\tilde{S}_k}{(1-\underline{\hbar}_k^H\underline{\mathcal{F}}_k)}}$$

finally we get

$$\Delta L(\tilde{S}_k)=\ln\frac{P(\tilde{S}_k|S_k=+1)}{P(\tilde{S}_k|S_k=-1)}=4\frac{\mathrm{Re}(\tilde{S}_k)}{(1-\underline{\hbar}_k^H\underline{\mathcal{F}}_k)}$$

after calculating the difference, we use it to update the priors as

$$L_{new}(S_k)=L(S_k)+\Delta L(\tilde{S}_k)$$

we evaluate $\bar{S}_{k,new}$ as follows

$$\bar{S}_{k,new}=\sum_r rP(S_k=r|\tilde{S}_k) \tag{B.5}$$

In the case of BPSK, equation (B.5) becomes

$$\bar{S}_{k,new}=(+1)*P(S_k=+1|\tilde{S}_k)+(-1)*P(S_k=-1|\tilde{S}_k) \tag{B.6}$$

The summation of possible probabilities is equal to 1

$$P(S_k=+1|\tilde{S}_k)+P(S_k=-1|\tilde{S}_k)=1 \tag{B.7}$$

by inserting (B.7) into (B.6) and using (B.2), we get

$$P(S_k=+1|\tilde{S}_k)=\frac{e^{L(S_k|\tilde{S}_k)}}{1+e^{L(S_k|\tilde{S}_k)}}$$

$$P(S_k=-1|\tilde{S}_k)=\frac{1}{1+e^{L(S_k|\tilde{S}_k)}}$$

and (B.6) is written as

$$\bar{S}_{k,new}=\frac{e^{L(S_k|\tilde{S}_k)}}{1+e^{L(S_k|\tilde{S}_k)}}-\frac{1}{1+e^{L(S_k|\tilde{S}_k)}}=\tanh(L(S_k|\tilde{S}_k)/2) \tag{B.8}$$

The covariance $b_{k,new}$ can be written as follows

$$b_{k,new} = \sum_{r} (r - E\{S_k|\tilde{S}_k\})^2 P(S_k = r|\tilde{S}_k) = 1 - \bar{S}^2_{k,new}. \tag{B.9}$$

For QPSK modulation scheme that has been used for the simulation, the calculations described above become for both real and imaginary parts as following

$\Delta L(\tilde{S}_k) = \frac{4}{\sqrt{2}} \frac{\mathrm{Re}(\tilde{S}_k)}{(1-\underline{\hbar}_k^H \underline{\mathcal{F}}_k)}, \frac{4}{\sqrt{2}} \frac{\mathrm{Im}(\tilde{S}_k)}{(1-\underline{\hbar}_k^H \underline{\mathcal{F}}_k)}$

$\bar{S}_{k,new} = \frac{1}{\sqrt{2}} \tanh(L(S_k|\tilde{S}_k)/2)$ for real and imaginary parts

$b_{k,new} = \frac{1}{2} - \bar{S}^2_{k,new}$ for real and imaginary parts.

Bibliography

[1] R. Prasad, *OFDM for Wireless Communication Systems.* Boston London: Artech House, 2004. 1

[2] ETSI, *Digital Audio Broadcasting (DAB) to mobile, portable and fixed receivers.* ETSI EN, 300 401 V1.4.1 2006. 1, 18

[3] ——, *Digital Video Broadcasting (DVB); Interaction channel for Digital Terrestrial Television (RCT) incorporating Multiple Access OFDM.* ETSI. 1, 18

[4] C. Smith and J. Meyer, *3G Wireless with 802.16 and 802.11.* McGraw-Hill Professional, 2004. 1, 18, 97, 102

[5] M. Mouly and M. Pautet, "Current evolution of the GSM," *IEEE Personal Communication Magazin*, vol. 2, pp. 9–19, Oct. 1995. 2

[6] J. Korhonen, *Introduction to 3G Mobile Communications.* Boston London: Artech House, 2003. 2

[7] K. Kinoshita and M. Nakagawa, *Japanese Celullar Standard.* Boca Raton, FL: CRC Press, 1996. 2

[8] A. Ross and K. Gilhousen, *CDMA Technology and the IS-95 North American standard.* Boca Raton, FL: CRC Press, 1996. 2

[9] S. Ohmori, Y. Yamao, and N. Nakajima, "The future generations of mobile communications based on broadband access technologies," *IEEE Personal Communication Magazin*, vol. 38, no. 12, pp. 134–142, Dec. 2000. 2

[10] *3GPP, 3G TR25.848, V.0.6.0, May 2000.* 3

[11] P. Chaudhury, W. Mohr, and S. Onoe, "The 3GPP proposal for IMT-2000," *IEEE Communications Magazine*, vol. 37, no. 12, pp. 72–81, Dec. 1999. 3

[12] P. Lescuyer and T. Lucidarme, *Evolved Packet Systems (EPS): The LTE and SAE evolution of 3G UMTS.* John Wiley and Sons, 2008. 3

[13] S. Hara and R. Prasad, *Multicarrier Techniques for 4G Mobile Communications.* Boston London: Artech House, 2003. 3

[14] WiMAXForum, "Mobile WiMAX part I: A technical overview and performance evaluation." 5

[15] S. Hara and R. Prasad, *Multicarrier Techniques for 4G Mobile Communications.* Boston London, www.artechhouse.co: Artech Housem, 2003. 5, 59

[16] J. Linartz and A. Grokhov, "New equalization approach for OFDM over dispersive and rapidly time varying channel," in *PIMRC'00*, Sep. 2000. 7, 96

[17] Y. Liao and K. Chen, "Estimation of stationary phase noise by the autocorrelation of the ICI weighting function in OFDM systems," *IEEE Trans. Wireless Commun.*, vol. 5, no. 12, pp. 3370–3374, Dec. 2006.

[18] M. Chang, "A novel algorithm of interference self-cancellation for OFDM systems," *IEEE Trans. Wireless Commun.*, vol. 6, no. 8, pp. 2881–2893, Aug. 2007.

[19] W. J. nad K. Chang and Y. Cho, "An equalization technique for orthogonal frequency-division multiplexing systems in time-variant multipath channels," *IEEE Trans. Commun.*, vol. 47, no. 1, pp. 27–32, Jan. 1999. 72

[20] Y. Mostofi and D. Cox, "ICI mitigation for pilot-adided OFDM mobile systems," *IEEE Trans. Commun.*, vol. 4, no. 2, Mar. 765-774.

[21] V. Fischer, A. Kurpiers, and D. Karsunkc, "ICI reduction method for OFDM systems," in *8th International OFDM-Workshop, Hamburg, Germany*, Sep. 2003. 7, 68, 96

[22] C. Shannon, "A mathematic theory of communications," in *Bell Systems Technical Journal*, vol. 27, Jul. 1948, pp. 379–423. 7

[23] R. Blum, Y. Li, J. Winters, and Q. Yan, "Improved space-time coding for MIMO-OFDM wireless communications," *IEEE Trans. Commun.*, vol. 49, no. 11, pp. 1873–1878, Nov. 2001. 8

[24] I. Barhumi, G. Leus, and M. Moonen, "Optimal training design for MIMO OFDM systems in mobile wireless channels," *IEEE Trans. Signal Processing*, vol. 51, no. 6, pp. 1615–1624, Jun. 2003.

[25] P. Xia, S. Zhou, and G. Giannakis, "Adaptive MIMO-OFDM based on partial channel state information," *IEEE Trans. Signal Processing*, vol. 52, no. 1, pp. 202–213, Jan. 2004.

[26] A. van Zelst and T. Schenk, "Implementation of a MIMO OFDM-based wireless LAN system," *IEEE Trans. Signal Processing*, vol. 52, no. 2, pp. 483–494, Feb. 2004. 8

[27] H. Schulze and C. Lders, *Theory and Applications of OFDM and CDMA Wideband Wireless Communications*. New York: J. Wiley & Sons, 2005. 8, 12, 15, 35

[28] D. Wulich and L. Goldfeld, "Reduction of peak factor in orthogonal multicarrier modulation by amplitude limiting and coding," *IEEE Trans. Commun.*, vol. 47, no. 1, pp. 18–21, Jan. 1999. 8

[29] V. Tarokh and H. Jafarkhani, "On the computation and reduction of the peak-to-average power ratio in multicarrier communications," *IEEE Trans. Commun.*, vol. 48, no. 1, pp. 37–44, Jan. 2000.

[30] G. Yue and X. Wang, "A hybrid PAPR reduction scheme for coded OFDM," *IEEE Trans. Wireless Commun.*, vol. 5, no. 10, pp. 2712–2722, Oct. 2006.

[31] H. Lee and M. P. Fitz, "Unitary peak power reduction in multiple transmit antennas," *IEEE Trans. Commun.*, vol. 56, no. 2, pp. 234–244, Feb. 2008. 8

[32] M. Paetzold, *Mobile Fading Channels*. New York: J. Wiley & Sons, 2002. 13, 14, 15

[33] A. Molisch, *Wireless communications*. J. Wiley & Sons, 2005. 13

[34] J. S. Sadowsky and V. Kafedziski, "On the correlation and scattering functions of the WSSUS channel for mobile communications," *IEEE Trans. Veh. Technol.*, vol. 47, no. 2, pp. 270–282, Feb. 1998. 14, 89

[35] G. Grimmett and D. Stirzaker, *Probability and Random Processes*. Oxford University Press, Juli 2001. 15

[36] ETSI, *Digital Radio Mondiale (DRM)-System Specification*. ETSI TS, 101 980, V1.1.1, Sep. 2001. 16, 18, 66, 79, 90

[37] V. Veeravalli and A. Sayeed, *Wideband Wireless Channels: Statistical Modeling, Analysis and Simulation*. J. Wiley & Sons, 2005. 17

[38] F. Perez-Fontan and P. M. Espineira, *Modeling the Wireless Propagation Channel: A Simulation Approach with MATLAB (Wireless Communications and Mobile Computing)*. J. Wiley & Sons, 2008. 17

[39] T. Claasen and W. Mecklenbraeuker, "On stationary linear time-variant systems," vol. 29, no. 3, pp. 169–184, Mar. 1982. 17

[40] R. W. Chang, "Synthesis of band-limited orthogonal signals for multi-channel data transmission," *Bell System Technical Journal*, vol. 46, no. 1, pp. 1775–1796, Jan. 1966. 18

[41] S. B. Weinstein and P. M. Ebert, "Data transmission by frequency-division multiplexing using the discrete fourier transform," *IEEE Trans. Commun.*, vol. 19, no. 5, pp. 628–634, Oct. 1971. 18

[42] L. J. Cimini, "Analysis and simulation of a digital mobile channel using orthogonal frequency division multiplexing," *IEEE Trans. Commun.*, vol. 33, pp. 665–675, Jul. 1985. 18

[43] K. Fazel and S. Kaiser, *Multi-Carrier and Spread Spectrum Systems*. John Wiley & Sons, 2003. 18

[44] R. Nee and R. Prasad, *OFDM for Wireless Multimedia Communications*. Boston London: Artech House, 2000. 20

[45] W. Jeon, K. Chang, and Y. Cho, "An equalization technique for orthogonal frequency-division multiplexing systems in time-variant multipath channels," *IEEE Trans. Wireless Commun.*, vol. 47, pp. 27–32, Jan. 1999. 23

[46] M. Morelli and U. Mengali, "A comparison of pilot-aided channel estimation methods for OFDM systems," *IEEE Trans. Signal Processing*, vol. 49, no. 12, pp. 3065–3073, Dec. 2001. 29

[47] S. J. Grant and J. K. Cavers, "Multiuser channel estimation for detection of cochannel signals," *IEEE Trans. Commun.*, vol. 49, no. 10, pp. 1845–1855, Oct. 2001.

[48] R. Otnes and M. Tuechler, "Iterative channel estimation for turbo equalization of time-varying frequency-selective channels," *IEEE Trans. Wireless Commun.*, vol. 53, no. 1, pp. 132–137, Mar. 2007. 79

[49] Y. G. Li, L. J. Cimini, Jr., and N. R. Sollenberger, "Robust channel estimation for OFDM systems with rapid dispersive fading channels," *IEEE Trans. Commun.*, vol. 46, no. 7, pp. 902–915, Jul. 1998.

[50] Y. Zeng, A. R. Leyman, and T.-S. Ng, "Joint semiblind frequency offset and channel estimation for multiuser MIMO-OFDM uplink," *IEEE Trans. Commun.*, vol. 55, no. 12, pp. 2270–2278, Dec. 2007.

[51] S. Lee, K. Kwak, J. Kim, and D. Hong, "Channel estimation approach with variable pilot density to mitigate interference over time-selective cellular OFDM systems," *IEEE Trans. Wireless Commun.*, vol. 7, no. 7, pp. 2694–2704, Jul. 2008.

[52] F. Gao, T. Cui, and A. Nallanathan, "On channel estimation and optimal training design for amplify and forward relay networks," *IEEE Trans. Wireless Commun.*, vol. 7, no. 5, pp. 1907–1916, May 2008.

[53] A. S. Ling and L. B. Milstein, "Trade-off between diversity and channel estimation errors in asynchronous MC-DS-CDMA and MC-CDMA," *IEEE Trans. Commun.*, vol. 56, no. 4, pp. 584–597, Apr. 2008.

[54] Y.-S. Choi, P. J. Voltz, and F. A. Cassara, "On channel estimation and detection for multicarrier signals in fast and selective rayleigh fading channels," *IEEE Trans. Commun.*, vol. 49, no. 8, pp. 1375–1387, Aug. 2001.

[55] X. Chu, R. Murch, J. Liu, and M. Ghavami, "Pilot-channel-assisted log-likelihood-ratio selective rake combining for low-rate ultra-wideband communications," *IEEE Trans. Commun.*, vol. 56, no. 8, pp. 1313–1323, Aug. 2008. 29

[56] S. Roy and C. Li, "A subspace blind channel estimation method for OFDM systems without cyclic prefix," *IEEE Trans. Wireless Commun.*, vol. 1, no. 4, pp. 572–579, Oct. 2002. 29

[57] M. Hongbin Li, "Blind channel estimation for multicarrier systems with narrowband interference suppression," *IEEE Commun. Lett.*, vol. 7, no. 7, pp. 326–328, Jul. 2003.

[58] B. Muquet, M. de Courville, and P. Duhamel, "Subspace-based blind and semi-blind channel estimation for OFDM systems," *IEEE Trans. Signal Processing*, vol. 50, no. 7, pp. 1699–1712, Jul. 2002.

[59] F. Sanzi and M. C. Necker, "Totally blind APP channel estimation for mobile OFDM systems," *IEEE Commun. Lett.*, vol. 7, no. 11, pp. 517–519, Nov. 2003.

[60] A. Petropulu, R. Zhang, and R. Lin, "Blind OFDM channel estimation through simple linear precoding," *IEEE Trans. Wireless Commun.*, vol. 3, no. 2, pp. 647–655, Mar. 2004.

[61] S. Yatawatta and A. P. Petropulu, "Blind channel estimation in MIMO OFDM systems with multiuser interference," *IEEE Trans. Signal Processing*, vol. 54, no. 3, pp. 1054–1068, Mar. 2006.

[62] C. Li and S. Roy, "Subspace-based blind channel estimation for OFDM by exploiting virtual carriers," *IEEE Trans. Wireless Commun.*, vol. 2, no. 1, pp. 141–150, Jan. 2003. 29

[63] J. van de Beek, M. Sandell, and P. Oorjesson, "ML estimation of time and frequency offset in OFDM systems," *IEEE Trans. Signal Processing*, vol. 45, no. 7, pp. 1800–1805, Jul. 1997. 29

[64] X. Ma and G. Giannakis, "Unifying and optimizing null-subcarrier based frequency-offset estimators for OFDM," in *Proc. Int. Conf. Inform, Commun., Signal Processing, Singapore*, Oct. 2001. 29

[65] Y. J. LIM, D. S. HYUN, and S. K. PARK, "Pilot patterns for OFDM communication systems in a fast time-varying channel," *IEICE Trans. COMMUN*, vol. E89B, no. 1, pp. 243–246, Jan. 2006. 30

[66] O. Macchi and C. Macchi, *Adaptive Processing: The Least Mean Squares Approach with Applications in Transmission.* John Wiley and Sons, 23. Februar 1995. 31

[67] C. Rao, H. Toutenburg, A. Fieger, C. Heumann, T. Nittner, and S. Scheid, *Linear Models: Least Squares and Alternatives.* Springer Series in Statistics, 1999. 31

[68] J. Idier, L. Mugnier, and A. Blanc, "Statistical behavior of joint least-square estimation in the phase diversity context," *IEEE Trans. Image Processing.*, vol. 14, no. 12, pp. 2107–2116, Dec. 2005.

[69] J. Wolberg, *Data Analysis Using the Method of Least Squares: Extracting the Most Information from Experiments.* Springer, 2005. 31

[70] H. Trees, *Detection, Estimation, and Modulation Theory. Part I: Detection, Estimation, and Linear Modulation Theory.* John Wiley & Sons, 1968. 32

[71] H. Poor, *An introduction to signal detection and estimation.* Springer-Verlag, 1994.

[72] S. Kay, *Fundamentals of Statistical Processing, Volume I: Estimation Theory.* Prentice Hall Signal Processing Series, 1993. 32

[73] S. T. Karris, *Numerical Analysis Using MATLAB and Spreadsheets.* Orchard publications, Oct. 2001. 32, 38, 64, 65

[74] M. Barkat, *Signal Detection and Estimation.* 685 Canton Street, Norwood, MA 02062: ARTECH HOUSE, 2005. 33

[75] C. Sgraja and J. Linder, "Estimation of rapid time-variant channels for OFDM using wiener filtering," in *IEEE Proc. on Commun.*, vol. 4, May 2003, pp. 2390–2395. 33, 62, 96

[76] Y. Hua and T. Sarkar, "Matrix pencil method for estimating parameters of exponentiallydamped/undamped sinusoids in noise," *IEEE Trans. Acoustics, Speech and Signal Processing.*, vol. 38, no. 5, pp. 814–824, May 1990. 33, 34

[77] C. PAIGE, "Computing the generalized singular value decomposition," *SIAM J. Sci. Stat.*, vol. 7, pp. 1126–1146, Jul. 1986. 34

[78] R. Lucky, "Automatic equalization for digital communicationsn," *Bell System Tech. J.*, vol. 44, pp. 547–88, Apr. 1965. 35

[79] S. Alamouti, "A simple transmitter deversity technique for wireless communications," *IEEE J. Select. Areas Commun.*, vol. 16, no. 10, pp. 1451–1458, Oct. 1998. 36

[80] A. Viterbi, "Error bounds for convolutional codes and an asymptotically optimum decoding algorithm," *IEEE Trans. Inform. Theory*, vol. 2, pp. 260–269, Apr. 1967. 39

[81] Agilent, *Agilent N5182A MXG Vector Signal Generator: Data sheet.* ftp://ftp.testequity.com/pdf/n5182a.pdf: Agilent Technology, 2007. 43

[82] D. Mittelstrasz, *Design Einer Antenne Bestehend aus Primaerstrahler und Dielektrischer Linse fuer das ISM-Band 2.4 GHz.* Studienarbeit: Otto-von-Guericke Universitaet Magdeburg, 2007. 43

[83] A. Bandyopadhyay, M. Anis, A. Joestingmeier, T. Meyer, and A. Omar, "Analysis of a compact ultra-wideband antenna for radio frequency applications," in *Antennas and Propagation Society International Symposium, 2007*, vol. 9, Jun. 2007, pp. 1965–1968. 43

[84] Agilent, *Agilent EXA Signal Analyzer N9010A: Data Sheet.* http://cp.literature.agilent.com/litweb/pdf/5989-6529EN.pdf: Agilent Technology, 2009. 43

[85] T. RAPPAPORT, *Wireless Communications: Principles and Practice.* Prentice Hall, 2001. 44, 45

[86] J. Heiskala and J. Terry, *OFDM Wireless LANs: A Theoretical and Practical Guide.* Sams, 2001. 47

[87] T. Schmidl and D. Cox, "Robust frequency and timing synchronization for OFDM," *IEEE Trans. Commun.*, vol. 45, no. 12, pp. 1613–1621, Dec. 1997. 48

[88] D. Huang and D. Guek, "Performance analysis of OFDM burst synchronization algorithms," in *ICCS 2002:The 8th International Conference on Communication Systems, 2002*, vol. 4, Nov. 2002, pp. 245–249. 48

[89] J. Pierri, *Design and Implementation of an OFDM WLAN Synchronizer: Master thesis*. University of Waterloo, 2007. 50

[90] L. R. P. B. G. Leus, "Simple equalization of time-varying channels for OFDM," *IEEE Commun. Lett.*, vol. 9, no. 12, pp. 619–621, Jul. 2005. 55

[91] X. Cai and G. B. Giannakis, "Bounding performance and suppressing intercarrier interference in wireless mobile OFDM," *IEEE Trans. Commun.*, vol. 51, no. 12, pp. 2047–2056, Dec. 2003. 55

[92] Y. S. Choi, P. J. Voltz, and F. A. Cassara, "On channel estimation and detection for multicarrier signals in fast and selective rayleigh fading channels," *IEEE Trans. Commun.*, vol. 49, no. 8, pp. 1375–1387, Aug. 2001.

[93] G. Liu and W. Zhu, "Compensation of phase noise in OFDM systems using an ICI reduction scheme," *IEEE Trans. Broadcasting.*, vol. 50, no. 4, pp. 399–407, Dec. 2004. 55

[94] Y.-C. Liao and K.-C. Chen, "Estimation of stationary phase noise by the autocorrelation of the ICI weighting function in OFDM systems," *IEEE Trans. Wireless Commun.*, vol. 5, no. 12, pp. 3370–3374, Dec. 2006. 55

[95] S. Tang, K. Gong, J. Song, C. Pan, and Z. Yang, "Intercarrier interference cancellation with frequency diversity for OFDM systems," *IEEE Trans. Broadcasting.*, vol. 53, no. 1, pp. 132–137, Mar. 2007.

[96] S. Tomasin, A. Gorokhov, H. Yang, and J.-P. Linnartz, "Iterative interference cancellation and channel estimation for mobile OFDM," *IEEE Trans. Wireless Commun.*, vol. 4, no. 1, pp. 238–245, Jan. 2005.

[97] M.-J. Hao, "Decision feedback frequency offset estimation and tracking for general ICI self-cancellation based OFDM systems," *IEEE Trans. Broadcasting.*, vol. 53, no. 6, pp. 560–566, Jun. 2007.

[98] F. Munier, T. Eriksson, and A. Svensson, "An ICI reduction scheme for OFDM system with phase noise over fading channels," *IEEE Trans. Commun.*, vol. 56, no. 7, pp. 1119–1126, Jul. 2008.

[99] H. Steendam and M. Moeneclaey, "Analysis and optimization of the performance of OFDM on frequency-selective time-selective fading channels," *IEEE Trans. Commun.*, vol. 47, no. 12, pp. 1811–1819, Dec. 1999.

[100] W.-S. Hou and B.-S. Chen, "ICI cancellation for OFDM communication systems in time-varying multipath fading channels," *IEEE Trans. Wireless Commun.*, vol. 4, no. 5, pp. 2100–2110, Sep. 2005.

[101] H.-G. Ryu, Y. Li, and J.-S. Park, "An improved ICI reduction method in OFDM communication system," *IEEE Trans. Broadcasting.*, vol. 51, no. 3, pp. 395–400, Sep. 2005. 55

[102] P. Schniter, "Low-complexity equalization of OFDM in doubly-selective channels," *IEEE Trans. Signal Processing*, vol. 52, no. 4, pp. 1002–1011, Apr. 2004. 56, 74, 75, 76, 78

[103] M. Trott, *The Mathematica GuideBook for Programming.* New York: Springer-Verlag, 2004. 57

[104] Y. G. Li and L. J. Cimini, "Bound on the interchannel interference of OFDM in time-varying impairments," *IEEE Trans. Commun.*, vol. 49, no. 3, pp. 401–404, Mar. 2001. 60

[105] C. Runge, "Ueber empirische funktionen und die interpolation zwischen aequidistanten ordinaten," in *Zeitschrift fr Mathematik und Physik*, vol. 46, Jan. 1901, pp. 224–243. 66

[106] L. Rugini, P. Banelli, and G. Leus2, "Low-complexity banded equalizers for ofdm systems in doppler spread channels," *EURASIP Journal on Applied Signal Processing*, vol. 2006. 74

[107] A. R. Ali, *ICI Reduction for OFDM Systems Using Time Domain Preprocessing.* Master Thesis: TU Darmstadt, 2004. 76

[108] F. Harris, "On the use of windows for harmonic analysis with the discrete fourier transform," *Proceedings of the IEEE*, vol. 66, no. 1, pp. 51–83, Jan. 1978. 76

[109] M. Tuechler, A. Singer, and R. Koetter, "Minimum mean square error equalization using a priori information," *IEEE Trans. Signal Processing*, vol. 50, no. 3, pp. 673–683, Mar. 2002. 79

[110] H. Arslan, *Signal processing for mobile communications.* CRC press, 2004. 87

[111] V. Lau and S. Maric, "Variable rate adaptive modulation for DS-CDMA," *IEEE Trans. Commun.*, vol. 47, pp. 577–589, Apr. 1999. 87

[112] M. R. Souryal, B. R. Vojcic, and R. L. Pickholtz, "Adaptive modulation in Ad Hoc DS/CDMA packet radio networks," *IEEE Trans. Commun.*, vol. 54, no. 4, pp. 714–725, Apr. 2006.

[113] Z. Yahong, Z. Zhongpei, and W. Weiling, "Multicarrier DS-CDMA with adaptive modulation and power allocation," vol. 20, no. 3, pp. 177–182, 2003. 87

[114] A. Czylwik, "Adaptive OFDM for wideband radio channels," in *IEEE Global Telecommunicarions Conference Globecom*, vol. 1, Nov. 1996, pp. 713–718. 87, 94

[115] T. Keller and L. Hanzo, "Adaptive modulation technique for duplex OFDM transmission," *IEEE Trans. Veh. Technol.*, vol. 49, pp. 1893–1906, Apr. 2000.

[116] R. Grnheid and H. Rohling, "Adaptive modulation and multiple access for the OFDM transmission technique," vol. 13, no. 1, pp. 5–13, 2000.

[117] A. Czylwik, "Adaptive ofdm for wideband radio channels," in *proc. Globecom, London, U.K. 1996*, Dec. 1996, pp. 713–718. 87, 94

[118] T. Lim, L. Rasmussen, and H. Sugimoto, "An asynchronous multiuser CDMA detector based on the kalman filter," *IEEE J. Select. Areas Commun.*, vol. 16, pp. 1711–1722, Dec. 1998. 87

[119] D. Schafhuber, G. Matz, and F. Hlawatsch, "Adaptive wiener filters for time-varying channels estimation in wirelss OFDM systems," in *IEEE ICASSP*, vol. 4, Apr. 2003, pp. 688–691. 87

[120] J. Zander, "Performance of optimal transmitter power control in cellular radio systems," *IEEE Trans. Veh. Technol.*, vol. 41, no. 1, pp. 57–62, Feb. 1992. 87, 94

[121] S. Ulukus and R. D. Yates, "Stochastic power control for cellular radio systems," *IEEE Trans. Commun.*, vol. 46, no. 6, pp. 784–798, Jun. 1998. 87, 94

[122] I. Capoglu, Y. Li, and A. Swami, "Effect of doppler spread in OFDM-based UWB systems," *IEEE Trans. Wireless Commun.*, vol. 4, pp. 2559–2567, Sep. 2005. 89

[123] L. Hanzo, C. H. Wong, and M. S. Yee, *Adaptive wireless transceivers*. New York: J. Wiley & Sons, 2002. 93, 101

[124] I. Siaud and A. Ulmer, "A novel adaptive sub-carrier interleaving application to millimeter-wave WPAN OFDM systems," in *proc. of Portable Information Devices, 2007. PORTABLE07.* 93

[125] Z. Zhang and L. Lai, "A novel OFDM transmission scheme with length-adaptive cyclic prefix," vol. 5, no. 11, pp. 1336–1342, Nov. 2004. 95

[126] A. Ali, V. Nguyen, K. Kyamakya, and A. Omar, "Estimation of the channel-impulse-response length for adaptive OFDM systems based on information theoretic criteria," in *VTC2006*, vol. 4, May 2006, pp. 1888–1892. 95

[127] M. Oziewicz, "On application of MUSIC algorithm to time delay estimation in OFDM channels," *IEEE Trans. Broadcasting.*, vol. 51, no. 2, pp. 1–72, Jun. 2005. 95

[128] R. Negi and J. Cioffi, "Pilot tone selection for chanel estimation in a mobile OFDM system," *IEEE Trans. Consumer Electron.*, vol. 44, no. 8, pp. 1122–1128, Aug. 1998. 101

[129] I. Barhumi, G. Leus, and M. Moonen, "Optimal training design for MIMO OFDM systems in mobile wireless channels," *IEEE Trans. Signal Processing*, vol. 51, no. 6, pp. 1615–1624, Jun. 2003. 101

[130] B. Hassibi and B. Hochwald, "How much training is needed in multiple-antenna wireless links?" *IEEE Trans. Inform. Theory*, vol. 49, pp. 951–963, Apr. 2003. 101

[131] S. Adireddy and L. Tong, "Optimal placement of training for frequency-selective block-fading channels," *IEEE Trans. Inform. Theory*, vol. 48, pp. 2338–2353, Aug. 2002. 101

[132] M. Dong and L. Tong, "Optimal design and placement of pilot symbols for channel estimation," *IEEE Trans. Signal Processing*, vol. 50, no. 12, pp. 3055–3069, Dec. 2002. 101

[133] W. Zhang, X. Xia, and P. Chin, "Optimal training and pilot pattern design for OFDM systems in rayleigh fading," *IEEE Trans. Broadcasting.*, vol. 52, no. 12, pp. 505–514, Dec. 2006. 101